PolyPublie
Polytechnique Montréal

POLYTECHNIQUE MONTRÉAL
UNIVERSITÉ D'INGÉNIERIE

Titre: Title:	Design of a Hybrid Solar-Wind Microgrid Driving a PEM Electrolyzer for Scalable Hydrogen Production
Auteur: Author:	Hayfa Rhimi
Date:	2026
Type:	Mémoire ou thèse / Dissertation or Thesis
Référence: Citation:	Rhimi, H. (2026). Design of a Hybrid Solar-Wind Microgrid Driving a PEM Electrolyzer for Scalable Hydrogen Production [Mémoire de maîtrise, Polytechnique Montréal]. PolyPublie. https://publications.polymtl.ca/73210/

Document en libre accès dans PolyPublie
Open Access document in PolyPublie

URL de PolyPublie: PolyPublie URL:	https://publications.polymtl.ca/73210/
Directeurs de recherche: Advisors:	Daria Camilla Boffito, & Andreas Athienitis
Programme: Program:	Génie énergétique

Ce fichier a été téléchargé à partir de PolyPublie, le dépôt institutionnel de Polytechnique Montréal
This file has been downloaded from PolyPublie, the institutional repository of Polytechnique Montréal

https://publications.polymtl.ca

POLYTECHNIQUE MONTRÉAL

affiliée à l'Université de Montréal

Design of a Hybrid Solar-Wind Microgrid Driving a PEM Electrolyzer for Scalable Hydrogen Production

HAYFA RHIMI

Département de génie chimique

Mémoire présenté en vue de l'obtention du diplôme de *Maîtrise ès sciences appliquées*

Génie énergétique

Janvier 2026

© Hayfa Rhimi, 2026.

POLYTECHNIQUE MONTRÉAL

affiliée à l'Université de Montréal

Ce mémoire intitulé :

Design of a Hybrid Solar-Wind Microgrid Driving a PEM Electrolyzer for Scalable Hydrogen Production

présenté par **Hayfa RHIMI**

en vue de l'obtention du diplôme de *Maîtrise ès sciences appliquées*

a été dûment accepté par le jury d'examen constitué de :

Jérôme LE NY, président
Daria Camilla BOFFITO, membre et directrice de recherche
Andreas ATHIENITIS, membre et codirecteur de recherche
Sébastien LE DIGABEL , membre

DEDICATION

To Foufi, you deserve this and more.

ACKNOWLEDGEMENTS

First and foremost, I would like to express my at most appreciation for my academic supervisors Professor Daria Camilla Boffito and Professor Andreas Athienitis for without them, the completion of this project would not have been possible. Their expertise and their input directed me towards the right path, and I am forever grateful for this experience and the knowledge I acquired. Again, thank you Professor Daria for the financial support, the technical support and for accepting me in your EPIC team because it truly was an epic journey and thank you Professor Andreas for your technical support and your comments for without them I would not have been able to finish this work.

I would also like to extend my gratitude for my family, my father Mohamed Rhimi, my mother Salma Abbassi and my siblings, Abdallah and Chayma. I truly do not know where I would have been without their unwavering support. I am beyond blessed and privileged to have them, I get to experience unconditional love and support daily and I do not take it for granted. Thank you for always letting me be who I am, for listening, for being there and for always believing in me.

I would also like to thank my friends, Aziz and Firas for being one phone call away from laughter and telling me I can do this. Emna and Ons for being one phone call away from comfort and reassurance. They all have truly showed me that life is always easier when shared with people you love. Finally, Iheb, these two years have been a roller coaster, and he was there for every high and low, I would not have done any of this without my friend telling me not to give up, so thank you.

Thank you, Montreal, for a formative two years and for every single event, reason and person who have helped me throughout this journey too. Lastly, I would like to thank myself for never giving up and never letting life get its last kick.

RÉSUMÉ

L'attention mondiale croissante portée à la décarbonation et aux énergies durables a intensifié le développement de systèmes d'énergies renouvelables capables de fournir une électricité propre et fiable. Parmi ces systèmes, l'intégration des ressources solaires et éoliennes pour la production d'hydrogène vert par électrolyse suscite un intérêt croissant, en raison de son potentiel à transformer des sources renouvelables intermittentes en un combustible stable à forte densité énergétique. Toutefois, l'intermittence de ces ressources, combinée à une forte dépendance aux systèmes de stockage d'énergie et aux algorithmes de contrôle conventionnels, limite encore les performances des systèmes énergétiques hybrides.

Afin de répondre à ces défis, cette recherche présente la conception et le développement d'un micro-réseau hybride solaire–éolien basé sur la simulation, destiné à alimenter un électrolyseur à membrane échangeuse de protons (PEM) pour la production d'hydrogène vert. Ce travail intègre un jumeau numérique entièrement développé dans un environnement virtuel, sans nécessiter de prototype physique. Ce jumeau permet l'évaluation des performances en temps réel, l'optimisation du fonctionnement ainsi que la mise en œuvre de stratégies de contrôle prédictif sous des conditions environnementales variables.

L'étude est structurée autour de quatre objectifs principaux. Tout d'abord, un modèle détaillé de production solaire a été développé sous MATLAB/Simulink afin d'évaluer les profils de génération d'énergie pour différents niveaux d'irradiation. Ce modèle a ensuite été complété par l'intégration d'un sous-système éolien, permettant de prolonger la durée de fonctionnement du système en compensant l'intermittence de l'énergie solaire.

Dans une seconde étape, le modèle hybride a été transféré sous Python, où des couches avancées de contrôle et d'optimisation ont été implémentées. Un algorithme d'optimisation par essaim de particules (Particle Swarm Optimization : PSO) a été introduit afin d'optimiser les paramètres opérationnels du système. Une structure de contrôle prédictif (Model Predictive Control : MPC) a ensuite été intégrée pour coordonner la prise de décision en temps réel et garantir une optimisation continue des flux énergétiques à partir de données météorologiques prévisionnelles. La précision des prévisions météorologiques permet ainsi d'anticiper les fluctuations de l'irradiation solaire et de la vitesse du vent, améliorant à la fois la fiabilité et l'efficacité du système.

Les performances du système sont analysées à travers le suivi de la charge de l'électrolyseur, de l'état de charge (SoC) de la batterie et de la production d'hydrogène à partir de données météorologiques mesurées. Dans la configuration finale, la puissance photovoltaïque est dimensionnée à 1,0 fois la puissance nominale de l'électrolyseur, la puissance éolienne à 0,53, et la batterie présente une limite de puissance de 0,40 ainsi qu'une capacité énergétique équivalente à 6,7 heures de fonctionnement à pleine charge de l'électrolyseur. Sur une simulation annuelle, l'électrolyseur fonctionne de manière continue avec un facteur de capacité de 0,68 (sur la base du PCI) et une production moyenne d'hydrogène de 48,7 kg par jour. La batterie fournit en moyenne 13 % de la demande énergétique de l'électrolyseur, le reste étant assuré par les sources renouvelables, avec une consommation spécifique de 50 kWh par kilogramme d'hydrogène produit.

Une contribution majeure de ce travail réside dans sa scalabilité et son adaptabilité. Une interface de simulation interactive a été développée afin de permettre aux utilisateurs de modifier le dimensionnement du système, les paramètres de contrôle et les apports en énergies renouvelables, rendant ainsi l'ensemble du cadre reproductible et facilement adaptable à de nouveaux scénarios de conception ou à de nouvelles localisations géographiques. Cette flexibilité permet une analyse comparative du potentiel de production d'hydrogène renouvelable dans différents contextes climatiques et géographiques sans nécessiter de reconfiguration approfondie des modèles. Le cadre proposé constitue ainsi une base pour le développement futur de systèmes de planification énergétique renouvelable spécifiques à un site donné.

Dans l'ensemble, cette étude fournit une base méthodologique complète pour la simulation d'un système hybride solaire–éolien optimisé avec stockage alimentant un électrolyseur. Elle démontre comment un jumeau numérique basé sur la simulation, associé à des prévisions météorologiques précises, à un contrôle prédictif et à des algorithmes d'optimisation, peut constituer une étape préliminaire vers une mise en œuvre réelle. En offrant une plateforme virtuelle flexible, évolutive et entièrement intégrée, ce travail contribue à réduire l'écart entre la modélisation théorique et le déploiement pratique de micro-réseaux intelligents dédiés à la production d'hydrogène renouvelable.

ABSTRACT

The global attention towards decarbonization and sustainable energy has intensified the development of renewable energy systems capable of supplying clean and reliable power. Among these, the integration of solar and wind resources for green hydrogen production through electrolysis has gained attention as well due to its potential to transform intermittent renewable energy into a stable, high energy density fuel. However, this intermittence of these resources along with high dependency on energy storage systems and conventional control algorithms limit the performance of hybrid energy system. To address these challenges, this research presents the design and development of a simulation-based hybrid solar-wind microgrid that supplies a proton exchange membrane (PEM) electrolyser for green hydrogen production.

This work includes a digital twin that is constructed entirely in a virtual environment without the need for a physical prototype. The twin can perform real-time performance assessment, optimization and predict control under varying environmental conditions. The study is structured around four main objectives. First a detailed solar power model was developed on MATLAB/Simulink to evaluate the energy generation profile under different irradiance values. This was followed up by the integration of a wind power subsystem, enabling the system's operation to last longer by complementing the intermittency of solar energy.

In the second stage, the hybrid model was transferred to Python, where advance control and optimization layers were implemented. A particle Swarm Optimization (PSO) was introduced to the system to optimize its operational parameters. A Model Predictive Control (MPC) structure was then integrated to coordinate real-time decision making and ensuring that the energy flow is continuously optimized with respect to predicted weather data. The accurate weather forecasting allows the system to anticipate fluctuations in solar irradiance and wind speed. This coupling aims to enhance both the reliability and efficiency of the system. This study tracks electrolyzer loading, battery state of charge (SoC) and hydrogen output under measured meteorological data. In the final configuration, the PV generation is sized at 1.0 of the electrolyzer's rated power, the wind turbine at 0.53 and the battery has a power limit of 0.40 with an energy capacity of 6.7hours at full electrolyzer load. Over a year-long simulation, the electrolyzer operates continuously with an

annual capacity factor of 0.68 on an LHV basis and an average hydrogen production of 48.7 kg/day. The battery supplies an average of 13% of the electrolyzer's demand with the remainder being covered by the renewables. The electrolyzer's specific consumption is 50kwh/kg of hydrogen.

An important contribution of this work lies in its scalability and adaptability. A fully interactive simulation interface was developed to allow users to modify system sizing, control settings and renewable inputs, making the entire framework reproducible and easily adaptable to new design scenarios or new geographical locations. This flexibility enables comparative analysis of RE powered hydrogen production potential across different climates and geographical regions without the need for extensive model reconfiguration. The framework thus offers a foundation for the future development of location-specific renewable energy planning systems.

Overall, this study provides a complete methodological foundation for simulating an optimized hybrid solar wind with storage powering an electrolyser. The work demonstrates how a simulation-based twin, coupled with accurate weather forecasting, predictive control and optimization algorithms can serve as a precursor to real world implementation. By offering a flexible, scalable and fully virtual platform, this research contributes to bridging the gap between theoretical modeling and practical deployment of intelligent renewable hydrogen microgrids.

TABLE OF CONTENTS

LIST OF TABLES

LIST OF FIGURES

LISTE OF SYMBOLS AND ABBREVIATIONS

BESS: Battery Energy Storage System

CO_2: Carbon Dioxide

D: Duty Cycle

DE: Differential Evolution

DT: Digital Twin

GA: Genetic Algorithms

GHG: Greenhouse Gases

GHI: Global Horizontal Irradiance

HERS: Hybrid Renewable Energy Systems

IEEE: Institute of Electrical and Electronics Engineers

I: Current

IMPC: Intelligent Model Predictive Control

LCOH: Levelized Cost of Hydrogen

MPC: Model Predictive Control

MPPT: Maximum Power Point Tracking

P: Power

P&O: Perturb and Observe

PEM: Proton Exchange Membrane (electrolyzer or fuel cell, depending on context)

PID: Proportional–Integral–Derivative

PSO: Particle Swarm Optimization

PV: Photovoltaic

RE: Renewable Energy

SOC: State of Charge

TEA: Techno-Economic Analysis

V: Voltage

LIST OF APPENDICES

CHAPTER 1 INTRODUCTION

The transition to renewable energy is no longer a distant global goal but rather it has become a necessity. The excessive reliance on fossil fuels in the past decades has led to severe environmental impacts such as climate change along with health issues such as lung diseases, land exploitation and multiple other pressing existential threats [1]. These tragic consequences are attributed to greenhouse gas emissions (GHG) which are the direct result of fossil fuels usage making the energy sector the largest contributor [2]. Recognizing these consequences, countries worldwide have focused on taking action through new policies such as the 2015 Paris Agreement that represented an important global commitment to reduce greenhouse gas emissions and mitigate climate related risks [3]. This agreement has set ambitious goals to limit the global temperature increase to well below 2°C and set a framework for countries that contributed in this with regular progress reporting and gave financial support for developing countries [4]. Following this agreement, several countries have implemented policies to reduce their emissions like the European Union's European Green Deal aiming for carbon neutrality by 2050 , the United States rejoined Paris as well setting a goal of 50-52% emissions reduction by 2030 and Canada pledged to reduce its emissions by 40-50% by 2030 and invest in clean technology and green infrastructure [5] [6] [7]. Provincial climate frameworks in Canada joined the national objectives including British Columbia targeting a 40% emissions reduction by the same deadline [8], Alberta regulating its industrial emissions through its Technology Innovation and Emissions Reduction (TIER) program [9] and finally Quebec's Cap and Trade system linked with California via the Western Climate Initiative covering 80% of the province's GHG emissions [10].

Therefore, the global energy landscape has undergone and continues to undergo a big shift, moving towards cleaner and cost competitive renewable energy sources. Over the past two decades, advances in technology and the growing environmental awareness has accelerated the push towards renewable energy adaptation making an impact in how society consumes and produces energy [11]. Technologies such as solar photovoltaics (PV), wind turbines, hydroelectricity and biomass offer a way to decarbonization and allow access to clean energy in rural regions [12]. These technologies share the common advantage of sustainability, yet they also share the same limitations, their power output is variable and heavily dependent on weather conditions, such as solar irradiance, wind speed and water availability [13]. So ensuring a reliable and steady supply of power poses technical

challenges. This intermittency problem has encouraged the development of new energy architectures that offer flexibility, local generation and intelligent energy management. Instead of relying on large, centralized grids, modern power systems nowadays incorporate distributed resources that are capable of autonomous operations [14]. This shift shows how energy transition is not only about replacing fossil fuels but also about rethinking the structure and control of electrical networks.

In this light, microgrids have emerged as a solution for resilient and low-carbon energy systems. A microgrid can be defined as a localized energy system capable of operating independently (islanded microgrid), or in conjunction with the main grid. This is usually achieved by integrating renewable energy sources with storage systems [15]. The concept of these microgrids have existed for a long time. Dating back to 1882, when Thomas Eddison constructed the "Pearl Street Station" in Manhattan, New York, this concept had not yet been introduced, however today the station meets all criteria that define a microgrid [16]. Subsequently, they have evolved over time from isolated, localized power systems based on diesel generation to smart energy systems capable of integrating renewable energy, storage and automation. They have evolved from being static into dynamic and intelligent energy networks with the development of power electronics and control systems. University campuses, hospitals and remote communities often rely on microgrids to ensure uninterrupted operation and make use of locally available renewable resources [17].

Although they were initially developed for electricity access, their potential applications have expanded to include integration with important energy vectors such as green hydrogen, making them useful to decarbonizing several energy and carbon intensive sectors, including chemicals, metallurgy and transport [18]. Unlike conventional hydrogen, which is produced using fossil fuels, green hydrogen production relies on clean energy sources such as wind and solar. By integrating it with renewable energy powered microgrids, it is possible to create low emissions solutions tailored to the industry's needs.

In this study, we explore the configuration of a renewable energy powered microgrid that is optimized to supply a proton exchange membrane (PEM) electrolyzer, with a long-term vision of enabling sustainable hydrogen integration in industrial systems. However, this implementation is not straightforward as it requires balancing technical, economic and operational constraints. Integrating hydrogen production with intermittent energy sources presses technical challenges

when taking into consideration the sensitivity of the lifespan and efficiency of the electrolyser to the fluctuating input conditions [19]. These challenges range from high capital and storage costs to operational inefficiencies manifested in the ability to ensure a continuous energy supply. Therefore, leveraging hybrid resources such as wind and solar, compensates for energy gaps because their generation profiles are often complementary, allowing the system to operate more efficiently. In contrast to single source configurations, hybrid energy systems are better equipped to address power shortages [20] . By combining the strengths of different technologies, the systems can run for a full day without relying on storage systems therefore reducing overall costs.

The design of this systems requires a careful coordination between the generation profile, the storage available and the load components. Real time control complexities, load mismatches and dynamic weather conditions all together complicate this design and operation process. It is important to achieve a design that focuses on maximizing hydrogen yield while minimizing costs and maintaining a reliable system, which remains an open engineering challenge, particularly in off grid microgrids [21]. These uncertainties highlight the need for an approach that combines dynamic modelling and intelligent control to accurately capture the system's behaviour and improve the decision making. This integrated framework, implemented through MATLAB and Python-based modules forms the methodological foundation for this study.

The conception of the system followed an iterative approach aimed at designing, modelling and optimizing a hybrid solar wind microgrid system capable of powering an electrolyser to produce green hydrogen. The main objective is to allow the electrolyser to behave as a smart unit by enhancing its operational efficiency and autonomy. This is possible through integrating intelligent algorithms that enable it to manage its energy input dynamically depending on the available detailed solar and wind data and minimize reliance on the battery storage.

The project was originally simulated using MATLAB to develop a baseline simulation of the microgrid and evaluate its operational behaviour and storage dependency. As the study evolved, the modelling environment was transitioned to Python to allow for a greater flexibility. Python has increasingly become the preferred platform for scientific computing and energy system modelling because of its extensive libraries and big environment [22]. This migration enabled the development of a more adaptive and manageable model.

The research was structured in three sequential phases, each one building on the previous phase. The first one involved simulating a solar microgrid with energy storage to analyze the system's reliability and identify performance bottlenecks. The second phase introduced wind energy to form a hybrid configuration, addressing the limitations of solar only generation and reducing the reliance on costly storage solutions. The final phase focused on embedding control and optimization algorithms, allowing for autonomous management of power flow and improved use of renewable energy.

This incremental phase by phase process reflects an iterative hybrid system modelling philosophy, in which complex projects are explored gradually to be able to locate the influence of each design decision and better analyze the behaviour of the system under each step. By adapting this layer-by-layer method, the study achieved a clearer understanding of the relation between generation, storage and hydrogen production while validating the performance of each subsystem along the way. This methodological progression mirrors real world deployment practices, where microgrids are developed through upgrades rather than a full package integration due to technical, financial and logistical constraints.

The scope of this study is intentionally limited to the direct electrification of the electrolyser using a hybrid energy source. Downstream processes such as hydrogen storage, compression and furthermore were excluded from this work to maintain focus on the energy conversion and control aspects. While large scale hydrogen deployment is a long-term objective for decarbonization, this study focuses exclusively on its production.

Moreover, this study established a fundamental framework that can be adapted and scaled to diverse industrial and regional contexts through scalable sizing options and accessible weather conditions files that could be adapted to different regions and seasons.

Similarly, although economic aspects are briefly discussed for comparative purposes, this study does not include a full techno-economic assessment (TEA) or a life cycle evaluation. The exclusion of a detailed economic model is intentional as the research is primarily focused on the technical design, control and optimization of the hybrid microgrid rather than on its financial feasibility. Economic considerations were nevertheless factored into certain design decisions hence the inclusion of a wind energy source to mitigate dependence on battery storage, whose cost remains one of the most significant barriers to large scale systems. However, a comprehensive TEA would

require a dedicated analysis encompassing levelized costs of hydrogen, maintenance schedules and other variables. Such an assessment would need a complex financial model that extends beyond the framework of this project. Moreover, the costs of photovoltaic modules, wind turbines and battery systems continue to evolve rapidly therefore limiting the robustness and generalizability of any economic conclusions drawn at this stage [23].

The rest of the thesis is structured as follows; The first chapter provides a review of the relevant literature on renewable powered microgrids, sustainable hydrogen production approaches and existing control strategies for system control. The next chapter discusses the methodology followed to carry out this research, including the simulation environment, components, control logic and performance metrics. The article chapter presents the article that was submitted to IEEE transactions on sustainable energy. The results chapter presents the three-phase modelling approach, solar only configuration, adaptation of a hybrid system and optimization. The next chapter discusses the key findings, identifies the technical implications and highlights to possible limitations. Finally, the last chapter concludes the work with a summary of the contributions and recommendations for future research.

CHAPTER 2 LITERATURE REVIEW

The objective of this section is to examine the state of research on renewable powered electrolyzer systems, emphasizing hybrid solar wind microgrid configurations, energy management techniques, and intelligent control algorithms, to establish the technical foundation and research gap that motivate this work.

2.1 Overview Of Renewable-Powered Hydrogen Systems

The rapid global transition towards low-carbon energy systems has intensified research on renewable energy integration and energy conversion technologies. As countries commit to net-zero emissions targets, renewable energy sources such as solar and wind have become central to decarbonization strategies across multiple sectors due to their scalability, cost reduction [24]. However, there variability and dependence on environmental conditions pose significant challenges for continuous and reliable power supply, particularly for energy intensive processes that require stable operation.

One such process is water electrolysis, which enables the production of hydrogen through splitting of water molecules using electricity. In recent years research has increasingly focused on electrifying electrolysers directly through renewable energy systems, aiming to create cleaner and more efficient hydrogen production pathways [25]. Rather than relying on surplus or grid-stabilizing power, this approach seeks to design hybrid renewable microgrids that can operate autonomously while ensuring steady and optimized power delivery to the electrolyzer.

Advancements in hybrid system modelling, power electronics and research on control algorithms have made it easier to dynamically coordinate between generation, storage and load components in such systems [26]. Understanding how these renewable-powered electrolyzer systems are modelled and controlled is important to improve their efficiency, durability and economic feasibility. Some renewable powered electrolyzer systems operate through direct coupling; others incorporate intermediate storage to buffer variability and stabilize power delivery [27]. In this work, the latter configuration is adopted as illustrated in *Figure 2.1*.

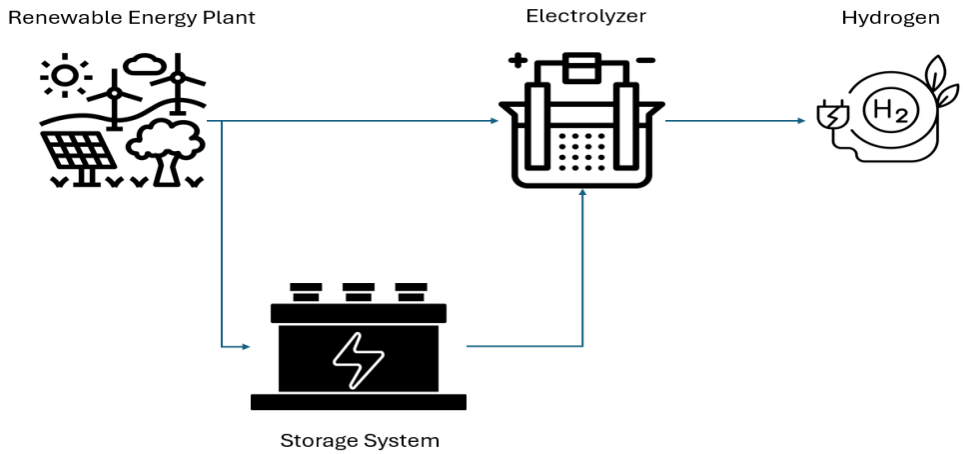

Figure 2.1: Schematic representation of the proposed model.

The following sections review the current state of research in this field, focusing on the systemic role of green powered electrolysis, the operational challenges of hybrid microgrids, and the control strategies developed to manage intermittency and optimize hydrogen production.

2.2 The Systemic Role of Renewable Powered Electrolysis

Green hydrogen is identified as an important tool for decarbonizing hard to electrify sectors such as aviation, shipping and heavy industries worldwide due to their intense energy consumption [28]. Hydrogen is increasingly recognized as a versatile energy carrier that can complement direct electrification and provide long term energy storage solutions. At present, approximately 96% of global hydrogen production is derived from fossil fuels through processes such as steam methane reforming, resulting in significant CO2 emissions, according to one study in 2025, global hydrogen production remains heavily dominated by fossil fuels, with natural gas and coal accounting for most of the output. Figure 2.2 illustrates this distribution, highlighting the limited share of hydrogen currently produced from renewable or by-product sources [29].

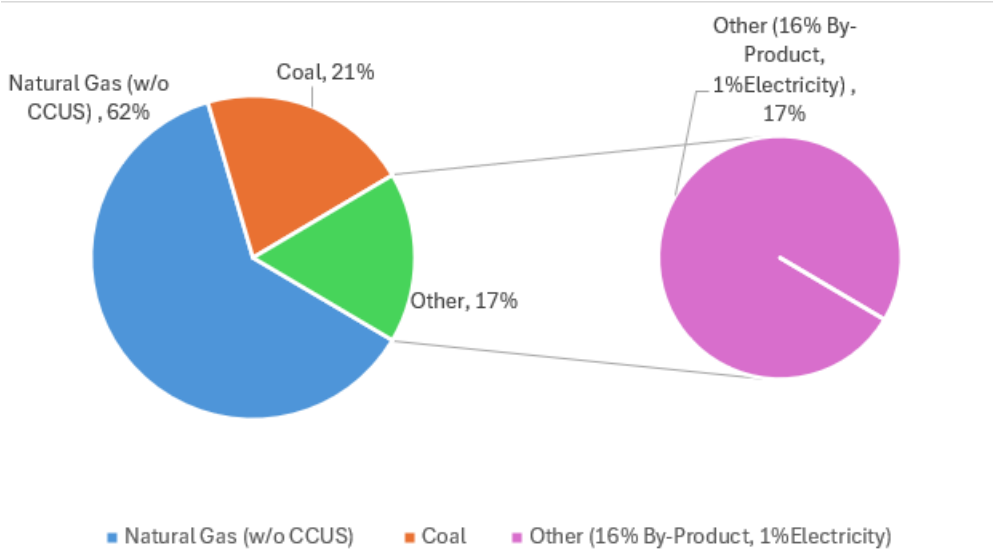

Figure 2.2: Global Hydrogen Production from different sources

Accelerated clean energy policies and decarbonization initiatives are expected to boost the global hydrogen market, which was estimated to be worth USD 130 billion in 2020 to become a multitrillion dollar industry by 2030 [30]. In this light, integrating PEM electrolysers with green sources is important to reach the 350 GW of installed electrolyser capacity target set by the International Renewable Energy Agency (IRENA) by 2030 [31]. In addition to facilitating the direct production of green hydrogen, renewable-powered electrolysis also makes grid balancing and large-scale energy storage possible. This integration is significant because it combines the gas, electricity and the industrial sectors into a single adaptable network that offers significant carbon reduction potential in addition to energy security [32].

2.3 Dynamic Operation Challenges

Because of their high current density performance, broad operating range (0-160% of nominal capacity) and quick startup time (less than one second), PEM electrolysers are frequently chosen for renewable integration [33]. These features makes them able to optimize the use of fluctuating energy sources by closely monitoring the variations. Dynamic operation, however, presents performance and control issues with varying inputs that have direct impact on the system's overall stability and efficiency. Regular power variations change the electrolyser's operating voltage and current density, which affects its immediate efficiency and hydrogen production [34]. Therefore,

system optimization requires precise dynamic modelling. Neglecting this power variability can result in a significant overestimation of hydrogen production with reported errors ranging from 5% to 24% according to one study named "Ignore variability, overestimate hydrogen production" [35]. According to their dynamic model, the sum of the components related to loss and reversibility represents the total cell voltage V_{cell} (Equation 2.1), to better understand and quantify how these losses collectively influence the overall performance of the electrolyzer:

$$V_{cell}=E_{rev}+V_{act}+V_{ohm}+V_{conc} \quad (2.1)$$

Where V_{cell} is the total cell voltage, E_{rev} is the reversible thermodynamic voltage (Nernst Potential), V_{act} is the activation overpotential due to electrochemical reaction kinetics, V_{ohm} is the ohmic voltage drop resulting from ionic and electronic resistance and V_{conc} is the concentration overpotential related to mass-transport limitations, all in voltage.

According to the Tafel equation (Equation 2.2) , the activation overpotential dominates under high current operation and grows logarithmically with current density.

$$Vact = \frac{RT}{\propto F} l\,n \frac{i}{i0} \quad (2.2)$$

Where R is the universal gas constant, T is the absolute temperature in Kelvin, $\propto$ is the charge transfer coefficient typically 0.5-1.0, F is the Faraday constant, i is the applied current density and i_0 is the exchange current density both in (A cm^{-2}).

Unwanted gas crossover and parasitic currents cause Faraday efficiency to decrease at very low current densities, as shown empirically in (Equation 2.3) [9]:

$$\eta_F = 1 - k\left(\frac{1}{i}\right) \quad (2.3)$$

Where k is the empirical gas-crossover coefficient (typically 1-5 mA cm^{-2}) and i is the applied current density (A cm^{-2}).

The overall stack efficiency (Equation 2.4), a valuable metric in system optimization, is obtained by combining voltage and Faraday efficiency:

$$\eta_{stack} = \frac{E_{rev}}{V_{cell}} \eta_F \tag{2.4}$$

Where η_{stack} is the overall stack energy efficiency, performance-oriented optimization models are based on these simplified relationships. They offer a framework for defining objective functions in optimization algorithms that aim to minimize losses or maximize hydrogen production under fluctuating renewable supply by directly connecting efficiency and hydrogen yield to operating current [36].

These models allow optimization techniques to dynamically modify the electrolyzer input in renewable-powered systems, where power availability fluctuates constantly, in order to maintain near-optimal efficiency. Therefore, the goal of this work and current research is to develop optimization and control strategies that maintain efficient operation and decrease the impact of variability on hydrogen production, rather than focusing on material degradation.

2.4 Integration with Hybrid Renewable Energy

As was previously mentioned, the potential for continuous and low-emission hydrogen production has made the integration of renewable energy systems with PEM electrolysers a key area of study for green hydrogen. Numerous hybrid and poly-generation configurations have been studied recently in an effort to improve the system's energy utilization and solve the intermittency issues that come with green energy. In order to provide a steady and affordable supply of electricity, hybrid renewable energy systems (HERS) usually combine two or more renewable sources, most commonly solar photovoltaic (PV), wind, geothermal, biomass or hydroelectricity, couple with energy storage systems in some cases [37].

According to a thorough analysis paper done on the hybridization concept for microgrids [38], multi-source hybridization continuously performs better than single-source systems in terms of sustainability and efficiency. Combining renewable sources enables the simultaneous production of heat, electricity, hydrogen and other energy vectors, sometimes reaching overall efficiencies of

over 60%, according to their comparative study of 21 poly-generation configurations [39]. Solar parabolic and solar biomass systems performed reasonably well among the configurations examined, but they were limited in their scalability, required complicated thermal management and they were dependent on the availability of local resources which was not optimal. Geothermal-solar hybrids have also been demonstrated to improve heating and desalination applications, but they are still considered capital intensive and geographically limited making them not adaptable to certain locations [40]. Regardless of the time of day or the weather, biomass-based systems offered reliable power that could continuously produce electricity but were less sustainable due to feedstock logistics and carbon emissions [41].

On the other hand, solar-wind hybrid systems have consistently shown the best balance between efficiency, scalability and resource availability. A more reliable energy source is made possible by the complementary relationship between the solar profile and the unpredictable yet nocturnal wind resource. PV-Wind systems outperformed standalone solar or wind configurations in this dataset, achieving energy efficiencies ranging from 55% to 77% [42]. These outcomes are consistent with another study that reported significant savings in levelized hydrogen costs when compared to single source systems after optimizing a PV-Wind hybrid plant at Kuwait's Shagaya Renewable Energy Power Park [43]. The ability of this coupling to reduce battery cycling depth, smooth short-term fluctuations and prolong the electrolyser's operating life is one of its major benefits.

Complementary energy generation is made possible through this integration, while wind tends to peak in the evening, at night or during seasons where there is less solar availability, solar irradiance provides consistent power during the day [44]. This feature reduces the need for storage system backup most of the time. Additionally, merging them would enable a shared power conditioning infrastructure, usually compromising pitch-controlled wind turbines, maximum power point tracking (MPPT) controllers for PV arrays and other control strategies to guarantee smoother PEM stack operation, reduce transient stress and extend the system's lifetime [45].

Their advantage is further demonstrated by empirical analysis. According to a study carried out in 2020 , they used TRNSYS to simulate a PV-Wind electrolysis system, hydrogen production reached 6500 NM^3 per year with PV contributing 310 MWh and wind 75MWh, resulting in an energy efficiency improvement of more than 11% when compared to a PV-only setup [46]. This hybrid configuration showed a low life cycle cost and a high renewable fraction among all tested

systems, according to another study centred on the optimization of a solar wind multigeneration system for electricity desalination and hydrogen production [47]. Solar-Wind systems not only perform better but are also more flexible for off-grid and decentralized microgrid applications, where grid backup is not available.

This conclusion forms the rationale for adopting the solar wind combination used in the present study, which seeks to design, model and optimize a hybrid renewable microgrid supplying a PEM electrolyzer for sustainable hydrogen generation.

2.5 Optimization and Smart Control of Renewable Powered Electrolyzers

These systems must constantly deal with fast and unpredictable power swings while the electrolyser itself reacts much more slowly because of its thermal and pressure dynamics. Therefore, these two timescales rarely align, and when the control strategy cannot manage the gap, the result is efficiency losses and unstable hydrogen production in the long run coupled with faster component degradation [48]. Even though research in this field has advanced quickly, most existing control methods struggle still to keep performance stable during significant fluctuations.

A study that has reviewed the main control strategies used in electrolysers and found that classical proportional-integral-derivative (PID) controllers are still the standard in most applications. They work reasonably well in steady state operation but start to show limits when the system is exposed to sudden change [49]. The study also noted that while more advanced methods like MPC or fuzzy logic can change the multiple variables at once and respect system constraints, they are not widely used yet. The main reasons for this are the added complexity and high computational demand. In practice, many controls are still tuned manually and statically, meaning they perform well only under conditions that are like those they were tuned for [50].

The issue becomes clearer when looking at how control systems behave under real renewable generation profiles. One paper discussed this challenge in the context of integrating photovoltaics to electrify an electrolyser, they pointed out that while electrical inputs from solar panels can change almost instantly, the electrolyser's parameters take longer to respond. As a consequence, many controllers either overshoot or undershoot their setpoints, leading to efficiency drops of up to 5% [51]. A more recent study showed how predictive control can help mitigate these problems, they have tested a nonlinear model predictive controller (NMPC) on an alkaline electrolyser and compared three approaches: a basic PID, a reactive NMPC using only current power data and an

anticipatory NMPC that incorporated four hours renewable forecasts. This showed how the predictive version achieved a modest but meaningful 1.58% increase in hydrogen production by adjusting operation in advance to power changes [52]. The other two controllers remained slower to react, illustrating how forecast can noticeably improve both efficiency and stability.

Furthermore, another study examined the issues faced by PEM electrolysers when coupled directly with intermittent energy sources. Using a 1MW PEM pilot plant connected to a 20LW solar farm in Hungary, the authors combined a techno-economic modelling with practical insights to evaluate how variable photovoltaic power affects electrolyser performance. Their analysis revealed that while dynamic operation enables flexibility and better utilization of renewable energy, it also introduces significant stresses across thermal and electrochemical domains [53]. The study claimed that the start-stop cycles were the main reason for degradation, noting that residual gases in the electrodes can trigger reverse, fuel-cell-like reactions that corrode catalyst layers.

The same study also highlighted several operational weaknesses that current systems and control strategies fail to address, under varying renewable input, the electrolyser experiences temperature drifts, pressure imbalances and product contamination, all of which are linked directly the decrease of hydrogen purity and accelerate the degradation process. Although this study offered good insight on the degradation aspect, the work did not quantify the impact of dynamic operation on long-term performance or suggest active control strategies to minimize these effects. In the end, the paper highlights a significant gap in the existing literature stating that most PEM systems are still made for quasi-steady operation, and not much is explored about how control or operational strategies might be modified to deal with the actual variability of RE power inputs.

In another study, the authors designed several control and power-sharing strategies for a group of PEM electrolysers operating under fluctuating wind conditions. Their goal was to limit the negative impact of renewable variability on individual stacks. By testing different load-balancing and equal-distribution methods through simulation, they found that hydrogen production increased by about 6% when power was allocated evenly and coordinated across the units. This outcome is significant because it highlights how smarter power management can mitigate uneven loading and reduce long-term degradation in dynamic renewable systems, however they state that the electrolyzer's utilization is only 20.2% [54]. Despite this advancement, the control strategy still uses predetermined logic to switch and balance the power among units and is ruled-based rather than

optimization-driven. Since the model lacks a forecasting or predictive element, it only responds to changes after they happen rather than regulating itself to the change. This reactive nature limits the system's ability to optimize efficiency and limits its ability to manage abrupt drops in the power input. Therefore, even though the study offers a significant and useful step to reducing the operational stress, it does not fully illustrate a truly adaptive control framework that supports a continuous hydrogen production and prevents system shutdown for long periods.

This gap opens the way for a more integrated framework combining system level optimization with dynamic, forecast based control to try and increase the system's efficiency or the electrolyzer's utilization top up to 50%-60% . The next section explores how metaheuristic optimization techniques have been applied to renewable powered systems and how their strengths can complement predictive control models to form a smarter and a more adaptive energy management strategy.

2.5.1 Metaheuristic Optimization Methods in Literature

Metaheuristic Optimization is a broad set of search methods created to solve complex problems that would not be solved following traditional mathematical approaches. Instead of relying on predefined equations , these methods follow a random structure meaning they explore many possible solutions throughout the time period and learn which directions lead to better results making them a well-suited approach for problems that are not linear or filled with uncertainty, which is often the case in real engineering systems. Unlike classical methods, these do not require a perfectly defined model, yet they still perform well even with incomplete or scattered data [55].

Among the most common algorithms we find Particle Swarm Optimization (PSO), Genetic Algorithms (GA) and Differential Evolution (DE). PSO was inspired by how birds flock or fish swim together, random in nature but each "particle" in this case is adjusting its position based on its experience and what others around it have learned, creating a synchronized environment out of randomness [56]. This mix of individual learning and collective sharing helps the swarm gradually find good solutions without getting stuck too early. GA, however, take a different more organized approach, imitating the process of biological evolution. They develop a population of potential solutions over many generations through approaches like how nature works, selection, crossover and mutation [57]. DE is simpler but still delivers promising results, it works by combining and

adjusting candidate solutions through random differences which helps it converge quickly and adapt to varying situations.

In renewable and hybrid energy systems, they have become more common because they usually involve competing goals such as trying to minimize cost while also maximize efficiency. While traditional methods often struggle to deliver a good output with these systems since they involve non-linear behaviour and variable inputs, metaheuristic methods can handle these challenges by searching large and irregular solution spaces without neglecting the physical or economic aspects. Several studies have pointed out the strengths of these algorithms, one noted that they have a strong global search ability which makes them more reliable, the authors discussed how swarm-based and evolutionary techniques tend to stay stable even when the input fluctuates [58]. Another paper emphasized how flexible and adaptable these algorithms can be especially in multi-objective solutions, unlike conventional methods that may struggle with conflicting objectives, metaheuristic strategies can simultaneously consider multiple criteria and generate a set of adaptable solutions. This fits real world scenarios where decision makers must balance competing goals [59].

Table 2.1: Key Characteristics of Traditional and Metaheuristic Optimization Methods Reported in the Literature

Aspect	Metaheuristic Algorithms	Traditional Methods
Search Space Flexibility	Can handle non-linear, non-differentiable, multi-modal problems and noisy/unstructured search spaces [60].	Often require convexity or explicit analytical models and struggle with highly irregular environments [63], [66].
Assumptions and Model Requirements	Fewer assumptions and less need for full model specifications [60].	Require exact mathematical formulation and continuous objective functions [63].

Computational Cost and Convergence Speed	Require many function evaluations, can be slower in convergence and parameter tuning can be complex [61].	For well-behaved problems they converge quickly and the computational cost is predictable [64].
Scalability	More scalable for systems with mixed discrete, continuous decision variables. [60].	Modelling becomes complex when the system enlarges, or many discrete variables exist [65].
Solution guarantee/Optimality	No guarantee of finding true global optimum, results vary between runs. [62].	Optimality well defined especially in linear programming [64]
Applicability in hybrid/renewable systems	Useful for varying conditions and complex models. [61], [62].	Requires simplifying assumptions and needs a well defined subsystem [66]

As summarized in Table2.1, metaheuristic algorithms have advantages over traditional optimization techniques, however despite their robustness, they still rely on static parameter settings. Once initialized, their internal search behaviour does not automatically adapt to rapid environment change. As a result, they can gradually lose efficiency when there is a major shift in input conditions over time, where he electrolyzer's capacity factor or utilization of energy becomes low [67].

To address this, the present works proposed a hybrid intelligent control framework that integrates the benefits of metaheuristic algorithms (specifically PSO) with Predictive Model Control (MPC) so that the model could adjust its operating strategy according to forecasted solar and wind variations.

Particle Swarm Optimization: Principles and Applications:

Before introducing the specific working principle of PSO, it is important to understand the general structure of most metaheuristic algorithms. Regardless of their different roles and variables, they all share a common iterative logic starting with a sum of candidate solutions, evaluate each one using a defined objective function then progressively improve this sum otherwise called as "Population" through adaptive rules until a termination condition is reached [68]. A technical report conducted by multiple universities states that these generic algorithms can be summarized in five main stages:

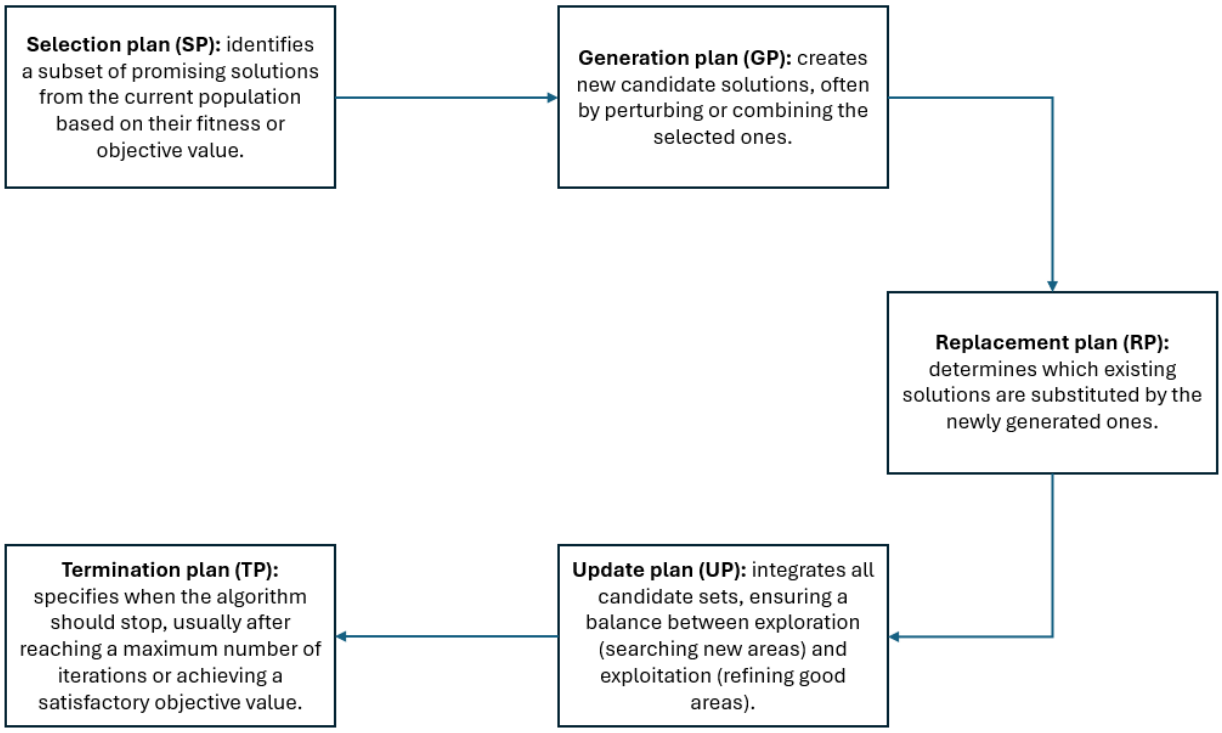

Figure 2.3: Main stages of a generic metaheuristic framework [68].

So the algorithm begins by randomly initializing a population of N solutions within the problem's search space. Each particle of this population, St, represents a potential solution vector that should satisfy the system's constraints. Their performance is evaluated using an objective function, f(x), which quantifies the quality of the solution so basically it is rating the solution in terms of suitability to the problem. However, not every candidate solution is feasible, to handle this, a constraint violation (CV) function is introduced as a measure to see how much a solution violates the problems limits [36]:

$$CV(\boldsymbol{x/p}) = \sum_{j=1}^{J} \langle g_j(\boldsymbol{x/p}) \rangle \tag{2.5}$$

Where $g_j(x/p)$ represents the j^{th} constraint function, and the operator $\langle \propto \rangle$ takes the value of $|\propto|$ if $\propto < 0$ and 0 if otherwise.

This means that $CV(\mathbf{x/p})$ is equal to zero for feasible solutions and positive for infeasible ones, with higher values meaning there are greater constraint violations.

The evaluation phase is carried out by combining the objective function f(x) and the constraint violation function CV to determine the performance of each candidate. The common comparison strategy between the two solutions A and B is defined as follows according to the authors:

- **If both A and B are feasible choose the one with the smaller f value.**
- **If one is feasible and the other is not, choose the feasible one.**
- **If both are not feasible then choose the one with the smaller CV value.**

Through this process, the algorithm continuously refines its population by selecting better solutions, producing new candidates and ignoring poor ones. Then step 6 to 12 in this framework are repeating iteratively until the termination plan is satisfied. At the end the best performance solution x_j^* is taken as the nearest optimal result [68].

For PSO, in the algorithm, each particle represents one possible solution and moves through the search space with a specific position and velocity. In the report they state that during each iteration, the particle updates its movement by considering two reference points: the best position it has personally reached defined as (P_{best}) and the best position found by the entire group (G_{best}). At every iteration, the velocity of the particle is influenced by three main points: The first is the inertia term, which allows the particle to maintain some of its previous motion, allowing the swarm to explore new regions instead of immediately converging. The second is P_{best} and the third is G_{best} [36]. These effects are controlled by specific parameters which are the inertia weight (W) and the acceleration coefficients (C_1 and C_2). The acceleration coefficients define how strongly a particle is influenced by its own memory (C_1) and by the group knowledge also defined as the collective knowledge (C_2). By using these mechanisms, every particle adjusts its direction and step size, maintaining a balance between exploring new areas and improving already discovered efficient areas. When the maximum number of iterations is reached, this iteration comes to an end.

2.5.2 Model Predictive Control: Principles and Applications:

MPC has gained attention in the field of renewable energy systems due its ability to deal with dynamic environments and help with the optimization of the system. It works by predicting future states and adjusting control actions in real time to minimize or maximize the intended function which is heavily affected by the gap between predicted values and actual system behaviour. In the context of hybrid energy systems, the MPC algorithm can minimize the error between predicted and reference voltages. A study explains its mechanism through three parts: one for the PV boost converter, another for the generation side current control and the third is for grid side inverter control in cases of grid connected systems [69]. This multi layered structure allows the systems a fast transient response and ensures steady-state performance which is a must in managing fluctuating input. They state that this method provides robustness against parameter variations and strengthens the system against sudden variabilities which makes it suitable for real world applications where environmental conditions constantly change.

In a different but related study, they used Intelligent Model Predictive Control (IMPC) in combination with neural network to explore how to manage a hybrid energy powered system along with battery energy storage system (BESS). This integration showed high accuracy predictions, the IMPC reduced the peak battery state of charge (SoC) by 26.7% for solar and by 7.3% for wind [70]. This predictive control is important for managing battery life and reduce the need for large scale energy storage systems which as discussed before could be expensive.

This algorithm is performed using this objective function [39]:

$$J = \sum_{t=1}^{N} \left(|P_{\text{target}}(t) - P_{\text{actual}}(t)|^2 + \lambda |\text{SoC}(t) - \text{SoC}_{\text{target}}(t)|^2 \right) \tag{2.6}$$

Where $P_{\text{target}}(t)$ is the predicted power at time t and $P_{\text{actual}}(t)$ is for the actual power, then $\text{SoC}(t)$ and $\text{SoC}_{\text{target}}(t)$ are respectively for the battery state of charge at time t and the target of SoC, λ is the weight factor and N is the prediction horizon, it determines the importance of the two terms in the function, a higher value means we should give attention to controlling the battery SoC while a lower value means we focus on matching the power generation to the target. The squared terms in the objective function are introduced to penalize large deviations more severely while

ensuring a smooth and differentiable cost function suitable for optimization. This quadratic formulation prevents positive and negative errors from canceling out and provides a stable gradient for model predictive control. The first part of the equation is the Power Tracking element which gives us an idea about how far the actual power is from the desired power, the function works to minimize this mismatch so the lower the error the better the system is at maintaining a stable power supply despite fluctuations. The second part is for the battery SoC control, it ensures that the battery stays within an optimal charge range avoiding overcharging or undercharging.

In solar-wind hybrid systems, the MPC algorithm works by continuously predicting how much power will be generated from the sources over a time horizon and adjusts the battery's charging or discharging behaviour and the final output. By doing so, the power from solar and wind is maximized and delivered smoothly without causing power surges or dips, the battery storage is used efficiently to maintain a good battery life and the overall energy balance is maintained [71].

However, inadequate or inaccurate meteorological data in these systems can lead to poor modeling outcomes such as low energy yield or bad storage management, a study demonstrated that incorporating detailed atmospheric characteristics into forecasting models enhance the accuracy of the energy prediction [72]. Data such as solar irradiance, wind speed and temperature are crucial for a precise forecast as it allows for more effective optimization.

2.5.3 Digital Twin: Principles and Applications

The concept of Digital Twin (DT) first appeared in aerospace engineering; NASA used it 2002 to simulate and monitor spacecraft performance remotely. To do that they created a digital copy of the system that can be tested under different operating conditions without risking the real equipment [73]. Over the last decade, the idea integrated itself in other engineering fields, including power systems and renewable energy. The strength of the DT in energy systems is that can combine simulation models with real-time or simulated data to understand, predict and improve the overall system behaviour. It can be described a virtual representation of a physical energy asset or process that continuously receives data to update its internal state and predict future performance [74].

One review describes how DTs in renewable energy systems are not viewed as complete lifecycle tools, covering the design, the operation and the maintenance phases of energy assets. During the design phase, it allows engineers to test different configurations visually before any physical

components are built. This virtual prototyping reduces design costs and the development time [75]. This study found that early-stage simulation avoided more than 15% of potential design efficiencies later discovered in the field. The same paper pointed out that during maintenance, DT's become valuable predictive tools. The DT can "predict" potential faults before they occur through analysing changes in the system's operating variables such as vibration amplitude in a wind turbine or voltage drift in batteries. The authors cited that they can reduce downtime by 25% and increase yearly energy yield by 10-20%.

A more recent study explores their application in smart grids and hybrid renewable systems. The authors highlight that DTs can integrate data from multiple sources, solar panels, wind turbines and energy storage systems to create a unified view of the entire microgrid. They state that they can simulate the combined power output of a hybrid solar wind system using the standard aerodynamic equations [76]. They also emphasize that DTs can also manage the energy storage systems as it is able to track the state of charge SoC and state of health SoH to control charging and discharging operations more efficiently.

This layered approach makes them adaptable to different scales however they warn that these systems rely heavily on data availability and standardization. Differences in data quality, measurement frequency and communication style could cause issues.

More recent research has examined the digital twin concept that exist only in virtual environments, operating without a direct connection to a physical element. This approach is often called "Simulation-based" or "Conceptual" DT, it has become important in the development and validation of renewable energy systems [77]. These twins replicate the structure, parameters and operating logic of real-world systems using historical data to trigger sensor feedback.

In 2023, a study stated that these simulation-driven DTs serve as a foundation for the digitalization of renewable systems, enabling model validation, scenario analysis and control design before field implementation [78]. Their review highlights that many early-stage applications in renewable energy systems are carried out without physical elements, since virtual prototyping and predictive modelling can capture the same operational dynamics through numerical simulations. In these cases, the DT acts as a virtual laboratory that mirrors expected physical behaviour using deterministic or data-driven models.

Another paper classifies these systems as model driven DTs, where the fidelity of the simulation replaces real world sensing. Their review of smart energy systems explains that many current DT architectures are designed without an existing physical twin, in these studies, it behaves as an experimental platform for testing control logic, forecasting algorithms and optimization strategies and overall assessing the efficiency of the system at each iteration [79]. One author explains that the absence of a physical twin does not diminish the twin's analytical value, on the contrary, it allows researchers to conduct parametric studies and stress tests across diverse operational conditions, something that is infeasible in real world systems. To prove this, the author examined a simulation-based twin of a distributed energy network that was developed to study the fault propagation and voltage recovery, the results showed that the virtual model accurately reflected expected field responses [80].

2.6 Research Gap

The reviewed literature on renewable-powered electrolyser systems mainly focuses on optimizing the energy flow between the renewable sources, the energy storage systems and the electrolyser unit through either traditional control or energy management techniques such as the PI control or Fuzzy logic control etc. Most existing models in literature use steady-state or quasi-dynamic assumptions, simplifying the behaviour in-between the electrolyser and the renewable energy sources. This results in incomplete understanding of how system performance really evolves under fluctuating weather conditions or load disturbances. In several studies, the operational behaviour of the electrolyser is treated as a static component, neglecting the thermal dynamics. Furthermore, the majority of these models isolate control development from the physical behaviour of the RE systems leading to an underestimated representation of hybrid operations. This pushes the need for a more integrated framework that takes into consideration all of the system's characteristics to better simulate the operational conditions.

Secondly, while the digital twin technology has emerged as a promising approach for modelling and optimization, its applications in such systems are still understudied. Most of the existing research focuses on systems with direct physical connectivity, where the "twin" continuously receives real-time data from sensors. Far fewer studies investigate simulation only DTs, which

exist entirely in a virtual environment. Recent reviews emphasize that these conceptual twins are a great to understand the system before any hardware investment [81],[82]. However, even in these studies, the integration of accurate weather forecasting with predictive control remains under-developed. MPC control, despite it being well-established for optimizing multi-variable systems, is rarely combined with dynamic weather forecasting in virtual environments.

Finally, the literature also shows a methodological gap for linking optimization algorithms with DT based energy management. While metaheuristic algorithms such as PSO and GA have been applied successfully showing promising results, they are often implemented as isolated modules rather than as adaptive, feedback-driven layers within a DT. The capacity factors stated in literature remain below 50% in most cases, the few cases where it reaches values from 50%-80% are when there is excess energy generation (large sizing of renewable energy sources) which not only is it not economically beneficial but also curtailed energy values increase without a backup plan to utilize it. They also mention large energy storage systems to increase the utilization values, but this also circles back to the economic feasibility of the study. There is therefore a clear need for a comprehensive methodological framework that merges these three layers, forecasting control and optimization into one digital structure capable of handling dynamic conditions, improving the electrolyzer’s capacity factor without large investment in RE sources or BESS.

CHAPTER 3 METHODOLOGY

3.1 Overview of the Approach

The methodology adopted in this research follows a structured, multi-layered process aimed at developing and optimizing a hybrid solar-wind energy system to electrify an electrolyser for green hydrogen production. The project begins with creating a basic model of a solar powered only electrolyser and battery storage system, then progressively expands by adding a wind energy source then by integrating advanced optimization techniques. The final step introduces weather forecasting data, an MPC layer with the PSO algorithm and a DT model to optimize the entire system's performance.

3.2 Project Phases

This project can be divided into the following key steps:

1. Solar energy simulation: Initial simulation of a solar energy generation system using Matlab/Simulink to electrify an electrolyser model and include battery storage.
2. Wind Energy Integration: Incorporating wind energy into the system to make it a hybrid energy system, expanding the model to handle both solar and wind energy outputs and adding control algorithms.
3. Python Transition: Transfer of the model to Python, integration of accurate weather forecast data and implementation of the PSO algorithm.
4. Optimization with PSO and DT to create a Smart Electrolyser: Simulating a real-time operation and predictive maintenance then allowing the system to be scalable and adaptable.

3.3 Research Goals

This research seeks to:

- Develop an autonomous and scalable hybrid renewable energy system: through combining solar and wind power, the goal here is to create a self-sustaining system capable of efficiently powering an electrolyser for hydrogen production. The system in the end should be adaptable and scalable for different applications and locations.

- Optimize system performance for hydrogen production: Using advanced optimization techniques found in literature, this work tested out the coupling of different optimization methods to enhance the energy efficiency and improve the hydrogen production rates.
- Create a smart electrolyser system: This works aims to develop a smart electrolyser that not only integrates renewable energy sources efficiently overcoming the intermittency challenges but also adapts to changing conditions, allowing for an autonomous operation.

3.4 System Architecture and Design

In this section, we will explore the design and overall architecture of the systems created, these diagrams will give a clear visual representation of the key components of each system and their relationship. These visuals are important to understand how the system was built to help achieve the objectives.

1. **Solar Green Hydrogen Microgrid:**

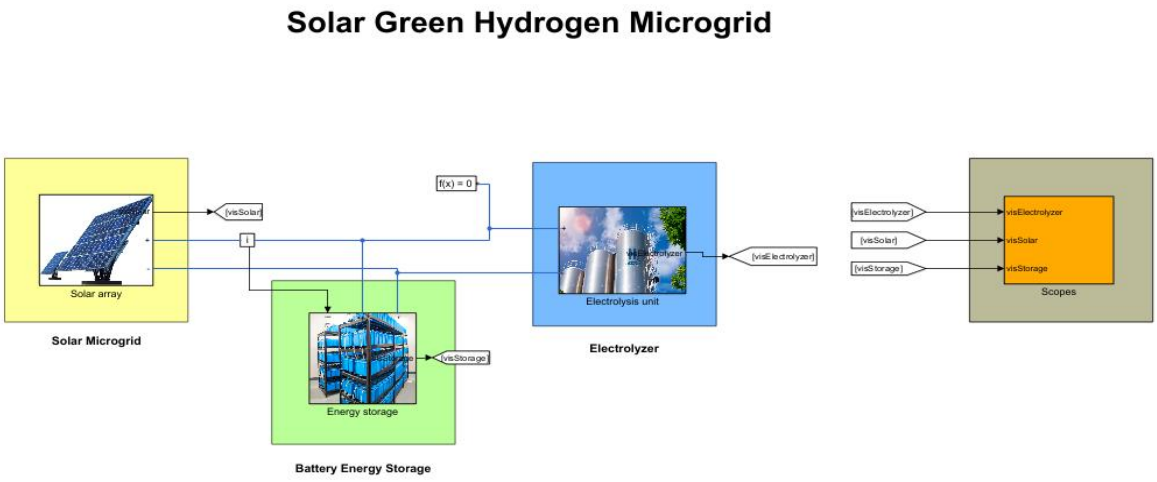

Figure 3.4: Matlab/Simulink model of the solar green hydrogen microgrid

This diagram depicts the integration of solar power, battery storage and the electrolyser system. It shows how solar energy is harnessed, stored and used to produce hydrogen through electrolysis. This serves as a foundational illustration of the system's key components. Later in the methodology, we will highlight the roles of each element and the methods used to simulate them.

2. Solar and Wind Green Hydrogen Microgrid:

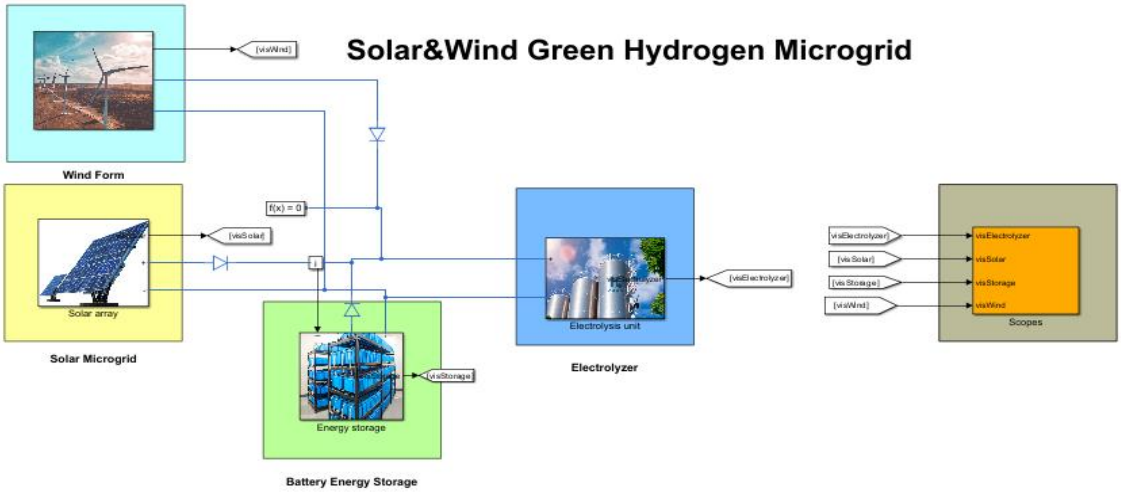

Figure 3.5: Matlab/Simulink model of the solar and wind green hydrogen microgrid

As the Figure3.5 shows, this model expands on the first by introducing wind energy into the renewable energy source. It shows how both the solar and the wind are integrated into the system providing a complementary and diverse energy supply. This setup was built to help manage fluctuations in energy production and reduce reliance on the storage system.

3. Python Model of Solar and Wind Microgrid

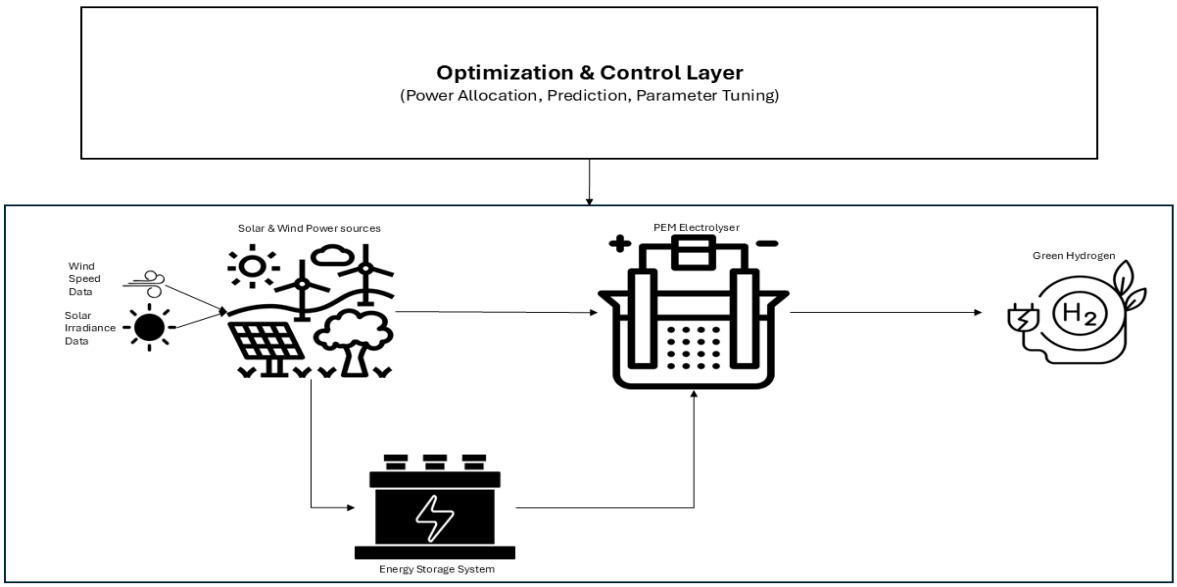

Figure 3.6: Python model of the solar and wind green hydrogen microgrid

3.5 Methodological Framework and Design Steps

This section presents the methodological framework and the systematic steps used to design, simulate and optimize the renewable energy system. This framework outlines the processes involved in creating the model and integrating diverse energy sources and storage to reach the objective of an efficient and sustainable operation. Each phase, from system design and component integration to performance optimization, is elaborated upon to provide a clear structure and show how the system gradually enhanced with each step.

3.5.1 Solar System Modeling and Simulation

This subsection outlines the basic approach used to model and simulate the solar energy system, it is designed to simulate the renewable energy generation based on standard parameters, without complex optimisation techniques. The primary goal for this simulation was to observe the interaction between the solar array, battery storage and electrolyser without accounting for power losses, power mismatches, major fluctuations and any variables that need control. The model considers fundamental factors such as solar irradiance, panel configuration, with a focus on how the solar array responds to normal varying sunlight conditions during the week. This model was kept basic to provide a clear understanding of how the solar cells contribute to the system's overall energy balance.

Solar Array Modeling

In PV power generation systems, the DC/DCconverters are typically used as interfaces between the load and the solar panel to enable efficient power transfer and maximum energy, in our case the load is the electrolyser. The load has to be controlled to its optimal voltage and current of the solar panel, in other words the Maximum Power Point (MPP). During this simulation, the DC/DC converter was simulated along with an MPPT system that searches and maintains the MPP under varying conditions. The converter is integrated directly with the solar panels, furthermore, for a smoother operation, a buck-boost converter is used to regulate the power from the solar array so that the voltage and current are kept within the range of optimal operation.

The MPPT used the Perturb and Observe (P&O) algorithm to maximize the energy output from the solar panel despite changes in solar irradiation. This DC/DC conversion with MPPT ensures that the solar array is operated efficiently with minimal power losses and maximum energy transfer to the system.

The PV module generates energy based on the available solar irradiance providing the initial input power. The MPPT controller continuously adjusts the operating point of the PV module by optimizing the voltage and current to extract the maximum available power. The buck/boost converter is responsible for regulating the output power, converting the variable voltage from the solar array to stable power supply that could either be used to charge the battery or run the electrolyser. This diagram provides a conceptual overview of how these components interact.

- **Solar Array:**

The solar array is represented using the Solar Cell block, which models a typical photovoltaic module. Using the Simscape Electrical library in MATLAB, this block implements a classical single solar cell as a resistance R_s, and a shunt resistance R_p in this equivalent circuit [83]:

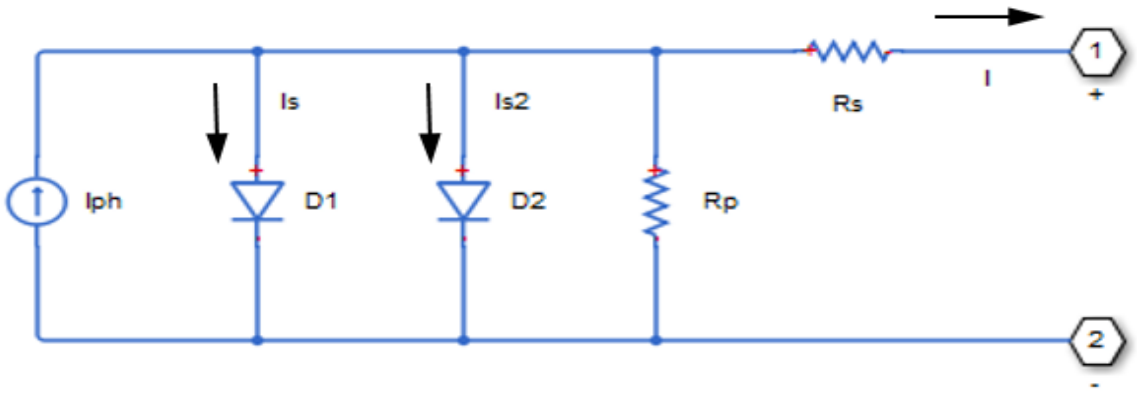

Figure 3.7: The Equivalent Circuit Diagram of a Solar Induced Current in Matlab

the output current of the cell is given by a nonlinear equation as follows:

$$I = I_{ph} - I_s\left(\exp\left(\frac{V + I R_s}{N V_T}\right) - 1\right) - I_{s2}\left(\exp\left(\frac{V + I R_s}{N_2 V_T}\right) - 1\right) - \frac{V + I R_s}{R_p} \quad (3.7)$$

Where I_{ph} is the solar induced current given by this equation:

$$I_{ph} = I_{ph0} \frac{I_r}{I_{r0}} \quad (3.8)$$

Where I_r is the irradiance in W/m², I_{ph0} is the solar generated current for the Irradiance I_{r0}.

In Equation 3.7 , I_s is the saturation current for the first diode and I_{s2} is for the second one measure in Ampere (A), the thermal voltage V_T is defined as kT/q, where k represents Boltzmann's constant, T is the device simulation temperature in kelvin, and q is the elementary charge of an electron. The parameters $N$and N_2denote the quality factors of the first and second diodes, respectively. These coefficients describe how closely each diode behaves compared to an ideal diode, lower values indicate more ideal characteristics, while higher values reflect increased recombination effects within the junction. Finally, V refers to the voltage measured across the electrical terminals of the solar cell.

This equation helps us understand how the solar panel reacts when sunlight or temperature changes. It shows how the current and voltage move together so that we can get the power outcome. These results are then sent to the MPPT controller and the DC/DC converter.

- **Maximum Power Point Tracker (MPPT)**

The MPPT in this study uses the P&O algorithm as mentioned earlier, this method continuously monitors the PV array's voltage and current V&I then adjusts the duty cycle D of the DC/DC converter accordingly to maximize the power output. Its mechanism is simple, based on four main parameters, the initial duty ratio D_{init}, the upper and the lower bounds of D (D_{max} and D_{min}), and the step increment ΔD which is used to increase or decrease D [84]. These limits makes sure that the converter operates within its design limits. So at each instant , the controller computes the current Power then compares it with old Power to determine the direction of the perturbation. The voltage change ΔV and the power change ΔP are calculated to determine what decision to make for the duty cycle, it goes as follows:

If $\Delta P > 0$and $\Delta V > 0$, the duty cycle $D$is increased to move toward the maximum power point.

If $\Delta P < 0$and $\Delta V > 0$, $D$is decreased to reverse the perturbation direction.

If the new Dvalue exceeds its upper or lower limits, it is clamped to D_{max}or D_{min}.

This decision process is repeated, allowing the system to "observe" the effect of "perturbations" in duty cycle and keep the operation near $\frac{dP}{dV}$=0. The output is the duty cycle D which drives the buck boost converter connected to the PV array.

- **Buck-Boost Converter**

This is implemented using the same library Simscape Electrical, this allows the integration of the converter by specifying its type and controlling its duty cycle D.

The converter links the DC output of the PV array after passing through the MPPT and enables either stepping-up (boost) or stepping-down (buck) of the voltage based on the duty cycle D. By varying D, the converter adjusts the relationship between the input voltage V_{in} and the output voltage V_{out}. It uses the following generic relation [85]:

$$V_{out} = f_{type}(D)\, V_{in} \tag{3.9}$$

And

$$I_{in} = \frac{V_{out} I_{out}}{V_{in} \eta} \tag{3.10}$$

Where I_{out} is the converter's output current in A, η is the converter efficiency and $f_{type}(D)$ is the gain function that depends on whether we pick the converter as a buck, boost or a buck-boost.

The ideal voltage gain for a buck-boost converter (under ideal conditions and neglecting losses) could be written as [85]:

$$\frac{V_{out}}{V_{in}} = \frac{D}{1-D} \tag{3.11}$$

So, in simple terms, this converter adjusts the voltage coming from the solar panel, when the sunlight is weak and the panel voltage drops, the converter boosts it up and when the sunlight is strong and the voltage gets too high , it bucks it down. By changing the duty cycle, it keeps the output voltage steady.

For the parameters and variables used, the simple cell temperature is assumed constant at 25°C, representing standard test conditions (STC). Temperature variations are not included at this stage

of the study as the main goal is to observe the impact of solar irradiance variabilities on the system's performance. T

Irradiance Data

The performance of the solar cell heavily depends on the incident solar irradiance (G) and the cell temperature (T). In the Simulink environment, this dependency is modelled through the photocurrent I_{ph} which increases similar to linear with the irradiance but slightly with the temperature, the relation is given by [86]:

$$I_{ph} = \left[I_{sc,ref} + \alpha_{Isc}(T - T_{ref})\right]\frac{G}{G_{ref}} \tag{3.12}$$

Where $I_{sc,ref}$ is the short circuit current at reference conditions, α_{Isc} is the temperature coefficient of short-circuit current, $T_{ref}\ and\ G_{ref}$ are the reference temperature (25°C) and reference irradiance (1000W/m²), then G is the instantaneous solar irradiance. G is introduced as a time-varying input to the solar cell block. The irradiance data used in this model is obtained from the Photovoltaic Geographical Information System (PVGIS) developed by the European Commission's Research Centre (JRC) [87]. PVGIS provides us with long term satellite derived datasets of the Global Horizontal Irradiance (GHI), which combines both direct and diffuse solar components incident on a horizontal plane. The dataset provides us with average hourly irradiance values, derived from multi-year meteorological records for each month.

For this study, the data corresponding to Montreal were extracted under normal conditions such as spring with clear sky irradiance behaviour. The profile it gave is a natural daily cycle, with a gradual increase after sunrise, peak during solar noon and decline towards sunset, providing us with a realistic input for the PV subsystem under constant cell temperature (25°C).

Irradiance Profile-Cold Winter Day (January, Montreal)

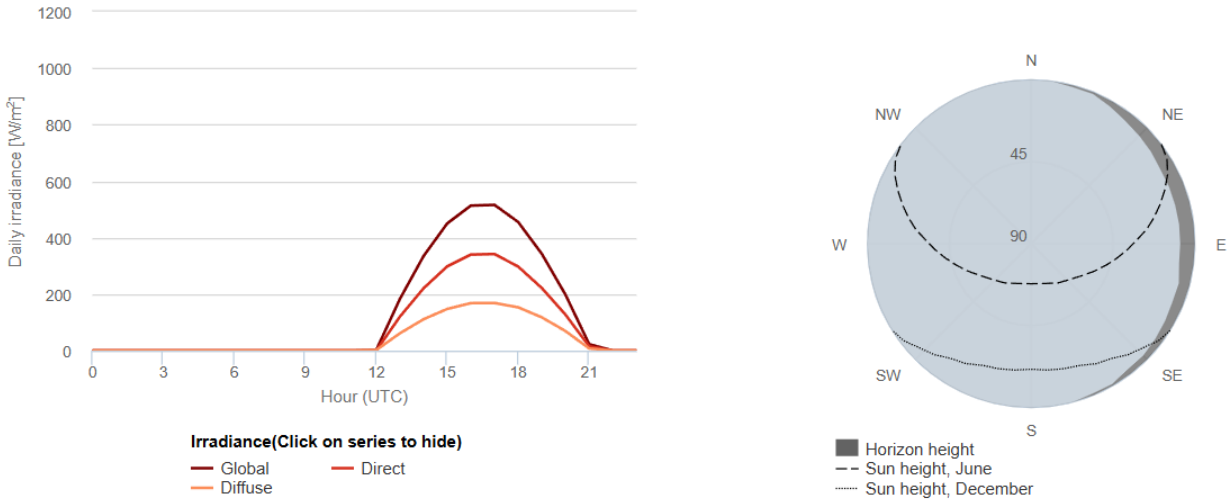

Figure 3.8: Average Global Horizontal Irradiance (GHI) in Montreal during a cold winter day (January) – data from PVGIS.

Irradiance Profile-Mild Spring Day (May, Montreal)

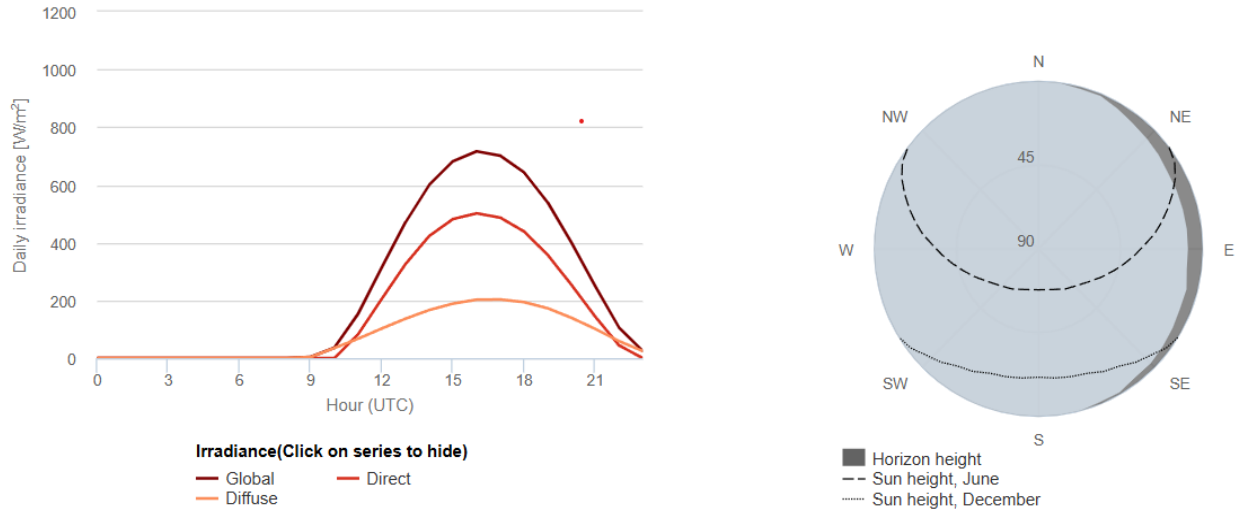

Figure 3.9: Average Global Horizontal Irradiance (GHI) in Montreal during a mild spring day (May) – data from PVGIS.

Irradiance Profile – Hot Summer Day (July, Montreal)

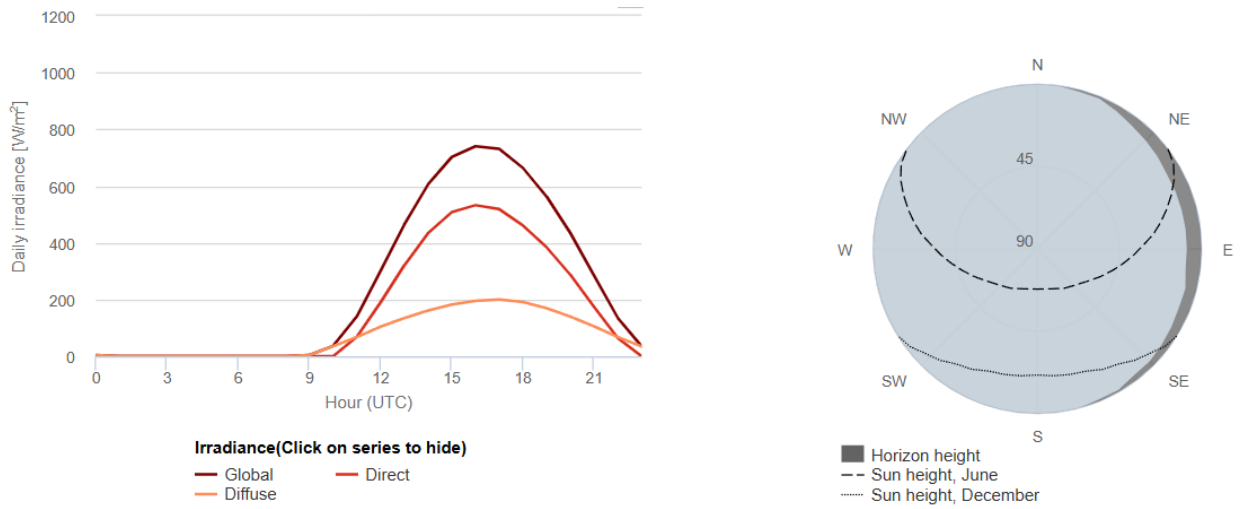

Figure 3.10: Average Global Horizontal Irradiance (GHI) in Montreal during a hot summer day (July) – data from PVGIS.

The data could be exported as an Excel (.xlsx) file and is used later a time-series input in MATLAB/Simulink, allowing the irradiance signal G(t) to drive the photovoltaic model dynamically over 24h period, allowing the system to simulate a typical day with its fluctuations.

The Energy Storage System

The Energy Storage System (ESS) serves as a critical element of the system as it ensures the system is still fed under low energy supply. Methodologically, the battery is modelled as a dynamic system that exchanges energy with the rest of the microgrid through a DC/DC converter, controlled according to the state of charge SoC and a reference current signal I_{ref}. The ESS operates usually under two modes: charging when there is excess power from the renewable energy generation and then discharging when the power demand exceeds the available renewable power.

The models are based on an equivalent electrical circuit, where the voltage-current relationship is expressed as [88]:

$$V_{batt} = E_0 - R_{int} I_{batt} \tag{3.13}$$

Where V_{batt} is the terminal voltage of the battery, E_0 is the open-circuit-voltage (OCV), R_{int} is the internal resistance and I_{batt} is the instantaneous current.

The state of charge SoC is the ratio between the current charge and its maximum capacity, representing the available energy stored in the system. It evolves as a function of current and time as follows [89]:

$$\mathrm{SoC}(t) = \mathrm{SoC}(t_0) - \frac{1}{C_{\mathrm{batt}}} \int_{t_0}^{t} I_{\mathrm{batt}}(t)\ dt \tag{3.14}$$

Where C_{batt} is the nominal capacity of the battery in Ampere-hours (Ah).

The SoC provides the control boundary for charging and discharging operations, when it falls below a given threshold (usually 30-35%), the control system interrupts discharge to prevent an over depletion of the battery, likewise, charging is limited at the given upper threshold to prevent overcharging.

This whole mechanism is controlled by the reference current I_{ref}, it controls the bidirectional operation of the battery system. It includes in its function both the solar current I_{solar} and the battery charge state (Q_{batt}). This ensures that when excess power is produced by the solar generator (I_{solar}>I_{load}), the surplus current charges the battery and in the opposite case it discharges so that we maintain a power balance across the system.

The DC/DC converter in this acts as a link between the battery and the DC bus that connects the system, it allows the charging and the discharging to be controlled through a duty cycle D as mentioned for the solar system as well, the output voltage of this is defined as [90]:

$$V_{out} = D\, V_{in} \tag{3.15}$$

Where V_{in} is the battery voltage in voltage. It continuously adjusts the duty cycle to ensure that the actual battery current follows the reference current, it is a closed loop cycle. An important thing to note is that during charging mode the converter maintains a positive I_{ref} and in the discharge it is a negative current.

Electrolyser

This part represents the key component of the system responsible for converting the renewable electrical energy into hydrogen through water electrolysis. In this work, a PEM electrolyser is used, it is well compatible with variable renewable energy. The main idea is to simulate how the electrical power supplied by the solar array and battery are fed to power the electrolyser.

This model is built around the physical relationship between the voltage, current, temperature and hydrogen flow rate. Each cell of the electrolyser requires a certain voltage to split water molecules and the total stack voltage depends on how many cells we have connected in series, the equation is [91]:

$$V_{stack} = N_{cell} V_{cell} \tag{3.16}$$

Where N_{cell} is the number of cells and V_{cell} is the voltage per cell in voltage (V). This voltage is made up by several parts, the first one is the reversible voltage (V_{rev}) which is the minimum theoretical voltage needed for water electrolysis. The other parts are the losses discussed in the literature such as the activation losses (η_{act}), the ohmic resistance inside the electrolyte (η_{ohm}) and the concentration effects at higher current (η_{conc}) the total voltage is given by :

$$V_{cell} = V_{rev} + \eta_{act} + \eta_{ohm} + \eta_{conc} \tag{3.17}$$

The reversible voltage in this equation is dependent on the operating temperature and pressure as described by the Nernst equation [92]:

$$V_{\text{rev}} = 1.229 - 0.9 \times 10^{-3}(T - 298.15) + \frac{4.308 \times 10^{-5} T}{2} ln\left(p_{\text{H}_2}\, p_{\text{O}_2}^{0.5}\right) \tag{3.18}$$

This shows that increasing the temperature slightly reduces the energy needed to split the water molecules therefore the electrolyser is highly sensitive to temperature. For this reason, a thermal coupling is included in the model. The electrolyser temperature is managed through a heat source and thermal resistance that both represent the heat generation part and the hear exchange with the environment part.

The electrical power consumed by the electrolyser is given by [93]:

$$P_{elec} = V_{stack} I_{el} \tag{3.19}$$

In the integrated system, the electrolyser behaves as a variable load that depends on the power available to it. During high periods of solar generation, the electrolyser is supplied directly by it and when it drops, the battery compensates by discharging and maintaining the current required

for hydrogen production. The reference power or current of the electrolyser is defined by the available renewable power ($P_{available}$), the stack Voltage (V_{stack}) according to the equation [93] :

$$I_{el,ref} = \frac{P_{available}}{V_{stack}} \tag{3.20}$$

In summary, the electrolyser acts as the conversion bridge between renewable electricity and chemical energy, its operation depends on two main inputs:

- The available electrical power from the PV-Battery system
- The thermal conditions that influence its efficiency

3.5.2 Solar and Wind System Modelling and Simulation

The hybrid system extends on the already developed modelled of the solar system by adding a wind generation component to complement the solar generation. The goal of this integration is to reduce the continuous cycling and reliance on the battery storage unit. In this model, the solar array size was reduced compared to the standalone model to account for the additional power provided by the wind subsystem to meet the electrolyser's demand.

The model follows the same structure as the other one, the total energy supplied at any time is the sum of both sources, expressed as :

$$E_{renew}(t) = E_{solar}(t) + E_{wind}\ (\mathrm{t}) \tag{3.21}$$

The subsystem of the wind turbine converts kinetic energy of moving air into electrical power using a simplified aerodynamic model. The instantaneous electrical power produced by the wind turbine is determined by [94]:

$$P_{\mathrm{wind}} = \frac{1}{2}\,\rho\, A\, C_p\, v^3 \tag{3.22}$$

Where ρ is the air density (1.225kg/m3), A is the rotor swept area in m², $C_p = 0.4$ is the power coefficient representing aerodynamic efficiency, and v is the wind speed in meters per second (m/s). The wind speed profile was modelled to vary between 4m/s and 8 m/s over 24 hours, representing a moderate onshore wind regime.

Wind speed data were obtained from publicly available meteorological records, the dataset provides long-term monthly averages of maximum, minimum or extreme wind speeds over up to 5 years [95].

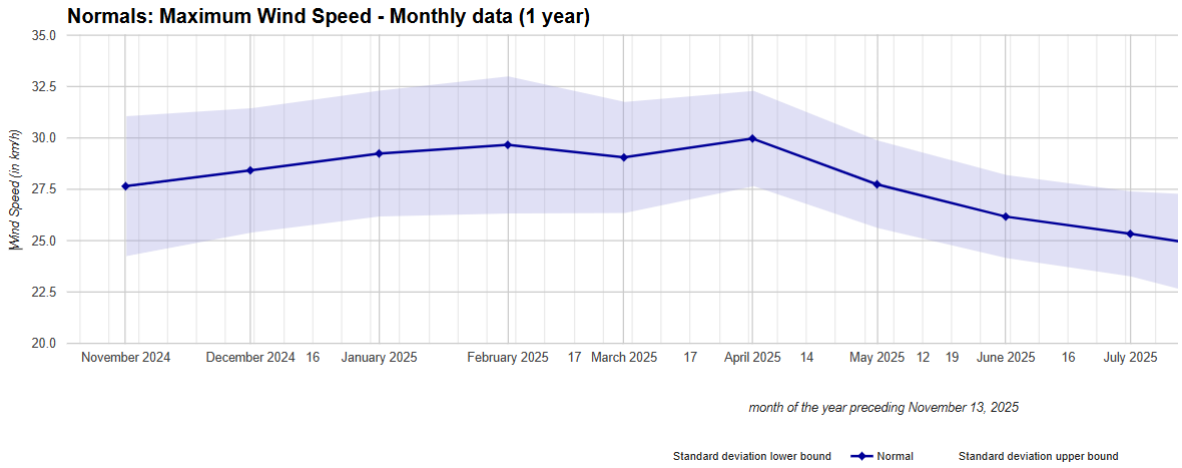

Figure 3.11: Wind Speed Profile

The power management is based on a simple rule that decides how the electricity from the solar array, wind turbine and the battery is shared. The goal is to make sure the electrolyzer always receives enough power to operate whenever renewable energy is available, while keeping the battery from being overused. The solar array provides most of the power when sunlight is strong while the wind turbine supports the system when the solar output is low, such as at night or during cloudy hours. When both sources produce power at the same time, the total renewable energy prioritizes the electrolyser and then the excess energy is stored in the battery. If the renewable generation drops below the electrolyser's demand the battery automatically discharges to make up the difference.

Then at the end there is a comparison between the stand-alone solar system and the hybrid system to show the decrease in the battery usage represented in Ah.

3.5.3 Optimized Hybrid System

This section will dive into the computational and control methodology developed to simulate the hybrid renewable microgrid in Python. The system operates in an autonomous mode, combining photovoltaic generation, wind turbines , a battery energy storage system and a PEM electrolyser.

The model runs in discrete time steps of one hour (Δt=1h) and integrates both predictive and optimization-based control layers to manage power flow, storage dynamic and hydrogen production.

Renewable Energy Inputs

The work begins with the import of weather-based time series representing the solar irradiance and the wind speed. At each time step t, the values are used to calculate the instantaneous power produced by the solar and wind subsystem.

For the PV generator, the power output depends linearly on the available irradiance G(t), the total active PV surface A_{pv} and the panel efficiency η_{pv} [95]:

$$P_{pv}(t) = A_{pv} \cdot G(t) \cdot \eta_{pv} \quad (3.23)$$

This simple linear model provides a realistic approximation for system-level energy flows and enables the use of measure irradiance and data directly.

The wind turbine output follows a cubic power relation between the cut-in V_{ci} , rater V_r and cut-out V_{co} speeds.

At each time step, the total renewable power available to the system is the sum of both sources, this combines profile provides the energy supply that feeds both on the electrolyser and the battery according to the active control strategy.

Battery Energy Storage System (BESS)

The battery plays a central role in stabilizing renewable energy fluctuations, it stores surplus energy during high renewable output periods and discharges when renewable generation is insufficient to sustain the electrolyser load.

As stated for the stand alone solar microgrid, the SoC evolves continuously as a function of the battery current and time according to the equation (3.14). To implement the model in a time-stepped simulation, we rewrite that equation over a small interval Δt. Using $P = VI$ and the battery's total energy capacity $E_{\text{batt}} = V_{\text{batt}}\, C_{\text{batt}}$ (Wh, or kWh with scaling), the SoC increment becomes:

$$\Delta \text{SoC} \approx -\frac{I_{\text{batt}}\,\Delta t}{C_{\text{batt}}} = \frac{1}{E_{\text{batt}}}\,P_{\text{net}}\,\Delta t \tag{3.25}$$

where $P_{\text{net}} > 0$ indicates charging and $P_{\text{net}} < 0$ indicates discharging.

So then the SoC is updated according to the following discrete equation [97]:

$$SOC_{t+1} = SOC_t + E_{batt}\left(\eta_{ch}P_{ch} - \frac{P_{dis}}{\eta_{dis}}\right)\Delta t \tag{3.26}$$

Where P_{ch} and P_{dis} are the charging and discharging powers (kW), η_{ch} and η_{dis} are the charge and discharge efficiencies, E_{batt} is the total capacity of the battery (kWh).

A saturation function ensures that the SoC remains between 0 and 1, even under numerical disturbances or ramp transients. This allows the model to remain stable over long simulations while accurately representing the available stored energy.

Electrolyser Model

This subsystem is defined by its minimum and maximum power ratings and by its operational ramp limit which prevents instantaneous power charges that could damage the stack.

The hydrogen production rate (kg/h) is calculated from the electrolyser input power and its conversion efficiency:

$$\dot{m_{H_2}}(t) = \frac{P_{el}(t) \cdot \eta_{el}}{E_{H_2}} \tag{3.27}$$

Where E_{H_2} is the specific energy content of hydrogen (kWh/kg), the total hydrogen produced during the simulation is obtained by integrating $\dot{m_{H_2}}(t)$ over time. This model captures both the instantaneous power consumption and the cumulative production behaviour of the electrolyser [98].

Instead of assuming a steady load, the model explicitly resolves the electrolyzer's internal dynamics, yielding a physically consistent operational response.

The electrolyzer is modelled using simplified operational, efficiency, and thermal dynamics. The electrical input power at time t is limited by the nominal capacity and defined as $P(t) = \min(P_{set}, P_{nom})$, with $P_{nom} = 150\text{kW}$. Startup behavior is represented by a linear ramp over a 2-hour period, while shutdown is assumed to be instantaneous when the unit is turned off.

The conversion efficiency is load-dependent and expressed as a linear function of the normalized operating power, with a nominal efficiency of 0.70 at full load and reduced performance at partial load. The hydrogen production rate is computed from the instantaneous power and efficiency using a higher heating value of 33.33 kWh/kg.

A simplified thermal model is included, where temperature increases due to conversion losses without active cooling, starting from an ambient condition of 25°C. A safety constraint is implemented such that the electrolyzer is automatically shut down when the temperature exceeds 80°C. Thermal losses are tracked during operation for performance analysis.

Power Flow and Energy Balance

This simulation is built to make sure there is an energy conversion across all subsystems at every time step.

The total renewable generation, which is the sum of the wind energy and the solar energy, is dynamically allocated among the electrolyser, the battery and the potential curtailment. This ensures that all power flows are physically consistent and that each control decision leads to a realistic system behaviour. The governing equation for the instantaneous power balance is given by :

$$P_{\text{ren}}(t) = P_{\text{el}}(t) + P_{\text{batt}}(t) + P_{\text{curt}}(t) \tag{3.28}$$

Where $P_{\text{curt}}(t)$ represents the curtailed or the unused power, the simulation logic enforces this balance iteratively. If the renewable generation exceed the combined capacity of the battery and electrolyser, the excess power is automatically assigned to curtailment ($P_{\text{curt}}(t)>0$). When the renewable output is low, the battery is allowed to discharge until it reaches its minimum SoC. This ensures that there is no artificial energy introduced into the system and that curtailment appears naturally as a residual term from the physical balance.

Internally, the battery update and electrolyser control are performed before this balance check, allowing the model to dynamically adjust the curtailment term. This means that the system continuously “closes the loop” to preserve energy even under rapidly changing solar and wind conditions.

The results of this stage are a complete time-resolved dataset of energy allocation, showing how RE is split between hydrogen production and storage at each hour of the simulation.

Supervisor Control Strategies

The system includes two distinct control models: a predictive control and a DT based controller. Both receive as inputs the current state of charge of the battery and a short-term forecast of renewable energy availability, then output two control actions: the target electrolyser power and the battery discharge/charge power. This allows a flexible trade-off between immediate hydrogen production and long-term energy stability.

Predictive Control :

This controller anticipates system behaviour over a fixed horizon N (24hours) by minimizing the objective function optimization problem was formulated following the standard quadratic predictive control framework widely used in renewable–hydrogen hybrid systems [99]. However, the cost function used in this work (Equation 3.29) was specifically tailored to the studied PV–battery–electrolyzer configuration, combining electrolyzer power tracking, SoC regulation, battery degradation minimization, and curtailment penalties to ensure efficient and stable hydrogen production.

$$J = \sum_{k=t}^{t+N-1} \left[w_1 (P_{\text{el}}(k) - P_{\text{set}})^2 + w_2 |P_{\text{batt}}(k)| + w_3 \left(SOC(k) - SOC_{\text{opt}} \right)^2 + w_4 P_{\text{curt}}(k) \right] \quad (3.29)$$

Where each term corresponds to a real physical objective:

-w_1: stabilizes electrolyzer operation.

-w_2: penalizes excessive charge–discharge cycles.

-w_3: encourages the battery to stay near its optimal SOC for flexibility.

-w_4: penalizes renewable energy waste.

The terms represent tracking-type objectives which aim to keep variables near a Reference value such as for power or SoC, the linear terms represent cost or constraint-type objectives, they aim to minimize usage or losses, not track a target.

The optimization problem is subject to the following operational and physical constraints, which ensure that the MPC decisions remain feasible and safe under real conditions.

-Power Balance:

$$P_{\text{ren}}(k) = P_{\text{el}}(k) + P_{\text{batt}}(k) + P_{\text{curt}}(k) \quad (3.30)$$

At each time step, the available renewable power (P_{ren}) is shared between the electrolyzer, the battery, and any curtailed surplus. This equality maintains the overall energy balance within the microgrid.

Curtailment can only occur when renewable generation exceeds the demand of the electrolyzer and the battery's charging capacity; negative values are physically meaningless.

The optimization is solved in a receding horizon fashion, only the first control command from the computed sequence is applied, after that the system moves forward one hour at a time and re-optimizes based on updated conditions. This approach resembles real-world adaptive control, new weather or load information always influences the energy dispatch. So, in summary, this controller optimizes the trade-off between hydrogen productivity and system longevity, making smooth transitions with foresight between charging, discharging, and production phases.

Digital Twin Controller:

Now the digital twin controller operates differently, instead of solving an optimization problem, it relies on virtual experimentation within the same simulation, environment. At every hour, the controller clones the system states, including the battery SoC and forecasted power, then runs three short, parallel internal simulation strategies over the forecast horizon.

Each strategy presents a possible operational mode like maxing out hydrogen by using all of the available renewable energy and discharging the battery aggressively. Prioritizing the battery charging to store energy for future hours reducing the immediate hydrogen output or balancing the system by operating the electrolyser at affixed setpoints using the battery to absorb or provide small deviations.

For each strategy, the digital twin computes a virtual time evolution of power flows and SoC using the same physical constraints as the main simulation, after simulating the horizon, it computes a performance score taken from standard decision-based control frameworks **[100]** then adapted to this system :

$$S = \sum_{t} P_{\text{el}}(t) - \alpha |SOC_{\text{end}} - SOC_{\text{opt}}| \tag{3.31}$$

This score rewards strategies that produce more hydrogen while discouraging large deviations from the target battery charge. The option with the highest score is then applied in the next control step. In this way, the controller can look ahead without complex calculations, it learns from its own simulated version of the system and picks the action that would perform best under the current forecast.

Particle Swarm Optimization for Post-Simulation

After running the main simulation, a post-optimization phase is introduced using PSO, this is not part of the control loop but a diagnostic step sued to determine whether the operational settings chosen by the controller are close to the global optimum for the same environment conditions. Each particle in the swarm represents a possible combination of electrolyser characteristics:

$x_i = [\eta_{el}, r_{max}, P_{set}]$

Where $\eta_{\text{el}}$is the efficiency, $r_{\max}$the ramp limit, and $P_{\text{set}}$the setpoint power. Each particle represents a possible configuration of the system for example, a combination of power setpoints or control parameters that influence the electrolyser's performance. Together, these parameters directly affect energy efficiency, power smoothness, and hydrogen production stability, making them suitable decision variables for optimization.

Each particle has a position $x_i$and a velocity v_i, which are updated at each iteration according to two main equations [101]:

$$v_i^{(k+1)} = \omega v_i^{(k)} + c_1 r_1 \left(p_i^{best} - x_i^{(k)}\right) + c_2 r_2 \left(g^{best} - x_i^{(k)}\right) \tag{3.32}$$

$$x_i^{(k+1)} = x_i^{(k)} + v_i^{(k+1)} \quad (3.33)$$

Where $v_i^{(k)}$ is the velocity of particle i at the iteration k, it is measured in the same units as the decision variables of each iteration, $x_i^{(k)}$ is the particle's current position as well. ω is dimensionless, it's the inertia weight, controlling how much of the previous velocity is kept. $c_1$and c_2 are acceleration coefficients, determining how strongly the particle is attracted to its own best solution and the global best solution respectively, $r_1$and r_2 are random numbers between 0 and 1, they add a stochastic element, then finally p_i^{best} and g^{best} represent respectively the best position found by particle I and the best position found by any particle in the entire swarm.

At each iteration, the algorithm evaluates how good each particle's current position is by calculating a fitness value, using a multi objective function. This function combines three performance indicators, the electrolyzer's efficiency, the smoothness of the power input, and the stability of hydrogen production. The objective function is defined as:

$$J(x) = -\eta_{el} + w_r\, \bar{\Delta P} + w_s\, \sigma_{H_2} \quad (3.34)$$

Where $\bar{\Delta P}$is the average ramp rate of the electrolyzer power signal and $\sigma_{H_2}$is the standard deviation of hourly hydrogen production. The objective function is formulated to maximize electrolyzer efficiency while penalizing excessive power ramping and hydrogen production variability.

3.6 Simulation Procedure and Outputs

The simulation reproduces the operation of the hybrid renewable hydrogen microgrid step by step. It combines the solar and wind generation, battery storage and hydrogen production in one consistent framework. The goal is to understand how these subsystems interact over time under real weather conditions and how different control strategies influence overall performance,this logic follows a logical sequence from input preparation to result visualization.

It runs in 7 main stages, each one corresponds to a specific part of the system's operation.

Step1: Initialization and parameters

This step sets all global parameters of the model including the total simulation duration, the time resolution, the electrical and storage capacities, efficiency factors and control settings. The user can choose between an automatic sizing model or a manual configuration offering flexibility.

In automatic mode, the system calculated the required photovoltaic and wind capacities based on the target daily hydrogen production, this ensures that the generation potential matches the electrolyser's energy demand while allowing for storage flexibility. In manual mode, the user defines all the systems components directly such as the peak power for the solar or the rated power for the wind, nominal capacity of the batteries. During this stage, initial conditions such as the starting SoC and the expected operation point of the electrolyser are also defined, ensuring consistency across the simulation.

Step 2: Weather data processing

The dynamic behaviour of the system depends heavily on the meteorological inputs, hourly data for solar irradiance and wind speed are imported and processsed. This stage corrects missing values and standardizes units to guarantee that the data are continuous and compatible with the energy models in the system. So the dataset introduced to the system represent a real environmental profile. This is an important step because gaps in the weather data could ruin the balance between renewable generation, storage and hydrogen production.

Step 3: Renewable energy generation modelling

After processing all the data, the simulation converts the weather data into actual renewable energy output. For the solar subsystem, irradiance values are tanslated into electrical power using the total surface area and the efficiency of the photovoltaic modules. The model accounts for real operating conditions such as the rated power limit and possible clipping when the available irradiance exceed nominal design capacity.

For the wind subsystem, the power output is derived from the introduced wind speed values using a characteristic power curve, the turbine generate energy only when the wind speed is between its cut-in and cut-out thresholds and increases cubically until it reaches the rated region. The combined solar and wind production defines the total energy available at each time step, this becomes the main input for the control and dispatch stages that follow.

Step4: Control and energy dispatch

This stage is the operational core of the simulation, it determines, hour by hour, how the available renewable energy is allocated among the electrolyser, the battery and the possible curtailment.

The control layer supervises the energy balance of the system while maintaining physical and operational limits.

In predictive control mode, the algorithm uses a forecast of upcoming renewable energy generation to anticipate changes and smooth the system's response, the objective is to keep the electrolyser within the safe operating range avoiding unnecessary battery cycling and prevent curtailment losses. While the digital twin simulates several control strategies in a virtual space of the system, each strategy represents a different logic, for example, maximizing hydrogen production, maintaining a balanced state of charge or prioritizing storage. The model evaluates their outcomes in real time and automatically selects the most effective option based on predefined performance indicators.

By doing this, the control layer reproduces how an intelligent microgrid would operate in practice, adapting dynamically to fluctuations while respecting the ramp-rate and power constraints.

Step5: Hydrogen production and storage dynamics

Once the control strategy defines the power sent to the electrolyser, the model converts this electrical energy into hydrogen. This depends on the electrolyser's rated capacity and efficiency. The hydrogen output is calculated overtime, allowing the evaluation of production patterns, interruptions and so on. This will show how the control influences the stability and continuity of hydrogen generation.

Step6: Post simulation analysis and optimization

After all of this is completed, the model compiles and analyses the results. The system performance is summarized through key indicators such as the total energy produced, the electricity delivered to the electrolyser, the hydrogen yield. This post-processing uses a particle swarm approach to explore alternative sets of operational parameters; it aims to identify conditions such as better ramp limits or improved efficiency values depending on the objective function variables. The results of this optimization are compared to the baseline simulation to quantify potential performance gains and highlight areas where control improvements would be most effective. This stage bridges

simulation and decision support, providing insight into how design or control choices affect the overall behaviour of the system.

Step7: Visualization and data export

This step is to interpret and export the results, the framework automatically generates graphical output that display the main energy flows, solar and wind production, battery charge and discharge, electrolyser operation and cumulative hydrogen production. Data can be exported in standard formats (CVS or image files) for reporting, documentation and further analysis. This transforms the simulation into clear, interpretable results, allowing both quantitative evaluation and visual understanding of system dynamics.

CHAPTER 4 ARTICLE 1: PREDICTIVE MODEL CONTROL AND PARTICLE SWARM OPTIMIZATION OF A HYBRID SOLAR-WIND MICROGRID DRIVING A PEM ELECTROLYZER FOR SCALABLE HYDROGEN PRODUCTION

Hayfa Rhimi, Andreas Athienitis and Daria Camilla Boffito

Name of the Journal: IEEE Transactions on Sustainable Energy

Submission Date: 11/12/2025

Abstract— Hybrid renewable microgrids that feed Proton Exchange Membrane (PEM) electrolyzers enable off-grid hydrogen production but require integrated design, sizing and control for good performance. We developed a Digital Twin (DT) of a solar-wind microgrid that supplies a PEM electrolyzer coupled with an energy storage system for a year-round assessment. The workflow starts with a solar standalone system on MATLAB/Simulink to assess the pattern of hydrogen production. Then a wind source is added to the system to provide complementary power generation and assess how it affects the hydrogen production pattern. Finally, the system is implemented in a Python program for optimization, it couples detailed component models with Particle Swarm Optimization (PSO) and Model Predictive Control (MPC) for short-horizon dispatch. This study tracks electrolyzer loading, battery state of charge (SoC)and hydrogen output under measured meteorological data. In the final configuration, the PV generation is sized as equal to the electrolyzer's rated power, the wind turbine at 53% and the battery has a power limit of 0.40 with an energy capacity of 6.7hours at full electrolyzer load. Over a year-long simulation, the electrolyzer operates continuously with an annual capacity factor of 0.68 on an LHV basis and an

This work was supported in part by the Canada Research Chairs (Engineering Process Intensifictaion and Catalysis – EPIC).

H. Rhimi is with Polytechnique Montréal, Montréal, QC H3T 1J4, Canada (hayfa.rhimi@polymtl.ca).
A. Athienitis is Professor with the Department of Building, Civil and Environmental Engineering, Concordia University, Montréal, QC H3G 1M8, Canada (e-mail: andreas.athienitis@concordia.ca).
D. C. Boffito is Professor with the Department of Chemical Engineering, Polytechnique Montréal, Montréal, QC H3T 1J4, Canada (e-mail: daria-camilla.boffito@polymtl.ca).

average hydrogen production of 48.7 kg/day. The battery supplies an average of 13% of the electrolyzer's demand with the remainder being covered by the renewables. The electrolyzer's specific consumption is 50kWh/kg of hydrogen.

Index Terms-- Battery energy storage, Digital twin, Electrolyzer, Hybrid renewable energy system, Hydrogen production, Model predictive control, Off-grid system, Particle swarm optimization, Solar power generation, Wind energy.

4.1 Introduction

Hydrogen energy presents several advantages, including zero-carbon emissions, high energy density, flexible conversion pathways and suitability for long-term storage and multi-energy integration [102]. Accelerating its development is a pathway to address climate change, enhance energy security and support sustainable development. Over the past decade, several national and regional initiatives have considered hydrogen as a crucial element to reach carbon neutrality. The European Union, Japan, and China have each adopted comprehensive hydrogen strategies that prioritize large-scale renewable energy–driven hydrogen production [103]-[104]. The European "Hydrogen Strategy for a Climate-Neutral Europe" presents a roadmap for deploying green hydrogen by 2030, while China's Medium and Long-Term Plan for the Development of the Hydrogen Energy Industry (2021–2035) identifies renewable-powered electrolysis as the primary focus for industrial growth [105]. Hydrogen serves as an important bridge among various energy vectors like electricity, gas, and heat, playing an increasingly vital role in creating flexible energy systems [106]. By converting excess renewable electricity into hydrogen through electrolysis, hydrogen systems can significantly enhance renewable energy (RE) utilization, offer seasonal energy storage, and facilitate cross-sector coupling for power, heating, and transportation applications [107]-[108]. Moreover, hydrogen functions both as a clean fuel and a key industrial feedstock, giving it a dual role in decarbonizing energy and industrial processes [109]-[110]. The advancement of renewable energy–based hydrogen projects worldwide point out the urgent need to develop reliable and efficient production systems capable of operating under varying environmental conditions [111]. While RE powered electrolysis offers a green pathway for hydrogen generation, it also presents complex operational challenges. Solar and wind energy, the most widely used renewable resources, exhibit significant intermittency considering their direct

dependency on the available solar irradiance and wind speed [112]-[113]. These fluctuations lead to power oscillations that impact electrolyzer efficiency, increase degradation rates, and limit system reliability [114]. Ensuring stable hydrogen production in an off-grid environment necessitates an integrated approach that combines hybrid renewable sources, storage systems, and advanced control techniques [115]. Hybrid microgrids have emerged as a promising configuration for such systems because they integrate solar and wind resources with energy storage, enabling flexible and continuous operation [116]. The dynamic modeling and control of PEM electrolyzers are of particular interest due to their fast transient response and high efficiency under fluctuating loads [117]. Authors have investigated hybrid renewable systems coupled to water electrolysis for off-grid hydrogen production. One paper reviewed these systems and highlighted that hybridization works well with PEM electrolyzers and they are particularly attractive for dynamic operation and for reducing hydrogen production costs [118]. Another study examined a 15MW PV park combined with wind turbines and battery storage showing how adding the wind and the storage increases the electrolyzer's utilization and smoothed the power profile relative to PV only generation [119]. Other works analyzed the performance of a 500KW grid system and compared the variable-load and constant power strategies, focusing on voltage and frequency stability and on limiting electrolyzer degradation in autonomous operation [120]. At the component level, a study developed and validated a detailed 1MW electrolyzer model for real-time simulation, enabling the study of fast active power and frequency support capabilities under realistic grid disturbances [121]. Complementing these works, another paper proposed a robust day-ahead optimization framework for a hybrid PEM electrolyzer with storage participating in frequency containment reserve markets and demonstrating that coordinated operation of hydrogen assets can provide a profitable hydrogen production [122]. However, to our knowledge, none of these works combined metaheuristic control algorithms with predictive control and real meteorological data for a fully off-grid solar and wind microgrid, along with a virtual DT that continuously tracks the behavior of the system at each iteration. No existing study, to our knowledge, explicitly targets increasing the electrolyzer capacity factor without relying on oversizing the renewable generation, especially the wind, or deploying very large battery capacities. Therefore, this paper presents an autonomous hybrid RE powered PEM electrolyzer for off-grid operation. A DT was developed to reproduce the electrical and operational behavior of the microgrid and its interaction with the PEM electrolyzer. The model presented uses real time meteorological datasets for solar irradiance and wind speed to

capture actual environmental variability and support adaptive energy management. The system combines an optimization layer, based on PSO, with an MPC strategy to coordinate the energy flow among solar, wind and storage units. These control mechanisms are designed to maintain continuous hydrogen production while limiting the impact of renewable fluctuations on the electrolyzer. The aim of the work is to achieve stable hydrogen generation without the need for grid backup. The proposed framework minimizes energy imbalance, improves renewable utilization and sustains electrolyzer efficiency under variable conditions, therefore achieving a relatively high-capacity factor compared to existing literature without oversizing the renewable sources or adding large battery capacities.. Simulation results show that the hybrid configuration isolates hydrogen output from RE intermittency, leading to a steady and reliable production profile. A sensitivity analysis to oversizing the RE sources and batteries was done to investigate its effects on the capacity factor and efficiency of the system. The DT also provides a flexible platform that can be adapted to different climates by updating the environmental datasets. The findings offer a practical reference for the planning and control of autonomous renewable hydrogen systems and contribute to the technical foundation for scalable off-grid energy infrastructures

4.2 Methodology

4.2.1 PV model

The solar array is represented using the Solar Cell block from the Simpscape Electrical library in Matlab. This block implements the standard single-diode photovoltaic equivalent circuit, consisting of a light-generated current source, a diode, a series resistance R_s , and a shunt resistance R_p. The output current of the cell is given by[123]:

$$I = I_{ph} - I_s\left(\exp\left(\frac{V + I R_s}{N V_T}\right) - 1\right) - I_{s2}\left(\exp\left(\frac{V + I R_s}{N_2 V_T}\right) - 1\right) - \frac{V + I R_s}{R_p} \quad (4.35)$$

where I_{ph} is the solar induced current given by this equation:

$$I_{ph} = I_{ph0}\frac{I_r}{I_{r0}} \quad (4.36)$$

where I_r is the solar irradiance (W/m²) and I_{ph0} is the solar generated current for the Irradiance I_{r0} .

I_s is the saturation current for the first diode and I_{s2} is for the second one (A). The thermal voltage $V_T$is defined as kT/q, where k represents Boltzmann's constant, $T$is the device temperature in kelvin, and q is the elementary charge of an electron. The parameters $N$and N_2denote the quality factors of the first and second diodes, respectively. These coefficients describe how closely each diode behaves compared to an ideal diode, lower values indicate a system closer to ideal behaviour., while higher values reflect increased recombination effects within the junction. Finally, V refers to the voltage measured across the electrical terminals of the solar cell.

The output is then transferred to an MPPT controller and a DC/DC converter. The MPPT controller continuously adjusts the operating point of the PV module by optimizing the voltage and current to extract the maximum available power. The buck/boost converter is responsible for regulating the output power, converting the variable voltage from the solar array to stable power supply that could either be used to charge the battery or run the electrolyzer [124].

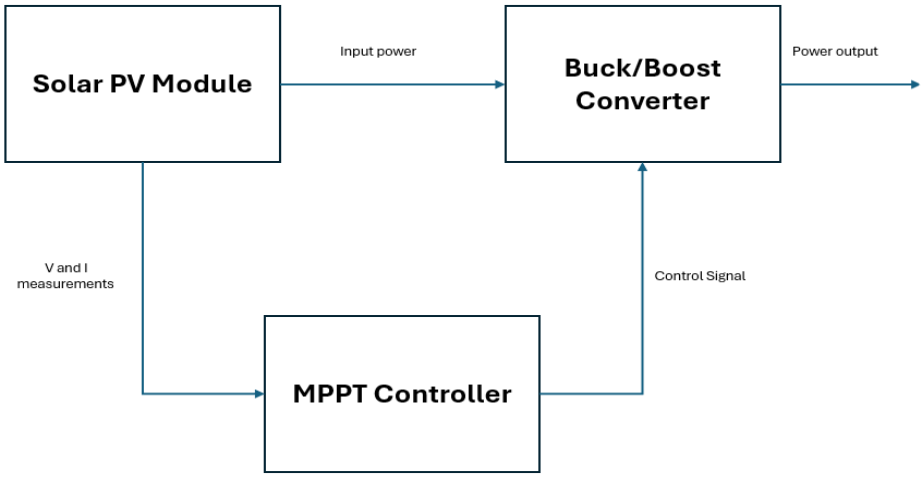

Figure 4.12: System Diagram: Solar PV with MPPT and Buck/Boost Converter

The MPPT in this study uses the P&O algorithm. As mentioned earlier, this method continuously monitors the PV array's voltage and current V&I . It then adjusts the duty cycle D of the DC/DC converter to maximize the power output. It makes decisions based on four main parameters, the initial duty ratio D_{init}, the upper and the lower bounds of D (D_{max} and D_{min}), and the step increment ΔD which is used to increase or decrease D [125] following:

-If $\Delta P > 0$and $\Delta V > 0$, $D$is increased to move toward the maximum power point.

-If $\Delta P < 0$and $\Delta V > 0$, $D$is decreased to reverse the perturbation direction.

- If the new Dvalue exceeds its upper or lower limits, it is kept within D_{max}or D_{min}.

This decision process is repeated, allowing the system to "observe" the effect of "perturbations" in D and keep the operation near $\frac{dP}{dV}$=0. The output is

D which drives the buck boost converter connected to the PV array.

The converter links the DC output of the PV array after passing through the MPPT and enables either stepping-up (boost) or stepping-down (buck) of the voltage based on D. By varying D, the converter adjusts the relationship between the input voltage V_{in} and the output voltage V_{out}. It uses the following relation [126]:

$$V_{out} = f_{type}(D)\, V_{in} \tag{4.37}$$

$$I_{in} = \frac{V_{out} I_{out}}{V_{in} \eta} \tag{4.38}$$

Where I_{out} is the converter's output current in A, η is the converter efficiency and $f_{type}(D)$ is the gain function that depends on whether we consider the converter as a buck, boost or a buck-boost.

The ideal voltage gain for a buck-boost converter (under ideal conditions and neglecting losses) is [127] :

$$\frac{V_{out}}{V_{in}} = \frac{D}{1-D} \tag{4.39}$$

The performance of the solar cell heavily depends on the incident solar irradiance (G) and the cell temperature (T). This dependency is modelled through the photocurrent I_{ph} which increases similar to linear with the irradiance but slightly with the temperature, the relation is given by [128]:

$$I_{ph} = \left[I_{sc,ref} + \alpha_{Isc}\left(T - T_{ref}\right)\right] \frac{G}{G_{ref}} \tag{4.40}$$

where $I_{sc,ref}$ is the short circuit current at reference conditions, α_{Isc} is the temperature coefficient of short-circuit current, $T_{ref}\ and\ G_{ref}$ are the reference temperature (25°C) and reference

irradiance (1000W/m²), then G is the instantaneous solar irradiance. G is introduced as a time-varying input to the solar cell block. The irradiance data used in this model is obtained from the Photovoltaic Geographical Information System (PVGIS) developed by the European Commission's Research Centre (JRC) [129]. PVGIS provides a long-term satellite derived datasets of the Global Horizontal Irradiance (GHI), which combines both direct and diffuse solar components incident on a horizontal plane. The dataset provides the average hourly irradiance values, derived from multi-year meteorological records for each month, producing at the end an average day for the chosen location.

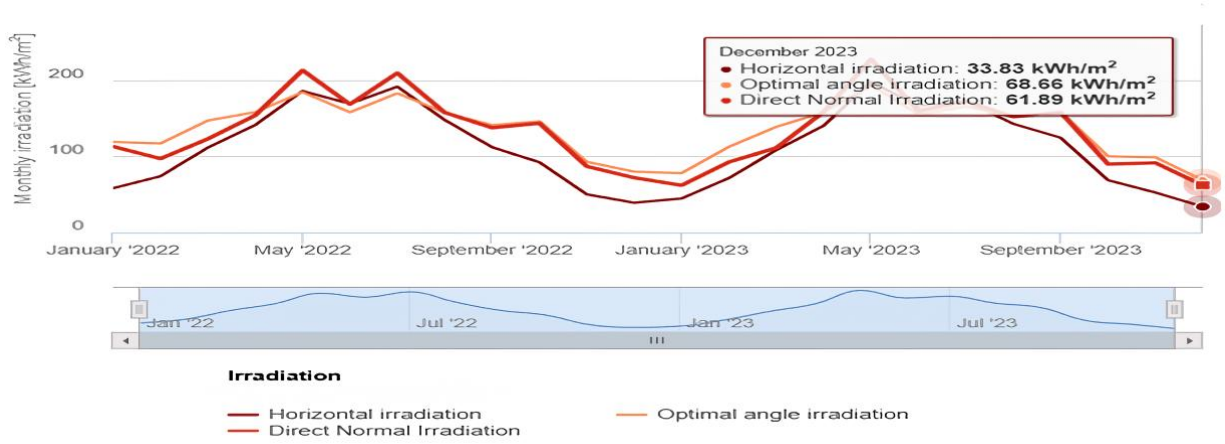

Figure 4.13: Annual solar irradiation profile from PVGIS (total monthly irradiance, kwh/m²)

4.2.2 The Energy Storage System

The battery is modelled as a dynamic system that exchanges energy with the rest of the microgrid through a DC/DC converter, controlled according to the state of charge SoC and a reference current signal I_{ref}. The ESS usually operates under two modes: a charging mode when there is excess power from the renewable energy generation and then a discharging mode when the power demand exceeds the available renewable power.

The models are based on an equivalent electrical circuit, where the voltage-current relationship is expressed as [130]:

$$V_{batt} = E_0 - R_{int} I_{batt} \tag{4.41}$$

Where V_{batt} is the termina voltage of the battery, E_0 is the open-circuit-voltage (OCV) which represents the theoretical battery voltage when no current flows, R_{int} is the internal resistance and I_{batt} is the instantaneous current.

The state of charge SoC is the ratio between the current charge and its maximum capacity, representing the available energy stored in the system. It evolves as a function of current and time as follows [131]:

$$\mathrm{SoC}(t) = \mathrm{SoC}(t_0) - \frac{1}{C_{\mathrm{batt}}} \int_{t_0}^{t} I_{\mathrm{batt}}(t)\ dt \tag{4.42}$$

This whole mechanism is ruled by the reference current I_{ref}. It controls the bidirectional operation of the battery system. It includes in its function both the solar current I_{solar} and the battery charge state (Q_{batt}). This ensures that when excess power is produced by the solar generator (I_{solar}>I_{load}), the surplus current charges the battery and in the opposite case it discharges so that a power balance across the system is maintained.

To implement the model in a time-stepped simulation, we rewrite (8) over a small interval Δt. Using $P = VI$and the battery's total energy capacity $E_{\mathrm{batt}} = V_{\mathrm{batt}}\, C_{\mathrm{batt}}$(Wh, or kWh with scaling), the SoC increment becomes:

$$\Delta\mathrm{SoC} \approx -\frac{I_{\mathrm{batt}}\,\Delta t}{C_{\mathrm{batt}}} = \frac{1}{E_{\mathrm{batt}}}\, P_{\mathrm{net}}\, \Delta t \tag{4.43}$$

where $P_{\mathrm{net}} > 0$ indicates that the ESS is charging and $P_{\mathrm{net}} < 0$ indicates that the ESS is discharging.

So then the SoC is updated according to the following discrete equation [*132*]:

$$SOC_{t+1} = SOC_t + E_{batt}\left(\eta_{ch} P_{ch} - \frac{P_{dis}}{\eta_{dis}}\right)\Delta t \tag{4.44}$$

Where P_{ch} and P_{dis} are the charging and discharging powers (kW), η_{ch} and η_{dis} are the charge and discharge efficiencies, E_{batt} is the total capacity of the battery (kWh). This model enforces the physical bounds :

$$SOC_{min} \le SOC_t \le SOC_{max}$$

$$-P_{dis}^{max} \le P_{batt}(t) \le P_{ch}^{max}$$

A saturation function ensures that the SoC remains between 0 and 1, even under numerical disturbances or ramp transients. This allows the model to remain numerically stable over long simulations while accurately representing the available stored energy.

The DC/DC converter in this acts as a link between the battery and the DC bus that connects the system. It allows the charging and the discharging to be controlled through a duty cycle. The output voltage of this is defined as [133]:

$$V_{out} = D\, V_{in} \tag{4.45}$$

where V_{in} is the battery voltage input. It continuously adjusts D to ensure that the actual battery current follows the reference current. It is a closed loop cycle. An important thing to note is that during charging mode the converter maintains a positive I_{ref} and in the discharge it is a negative current. Where C_{batt} is the nominal capacity of the battery in Ampere-hours (Ah).

4.2.3 Wind model

The subsystem of the wind turbine converts kinetic energy of moving air into electrical power using a simplified aerodynamic model. The instantaneous electrical power produced by the wind turbine is determined by [134]:

$$P_{\text{wind}} = \frac{1}{2}\, \rho\, A\, C_p\, v^3 \tag{4.46}$$

where ρ is the air density (1.225kg/m^3), A is the rotor swept area in m², C_p is the power coefficient representing aerodynamic efficiency, and v is the wind speed in meters per second (m/s). Since no experimental turbine data are available, the performance coefficient $C_p$was selected based on typical values reported in the literature. The theoretical upper limit of C_p, known as the Betz limit, is 0.593, while practical turbines generally achieve values between 0.35 and 0.45 depending on the blade geometry, tip speed ratio (λ), and pitch angle (β) [135]. For instance, studies have shown that a pitch angle of $\beta = 0°$yields a maximum $C_p$of approximately 0.45 for a 2 MW-class turbine, decreasing with larger pitch angles. Consequently, adopting $C_p = 0.4$ provides a realistic and conservative assumption representative of modern commercial turbines operating near optimal aerodynamic conditions.

The wind turbine output follows a cubic power relation between the cut-in V_{ci} , rater V_r and cut-out V_{co} speeds.

Below the cut-in speed or above the cut-out speed, the turbine produces no power. Between these limits, power increases cubically with wind velocity until the rated value P_{rated} is reached [136]:

$$P_{wind}(t) = 0 \qquad , v < v_{ci} \; or \; v \geq v_{co}$$

$$P_{wind}(t) = P_{rated} \frac{(v^3 - v_c i^3)}{(v_r^3 - v_c i^3)} \qquad , v_{ci} \leq v < v_r \tag{4.47}$$

$$P_{wind}(t) = P_{rated} \qquad , v_r \leq v < v_{co}$$

At each time step, the total renewable power available to the system is the sum of both solar and wind sources, this combined profile provides the energy supply that feeds both on the electrolyser and the battery according to the active control strategy.

Wind speed data were obtained from publicly available meteorological records, the dataset provides long-term monthly averages of maximum, minimum or extreme wind speeds over up to 5 years [137].

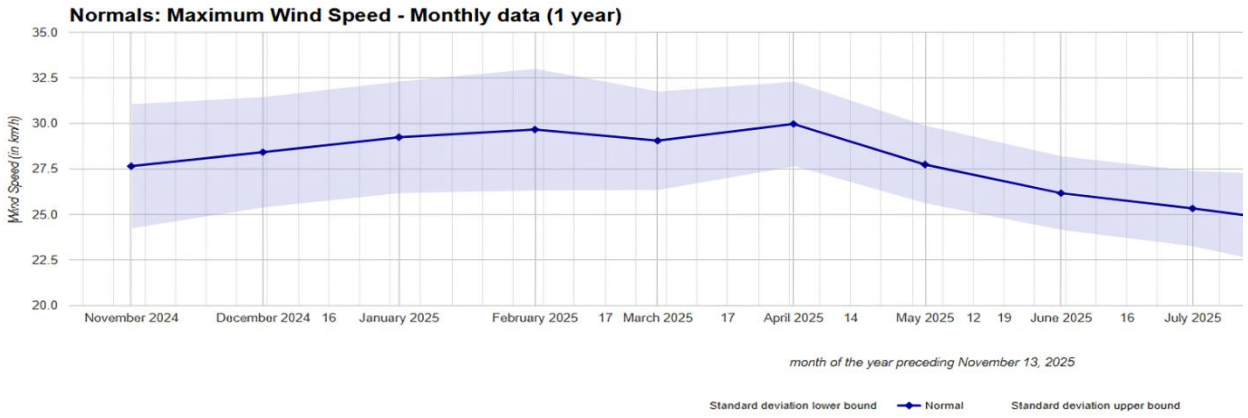

Figure 4.14: Example of a monthly maximum wind Speed profile of Montreal

4.2.4 Electrolyzer model

The electrolyzer module represents the conversion component that transforms the electrical energy supplied by the PV–Wind battery system into hydrogen through water electrolysis. Within the simulation environment, the electrolyzer is modeled as a dynamic load whose power input and hydrogen output evolve according to the available renewable power and operational constraints.

The instantaneous electrical power consumed by the electrolyzer is expressed as [138]:

$$P_{elec} = V_{stack} I_{el} \tag{4.48}$$

and the corresponding hydrogen production rate is obtained from the power-to-hydrogen conversion efficiency [39]:

$$\dot{m_{H_2}}(t) = \frac{P_{el}(t) \cdot \eta_{el}}{E_{H_2}} \tag{4.49}$$

where $E_{\mathrm{H_2}} = 33.33$ kWh/kg and the efficiency η_{el}varies with load and temperature [139].

In the hybrid microgrid simulation, the PEM electrolyser operates in interaction with the PV and battery subsystems. The power delivered to it is determined by the available renewable generation $P_{\mathrm{available}}$and the state of charge of the battery. During periods of high renewable output, the electrolyser runs near its nominal power to maximize hydrogen production, while under low-generation conditions it operates at partial load or idle to maintain system stability. The reference current is therefore computed dynamically as [140]:

$$I_{el,ref} = \frac{P_{available}}{V_{stack}} \tag{4.50}$$

This subsystem is defined by its minimum and maximum power ratings and by its operational ramp limit which prevents instantaneous power charges that could damage the stack, these operational constraints are expressed as:

$P_{el,min} \leq P_{el}(t) P_{el,max}$,

$$|P_{el}(t) - P_{el}(t-1)| \leq \Delta P_{el}^{max}$$

4.2.5 System Control and Optimization

After first analyzing how the solar and hybrid configurations behave without control, the final step if this study adds advanced control and optimization tools along with accurate weather data to improve efficiency and autonomy. The complete model includes a Model Predictive Controller (MPC) for real-time power management, a Digital Twin for predictive simulation and performance evaluation, and a Particle Swarm Optimization (PSO) algorithm for global parameter tuning.

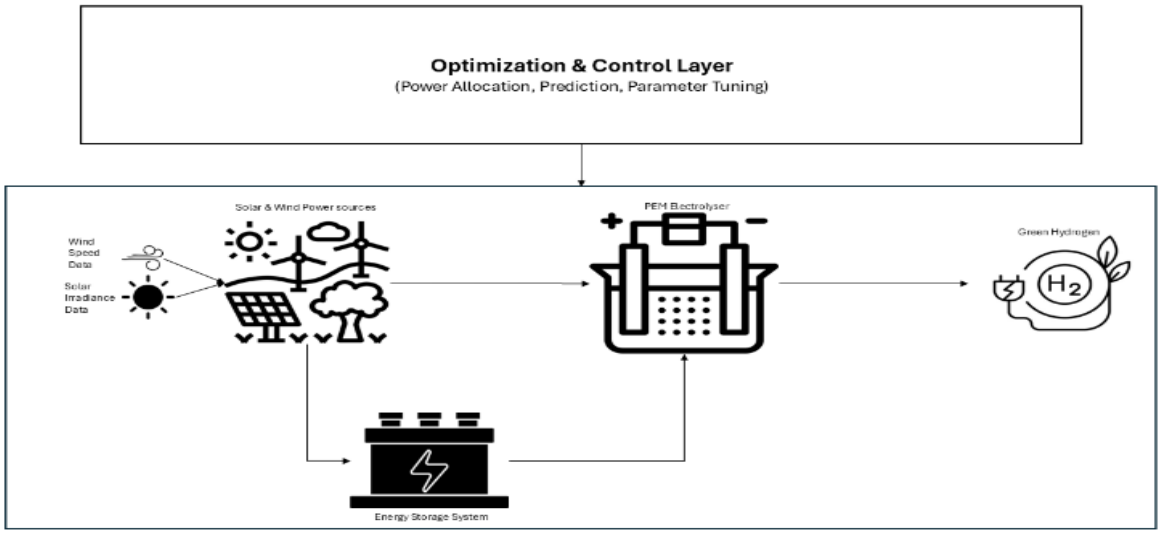

Figure 4.15: Schematic Representation of the Model implemented in Python

1) Model Predictive Control

An MPC was integrated to determine the optimal power distribution between the electrolyzer and the battery at each simulation step, based on the forecasted renewable generation and current battery state of charge (SoC).

The MPC optimization problem was formulated following the standard quadratic predictive control framework widely used in renewable hybrid systems [141]. However, the cost function used in this work was specifically tailored to the studied PV–battery–electrolyzer configuration, combining electrolyzer power tracking, SoC regulation, battery degradation minimization, and curtailment penalties to ensure efficient and stable hydrogen production.

$$J = \sum_{k=t}^{t+N-1} \left[w_1 (P_{\text{el}}(k) - P_{\text{set}})^2 + w_2 |P_{\text{batt}}(k)| + w_3 \left(SOC(k) - SOC_{\text{opt}} \right)^2 + w_4 P_{\text{curt}}(k) \right] \quad (4.51)$$

The optimization problem is subject to the following operational and physical constraints, which ensure that the MPC decisions remain feasible and safe under real conditions.

-*Power Balance:*

$$P_{\text{ren}}(k) = P_{\text{el}}(k) + P_{\text{batt}}(k) + P_{\text{curt}}(k) \quad (4.52)$$

At each time step, the available renewable power (P_{ren}) is shared between the electrolyzer, the battery, and any curtailed surplus. This equality maintains the overall energy balance within the microgrid.

-*Electrolyzer Power Limits:*

$$P_{\text{el,min}} \leq P_{\text{el}}(k) \leq P_{\text{el,max}}$$

The electrolyzer can only operate within its rated power range to avoid inefficiencies and prevent cell degradation under low or excessive load conditions.

-*Ramp Rate Limitation:*

$$|P_{el}(k) - P_{el}(k-1)| \leq \Delta P_{el}^{max}$$

This constraint restricts the rate of change of electrolyzer power between two consecutive time steps, accounting for the thermal and dynamic inertia of the stack and ensuring smooth transitions.

-*Battery Power Boundaries:*

$$-P_{batt}^{dis,max} \leq P_{batt}(k) \leq P_{batt}^{ch,max}$$

The battery is limited by its maximum charging and discharging capabilities, ensuring that converter and thermal specifications are respected.

-*SoC Boundaries:*

$$SoC_{min} \leq SoC(k) \leq SoC_{max}$$

The SoC must remain within safe operational limits to prevent overcharging and overdischarging. The controller predicts the SoC evolution over the entire horizon to guarantee that future control actions remain feasible.

-*Curtailment non-negativity:*

$$P_{curt}(k) \geq 0$$

Curtailment can only occur when renewable generation exceeds the demand of the electrolyzer and the battery's charging capacity; negative values are physically meaningless.

2) Digital Twin

The DT controller provides a simulation driven alternative, rather than solving a mathematical program at each time step, the DT relies on virtual experimentation within the same simulation environment to determine the best operational mode At each control step, the controller clones the current system state, including the battery state of charge (SoC) and the forecasted renewable generation and performs several short, parallel simulations over the prediction horizon [142].
Each internal simulation represents a possible operating strategy that can be improved. During each virtual scenario, the DT computes the time evolution of the power flows or SoC using the same physical constraints as the real system. At the end of the horizon, a performance score is calculated from standard decision-based control frameworks [143] then adapted to this system:

$$S = \sum_{t} P_{\text{el}}(t) - \alpha |SOC_{\text{end}} - SOC_{\text{opt}}| \tag{4.53}$$

The score favors strategies that maximize hydrogen production (P_{el}) while penalizing excessive deviation of the final SoC. The weight α adjusts the trade-off between production and battery-health. The strategy achieving the highest score S is selected.

3) Particle Swarm Optimization

This stage does not operate within the real-time control loop but serves as a diagnostic optimization layer, which verifies whether the operating conditions selected by the controller are close to the global optimum under the same environmental inputs.
Each particle in the swarm represents a possible combination of electrolyzer parameters :

$$x_i = \left[\eta_{el,rmax},\ P_{set} \right]$$

where $\eta_{el}$is the electrolyzer efficiency, $r_{max}$the ramp-rate limit, and P_{set} the operating setpoint. Particles evolve through iterative position and velocity updates given by [144]:

$$v_i^{(k+1)} = \omega v_i^{(k)} + c_1 r_1 \left(p_i^{best} - x_i^{(k)}\right) + c_2 r_2 \left(g^{best} - x_i^{(k)}\right) \tag{4.54}$$

$$x_i^{(k+1)} = x_i^{(k)} + v_i^{(k+1)} \tag{4.55}$$

where $v_i^{(k)}$ and $x_i^{(k)}$ denote the velocity and position of particle i at iteration k. ω is the inertia weight controlling exploration, c_1 and c_2 are acceleration coefficients that balance personal and global learning, while r_1 and r_2 are random numbers uniformly distributed in [0,1]. Each particle stores its best solution p_i^{best}, while the swarm tracks the overall global best g^{best}.

This is the multi-objective performance index $J(x)$:

$$J(x) = -\eta_{el} + w_r \, \bar{\Delta P} + w_s \, \sigma_{H_2} \tag{4.56}$$

Where $\bar{\Delta P}$ is the average ramp rate of the electrolyzer power signal and σ_{H_2} is the standard deviation of hourly hydrogen production.

Figure 4.16: Flowchart of the Particle Swarm Optimization (PSO) process applied to the hybrid solar–wind powered electrolyzer system.

4.3 Results and Discussion

To evaluate the performance of the proposed energy system, two main scenarios were investigated over 168h (a week), under two conditions: sunny days and cloudy days. A third investigation for the full year performance took place to understand the behavior of the system under extreme changes. The control architecture integrates three complementary layers, an MPC cost formulation, a DT look-ahead strategy selector and a PSO post optimization. The simulations operate with a discrete sampling time of 1-hour and a 24-hour prediction horizon. The MPC layer defines the objective landscape through four weighting parameters $w_1 = 0.5$ promoting hydrogen-production maximization, $w_2 = 0.1$ penalizing deviation from the optimal SoC reference, $w_3 = 0.5$ penalizing excessive battery usage, $w_4 = 1$ penalizing renewable curtailment. Building on this cost function, the DT controller evaluates three predefined strategies over the entire horizon: hydrogen maximization, battery charging and balanced operation. It computes for each trajectory the electrolyzer power, battery power and SoC evolution under the model constraints. A scalar score is then computed by combining total electrolyzer energy (proxy for hydrogen output) with the SoC deviation penalty. The strategy achieving the highest score is selected and only its first control action is applied. To further refine the system, a PSO post processing step is performed to tune the most influential parameters. It iteratively updates the particle's positions ($\eta_{el,rmax}$, P_{set}) to minimize the performance score.

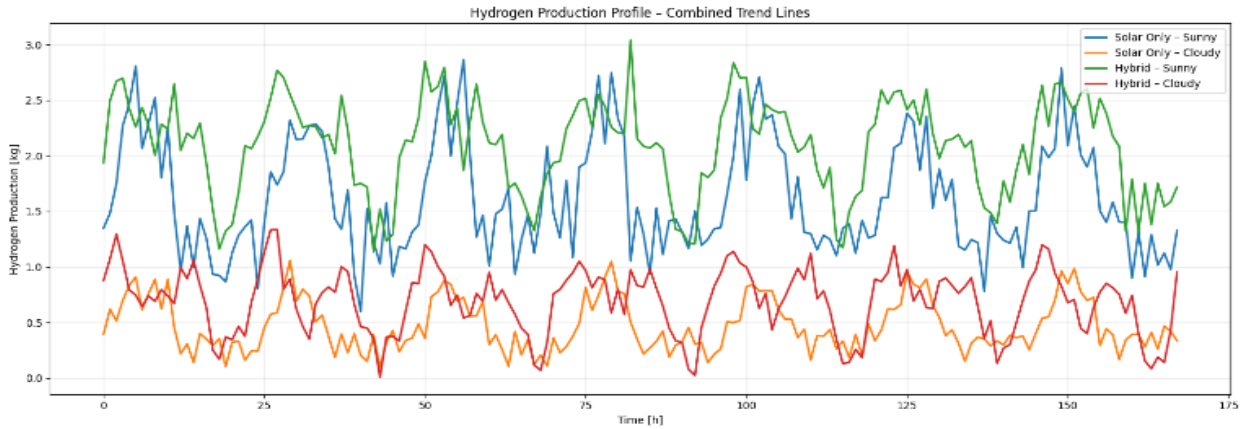

Figure 4.17: Comparative Hydrogen Production Profiles for Solar-Only and Hybrid Renewable Systems Under Sunny and Cloudy Conditions (Pre-Optimization)

The pre-optimization results show that hydrogen output closely tracks fluctuations in renewable generation, with solar-only and hybrid systems exhibiting strong sensitivity to irradiance and wind.

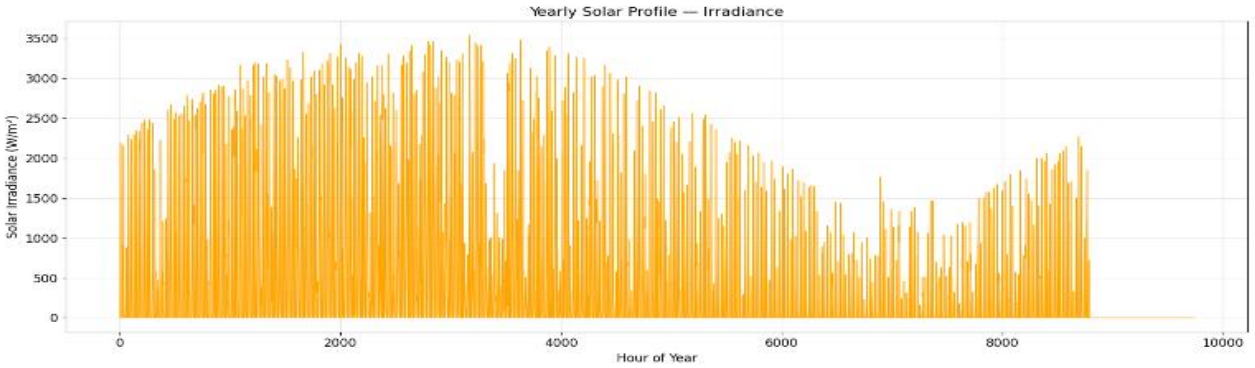

Figure 4.18: Yearly Solar Profile of Montreal derived from hourly data

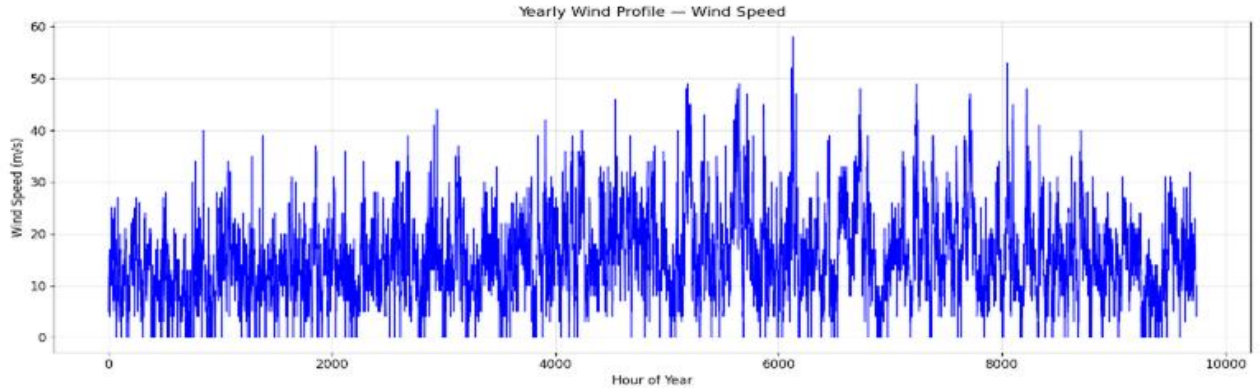

Figure 4.19: Yearly Wind Profile of Montreal derived from hourly data

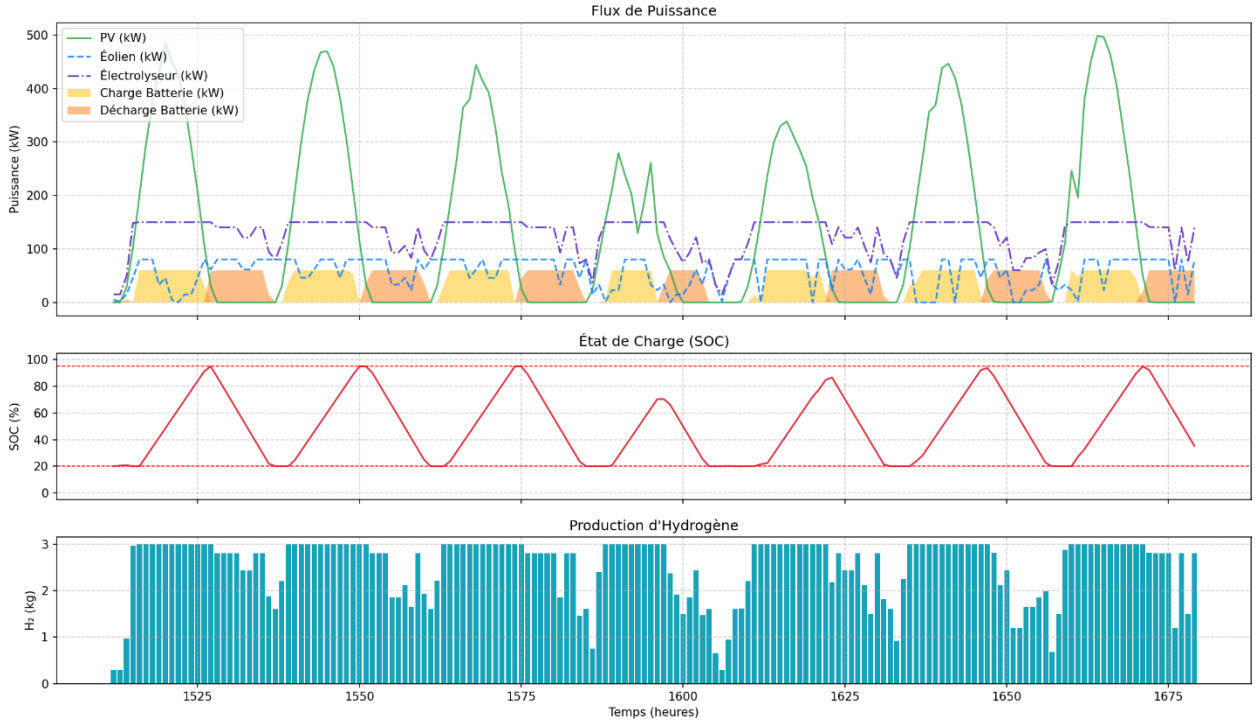

Figure 4.20: Power Flows, Battery SOC, and Hydrogen Production During Sunny days

During the representative sunny week (week 10), the hydrogen production profile exhibits limited sensitivity to short-term fluctuations in solar and wind generation. The system ensures that sufficient net power is maintained at the electrolyzer input throughout the diurnal cycle. Although the renewable inputs show significant intra-day variability, the coordinated action of the battery, contributing an average of 17% of the electrolyzer's hourly demand, effectively buffers high-frequency power deviations.

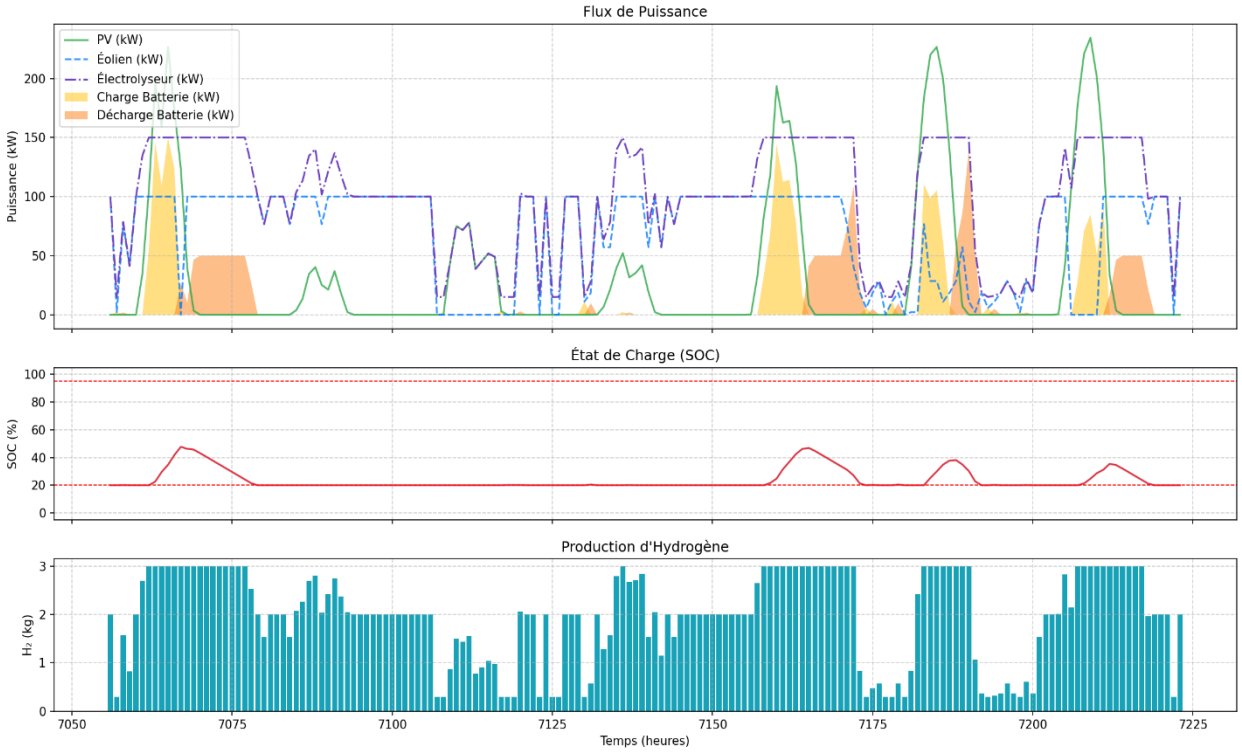

Figure 4.21: Power Flows, Battery SOC, and Hydrogen Production During Cloudy days

Week 43 represents the lowest renewable input conditions in the dataset with solar irradiance between 0 W/m² and 1076 W/m² . Despite the severe energy deficit, the system prevents production collapse. The electrolyzer continues to operate whenever short wind bursts occur and the battery, although constrained between 20% and 35% SoC still provides enough short-term support to maintain electrolyzer power above its minimal threshold. Hydrogen output is reduced between 0.5-2.5 kg/h.

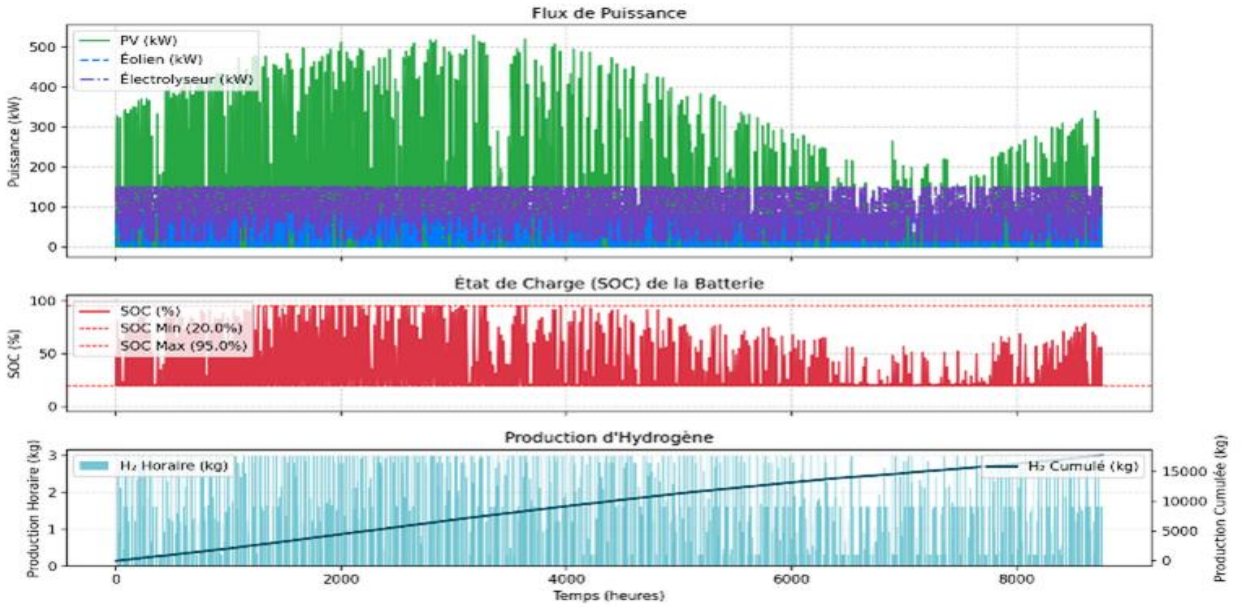

Figure 4.22: Annual Power Flows, Battery SOC, and Hydrogen Production

The annual simulation results confirm the effectiveness of the optimized hybrid configuration; the electrolyzer operates with a specific energy consumption of 50KWh/kg. The system maintains a high electrolyzer capacity factor of 0.68, significantly above typical off-grid hybrid installations, without relying on oversizing or excessive storage. Solar and wind supply 85% averagely over the year with the battery compensating for the rest preventing power shortages. The battery cycles within a 20-95% SoC window, charges fully in high-resource months and supports partial-load operation during renewable deficits. This design enables a total annual hydrogen production of nearly 17.8 tonnes. The cumulative hydrogen production grows consistently throughout the year, demonstrating that the system achieves ahigh utilization under realistic intermittency.

Table 4.2: Operating bounds of the Hybrid-PV-Wind-Battery-PEM Electrolyzer System

Component	Min	Max
PV Power (kW)	0	529.95
Wind Power (kW)	0	80
Electrolyzer Power (kW)	15	150
Battery Power (kW)	-60	60
Hydrogen Production (kg/h)	0.3	3
Battery SoC (%)	20%	95%
Curtailment (kW)	0	389

Table 4.3: State-of-the-Art Utilization Factors for PEM Electrolyzers in Hybrid Off-Grid Architectures

System Type	Value	Remarks	Ref.
Hybrid–wind–solar–battery (multiple global case studies)	53.7% (Miami case), up to ∼70% in wind-dominant climates	Wind-rich sites display high hydrogen production.	[44]
PV–and–Hybrid PV/Wind (System A & B)	9.20% (Sys A), 20.2% (Sys B)	Heavy PV-dependent systems display low capacity factors due to strong sensitivity to irradiance variability.	[45]
Hybrid–PV–Wind–Battery	41.5% (A), 65.5% (B), ≈66% (C), 82.0% (D)	Excess renewable generation and large battery sizing result in high hyrgoen production.	[46]
Hybrid off-grid systems (review)	61.34%	Benchmarks system-level performance limits in hybrid renewable configurations.	[47]
This Study	**67.6%**	**Achieves electrolyzer utilization levels typically requiring oversized renewable or storage systems.**	–

The hybrid solar-wind microgrid combined with MPC, DT and PSO achieves performance levels that exceed those reported for comparable off-grid PEM electrolyzer systems. The electrolyzer operates with an annual capacity factor of 0.676 which is aligned with the high end of hybrid systems that rely on substantial oversizing or large storage (up to 82% [46]). This configuration maintains a good utilization without oversizing the renewable generation: PV is sized at 1x the electrolyzer rating and wind at 0.53x, and the battery provides only 40% of the electrolyzer rated power with an average duration of 6.7h to maintain the system at a feasible economic standard. The system consistently stabilizes hydrogen production despite pronounced hourly fluctuations in irradiance and wind speed. During high-resource conditions, hydrogen output remains within a narrow 2-3kg/h band. The battery contributes an average of 13-17% of the electrolyzer input power depending on the week, primarily during morning-evening transitions and cloudy periods. This modest cycling contribution is enabled by the MPC penalty structure and DT trajectory selection, which together constrain the SoC to the 20-98% admissible band while preventing deep cycling and excessive ramping. Under worst-case renewable availability (week 43), hydrogen production remains between 0.5-2.5 kg/h, avoiding full outages despite sustained low irradiance and weak

wind speed values. The control architecture in the system preserves continuity of operation rather than prioritizing instantaneous yield. The PSO post-optimization improves the operational smoothness of the electrolyzer by tuning ramp limits and the swarm converges toward a solution that reduces hourly hydrogen standard deviation for a flatter production trajectory.

Relative to state-of-the-art performance benchmarks (Table II), the system achieves utilization levels typically reported only with a significant overcapacity, high curtailment ratios or very large battery banks. This software level optimization can substitute for hardware oversizing while improving the system's feasibility and reducing capital intensity in off-grid hydrogen microgrids.

4.4 Conclusion

This study tackled a hybrid solar-wind microgrid supplying a PEM electrolyzer along with a battery storage under real year-long meteorological conditions. The system demonstrated continuous hydrogen production without grid support or large energy storage systems or oversized renewable generation. It achieved a high annual utilization level and consistent specific energy performance while respecting the operational bounds. Sensitivity analysis on storage sizing confirms that doubling the battery capacity combined with a 67% PV and 25% wind oversizing, enables an electrolyzer capacity factor of 0.88, well above typical off-grid benchmarks. This validates that RE and storage oversizing can push capacity factors to be above 80% aligning with literature reported values. In addition, a fully interactive simulation interface was developed to allow users to modify system sizing, control settings and renewable inputs, making the entire framework reproducible and easily adaptable to new design scenarios or new geographical locations. Future work should extend the analysis to long-term component degradation, economic optimization and evaluation across diverse geographical locations to establish robust design guidelines for scalable off-grid hydrogen systems.

4.5 References

[102] S. G. Nnabuife, A. K. Hamzat, J. Whidborne, B. Kuang, and K. W. Jenkins, "Integration of renewable energy sources in tandem with electrolysis: A technology review for green hydrogen production," International Journal of Hydrogen Energy, vol. 107, pp. 218–240, Mar. 2025, doi: 10.1016/j.ijhydene.2024.06.342.

[103] K. K. Kurramovich, A. A. Abro, A. I. Vaseer, S. R. Ali, M. Murshed, and S. U. Khan, “Roadmap for carbon neutrality: the mediating role of clean energy development-related investments.,” Environ Sci Pollut Res, vol. 29, no. 23, pp. 34055–34074, Jan. 2022, doi: 10.1007/s11356-021-17985-3.

[104] Z. Ziobrowski and A. Rotkegel, “Assessment of Hydrogen Energy Industry Chain Based on Hydrogen Production Methods, Storage, and Utilization,” Energies, vol. 17, no. 8, p. 1808, Apr. 2024, doi: 10.3390/en17081808.

[105] F. Zhao, Z. Liu, X. Liu, and F. Bai, “A Review on Renewable Energy Transition under China’s Carbon Neutrality Target,” Sustainability, vol. 14, no. 22, p. 15006, Nov. 2022, doi: 10.3390/su142215006.

[106] P. Ge, Q. Hu, Q. Wu, Y. Ding, X. Dou, and Z. Wu, “Increasing operational flexibility of integrated energy systems by introducing power to hydrogen,” IET Renewable Power Gen, vol. 14, no. 3, pp. 372–380, Jan. 2020, doi: 10.1049/iet-rpg.2019.0663.

[107] J. Witte, H. Madi, U. Elber, P. Jansohn, and T. J. Schildhauer, “Grid-neutral hydrogen mobility: Dynamic modelling and techno-economic assessment of a renewable-powered hydrogen plant,” International Journal of Hydrogen Energy, vol. 78, pp. 52–67, June 2024, doi: 10.1016/j.ijhydene.2024.05.331.

[108] S. Samsatli and N. J. Samsatli, “The role of renewable hydrogen and inter-seasonal storage in decarbonising heat – Comprehensive optimisation of future renewable energy value chains,” Applied Energy, vol. 233–234, pp. 854–893, Nov. 2018, doi: 10.1016/j.apenergy.2018.09.159.

[109] R. Borup, J. Brouwer, and T. Krause, “Hydrogen is Essential for Industry and Transportation Decarbonization,” Electrochem. Soc. Interface, vol. 30, no. 4, pp. 79–84, Dec. 2021, doi: 10.1149/2.f18214if.

[110] A. Franco and M. Rocca, “Renewable Electricity and Green Hydrogen Integration for Decarbonization of ‘Hard-to-Abate’ Industrial Sectors,” Electricity, vol. 5, no. 3, pp. 471–490, July 2024, doi: 10.3390/electricity5030024.

[111] Q. Hassan, H. M. Salman, A. Z. Sameen, and S. Algburi, “Assessment of industrial-scale green hydrogen production using renewable energy,” Proceedings of the Institution of Mechanical

Engineers, Part A: Journal of Power and Energy, vol. 238, no. 3, pp. 569–587, Nov. 2023, doi: 10.1177/09576509231219339.

[112] W. Su, J. Wang, and J. Roh, “Stochastic Energy Scheduling in Microgrids With Intermittent Renewable Energy Resources,” IEEE Trans. Smart Grid, vol. 5, no. 4, pp. 1876–1883, July 2014, doi: 10.1109/tsg.2013.2280645.

[113] S. G. Nnabuife, A. K. Hamzat, K. A. Quainoo, C. K. Darko, and C. K. Agyemang, “Innovative Strategies for Combining Solar and Wind Energy with Green Hydrogen Systems,” Applied Sciences, vol. 14, no. 21, p. 9771, Oct. 2024, doi: 10.3390/app14219771.

[114] E. Kuhnert, K. Mayer, M. Heidinger, C. Rienessel, V. Hacker, and M. Bodner, “Impact of intermittent operation on photovoltaic-PEM electrolyzer systems: A degradation study based on accelerated stress testing,” International Journal of Hydrogen Energy, vol. 55, pp. 683–695, Dec. 2023, doi: 10.1016/j.ijhydene.2023.11.249.

[115] F. Dawood, M. Anda, and G. Shafiullah, “Stand-Alone Microgrid with 100% Renewable Energy: A Case Study with Hybrid Solar PV-Battery-Hydrogen,” Sustainability, vol. 12, no. 5, p. 2047, Mar. 2020, doi: 10.3390/su12052047.

[116] P. S. Kumar, K. V. S. M. Babu, V. Ramu, R. P. S. Chandrasena, and G. N. Srinivas, “Energy Management System for Small Scale Hybrid Wind Solar Battery Based Microgrid,” IEEE Access, vol. 8, pp. 8336–8345, Jan. 2020, doi: 10.1109/access.2020.2964052.

[117] R. Keller, E. Rauls, M. Hehemann, M. Müller, and M. Carmo, “An adaptive model-based feedforward temperature control of a 100 kW PEM electrolyzer,” Control Engineering Practice, vol. 120, p. 104992, Dec. 2021, doi: 10.1016/j.conengprac.2021.104992.

[118] M. Nasser, T. F. Megahed, S. Ookawara, H. Hassan, and M. Abd El-Hady, “A review of water electrolysis-based systems for hydrogen production using hybrid/solar/wind energy systems,” Environmental Science and Pollution Research, vol. 29, pp. 86994–87018, 2022.

[119] V. Papadopoulos, J. Desmet, J. Knockaert, and C. Develder, “Improving the utilization factor of a PEM electrolyser powered by a 15 MW PV park by combining wind power and battery storage – feasibility study,” International Journal of Hydrogen Energy, vol. 43, pp. 16468–16478, 2018.

[120] J. L. Llamazares, M. I. García, J. I. San Martín, and A. Ramos-Hernanz, “Stability analysis of an off-grid hybrid power plant for hydrogen production,” Renewable Energy and Power Quality Journal, vol. 23, 2025.

[121] B. W. Tuinema, M. J. M. van der Meulen, P. H. F. M. Leufkens, and H. Polinder, “Modelling of large-size electrolysers for real-time simulation and study of the possibility of frequency support by electrolysers,” unpublished manuscript, 2020.

[122] H. Khajeh, S. Seyyedeh-Barhagh, and H. Laaksonen, “Optimized operation of hybrid wind-hydrogen system to provide flexibility for transmission system needs,” IEEE Transactions on Sustainable Energy, vol. 16, no. 3, pp. 1576–1587, Jul. 2025.

[123] MathWorks, “Solar Cell,” Simscape Electrical Documentation, 2024. [Online]. Available: https://www.mathworks.com/help/sps/ref/solarcell.html

[124] S. Singh, S. Manna, A. K. Akella, and M. I. Hasan Mansoori, “Implementation of Perturb & Observe MPPT Technique using Boost converter in PV System,” Institute Of Electrical Electronics Engineers, July 2020, pp. 1–4. doi: 10.1109/cispsse49931.2020.9212203.

[125] MathWorks, “Average-Value DC–DC Converter,” Simscape Electrical Documentation, 2024. [Online]. Available: https://www.mathworks.com/help/sps/ref/averagevaluedcdcconverter.html

[126] P. Sanjeevikumar, F. Blaabjerg, P. W. Wheeler, J. Loncarski, and G. Grandi, “A simple MPPT algorithm for novel PV power generation system by high output voltage DC-DC boost converter,” Institute Of Electrical Electronics Engineers, Jan. 2015, pp. 214–220. doi: 10.1109/isie.2015.7281471.

[127] M. Hosseinpour, A. Seifi, S. H. Hosseini, and M. Ahmadi, “A new transformerless buck-boost converter with improved voltage gain and continuous input current,” IET Power Electronics, vol. 17, no. 4, pp. 534–550, Feb. 2024, doi: 10.1049/pel2.12671.

[128] MathWorks, “Solar Cell,” Simscape Electrical Documentation, 2024. [Online]. Available: https://www.mathworks.com/help/sps/ref/solarcell.html

[129] European Commission, Joint Research Centre (JRC), Photovoltaic Geographical Information System (PVGIS), 2024. [Online]. Available: https://re.jrc.ec.europa.eu/pvg_tools/en/

[130] M. J. Rana and M. A. Abido, “Energy management in DC microgrid with energy storage and model predictive controlled AC–DC converter,” IET Generation Trans & Dist, vol. 11, no. 15, pp. 3694–3702, July 2017, doi: 10.1049/iet-gtd.2016.1934.

[131] S. J. Moura, M. Krstic, and N. A. Chaturvedi, “Adaptive PDE Observer for Battery SOC/SOH Estimation,” American Society Of Mechanical Engineers, Oct. 2012, pp. 101–110.

[132] M. A. Syed and M. Khalid, “An Intelligent Model Predictive Control Strategy for Stable Solar-Wind Renewable Power Dispatch Coupled with Hydrogen Electrolyzer and Battery Energy Storage,” International Journal of Energy Research, vol. 2023, pp. 1–17, Mar. 2023, doi: 10.1155/2023/4531054.

[133] H. A. Mohamed, H. A. Khattab, G. A. Morsy, and A. Mobarka, “Design, control and performance analysis of DC-DC boost converter for stand-alone PV system,” Institute Of Electrical Electronics Engineers, Dec. 2016, pp. 101–106. doi: 10.1109/mepcon.2016.7836878.

[134] R. Wagner, S. M. Pedersen, M. S. Courtney, I. Antoniou, and H. E. Jørgensen, “The influence of the wind speed profile on wind turbine performance measurements,” Wind Energy, vol. 12, no. 4, pp. 348–362, Sept. 2008, doi: 10.1002/we.297.

[135] M. Bilgili, S. Tumse, B. Sahin, and M. Tontu, “Effect of Growth in Turbine Size on Rotor Aerodynamic Performance of Modern Commercial Large-Scale Wind Turbines,” Arab J Sci Eng, vol. 46, no. 8, pp. 7185–7195, Jan. 2021, doi: 10.1007/s13369-021-05364-6.

[136] N. Jargalsaikhan, H. Masrur, A. Iqbal, S. S. Rangarajan, S. Byambaa, and T. Senjyu, “A control algorithm to increase the efficient operation of wind energy conversion systems under extreme wind conditions,” Energy Reports, vol. 8, pp. 11429–11439, Sept. 2022, doi: 10.1016/j.egyr.2022.08.243.

[137] “Data Download for Montréal,” WeatherStats, Accessed: Nov. 24, 2025. *Online*. Available: https://montreal.weatherstats.ca/download.html

[138] S. Sood et al., “Generic Dynamical Model of PEM Electrolyser under Intermittent Sources,” Energies, vol. 13, no. 24, p. 6556, Dec. 2020, doi: 10.3390/en13246556.

[139] S. Gharibzadeh, R. Motallebzadeh, S. Jafarmadar, and A. Ebrahimpour, “Comprehensive optimization of an integrated energy system for power, hydrogen, and freshwater generation using high-temperature PEM fuel cell,” Case Studies in Thermal Engineering, vol. 56, p. 104181, Mar. 2024, doi: 10.1016/j.csite.2024.104181.

[140] S. Sood et al., “Generic Dynamical Model of PEM Electrolyser under Intermittent Sources,” Energies, vol. 13, no. 24, p. 6556, Dec. 2020, doi: 10.3390/en13246556.

[141] M. A. Arce, J. M. Guerrero, A. J. Calderón, and F. Jurado, “Model predictive control of hybrid renewable energy systems with battery storage and electrolyzer for hydrogen production,” Renewable Energy, vol. 141, pp. 300–312, Oct. 2019.

[142] A. B. Shafiee, H. Karimi, and M. Saif, “Digital twin-based predictive control for renewable-hydrogen hybrid systems,” IEEE Transactions on Energy Conversion, vol. 37, no. 3, pp. 2158–2170, Sept. 2022.

[143] J. Kennedy and R. Eberhart, “Particle swarm optimization,” in Proceedings of the IEEE International Conference on Neural Networks, Perth, WA, Australia, vol. 4, pp. 1942–1948, Dec. 1995.

[144] A. Khalilnejad, A. Sundararajan, and A. I. Sarwat, “Optimal design of hybrid wind/photovoltaic electrolyzer for maximum hydrogen production using imperialist competitive algorithm,” Journal of Modern Power Systems and Clean Energy, vol. 6, no. 1, pp. 40–49, 2018.

[145] M. Alharthi, “An analysis of hybrid renewable energy-based hydrogen production and power supply for off-grid systems,” Processes, vol. 12, 2024.

[146] T. Papadopoulos, P. Stathopoulos, and P. Tsiakaras, “Improving the utilization factor of a PEM electrolyzer powered by a 15 MW solar park,” International Journal of Hydrogen Energy, vol. 43, no. 1, pp. 214–226, 2018.

[147] M. Nasser, T. F. Megahed, S. Ookawara, and H. Hassan, “A review of water electrolysis–based systems for hydrogen production using hybrid/solar/wind energy systems,” Environmental Science and Pollution Research, vol. 29, pp. 86994–87018, 2022.

CHAPTER 5 RESULTS AND DISCUSSION

This chapter presents the results of the simulation and optimization process for the solar microgrid, the hybrid solar-wind microgrid and the final optimized configuration. The performance of each system is analyzed across several key metrics, including energy generation, storage behaviour and overall hydrogen production. These results are divided into three main sections: first the performance of the solar microgrid, followed by the solar wind hybrid system and finally the optimized system integrating PSO, MPC and DT technologies. Each section will present an analysis of the system behaviour, these results are examined to assess the effectiveness of each configuration highlighting the contribution of each component to the system's overall operation and gradually observe how they evolve.

5.1 Solar Power System

In this section, we will evaluate the performance of a basic solar power generation system under varying environmental conditions, focusing on two distinct scenarios: sunny days and cloudy days. The solar power output in these conditions is highly dependent on the weather affecting therefore the use of batteries and the electrolyser's operation.

The system being analysed is not optimized, it lacks advanced control or optimization mechanismes and relies on basic functionalities such as simple charging and discharging cycles for the batteries as well as generic weather data disregarding major fluctuations during the day. As a result, while the system does provide a foundation for understanding solar generation and how the electrolyser behaves, it does not yet account for more advanced energy management strategies.

The following graphs illustrate the solar power profiles for each scenario and will also show the system's dependence on the battery to store energy and supply the electrolyser at night. Additionally, we will view the hydrogen production over the course of the week, which is directly impacted by the available solar energy and battery storage capabilities. By comparing these profiles, we can assess the limitations of the system and understand where there needs to be interference.

Case1: Sunny Day

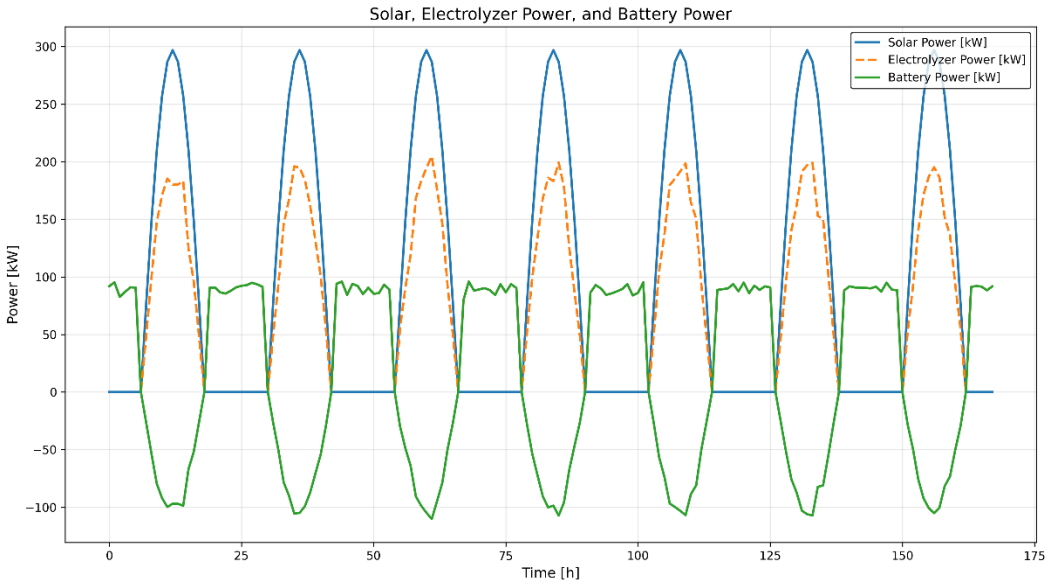

Figure 5.23: Solar, Electrolyzer Power, and Battery Power for Sunny Day Profile

The solar profile follows a typical sinusoidal curve due to the time-of-day variation in irradiance, where it increases in the morning, peaks at midday and decreases towards the evening reflecting a generic day without real world data but enough to present a sunny day at perfect conditions. The electrolyser is responsible for converting that electrical energy into hydrogen. As shown in the figure, during daylight hours, the electrolyser's power demand directly follows the available solar power. The solar system is designed to provide 2316kwh/day for the electrolyser, which is what it needs to produce 35kg of hydrogen daily [148]. To satisfy it, it needs to produce a surplus that will be stored to the batteries. Therefore, the electrolyser operates with the assumption that 65% of solar power is allocated to it. The electrolyser functions during the day as stated following the solar power with some fluctuations during peak sun hours and the battery is charging using that surplus power. The observed fluctuations in both electrolyser power and battery power are primarily due to the lack of advanced control mechanisms within the system. Without the right energy management, this system relies on simple, predefined cycles. So, the power demand experiences uncontrolled variability which leads to inefficiencies in energy utilization. During nighttime, there is no solar generation due to lack of irradiance, therefore as observed in the figure, the battery discharges and the electrolyser is powered by that battery discharge therefore following the same pattern.

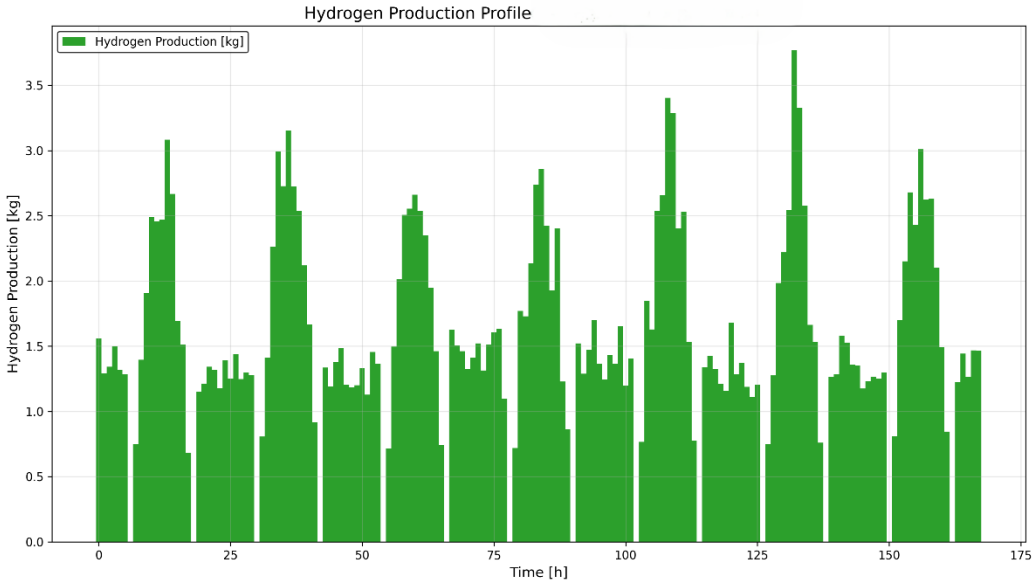

Figure 5.24: Hourly Hydrogen Production Profile on a Sunny Day

The hourly hydrogen production profile displays fluctuations in hydrogen production over a one-week period, based on the energy that was available to the electrolyser, the graphs illustrate how the production varies significantly hour by hour, with notable instabilities in the system. During the day, when the electrolyser is powered by available energy, production is higher, but it still is subject to random fluctuations due to the energy supply. At night when the electrolyser relies on battery power, hydrogen production drops and the instability continues as the battery fully discharges. This non uniform production decreases the overall hydrogen production over time.

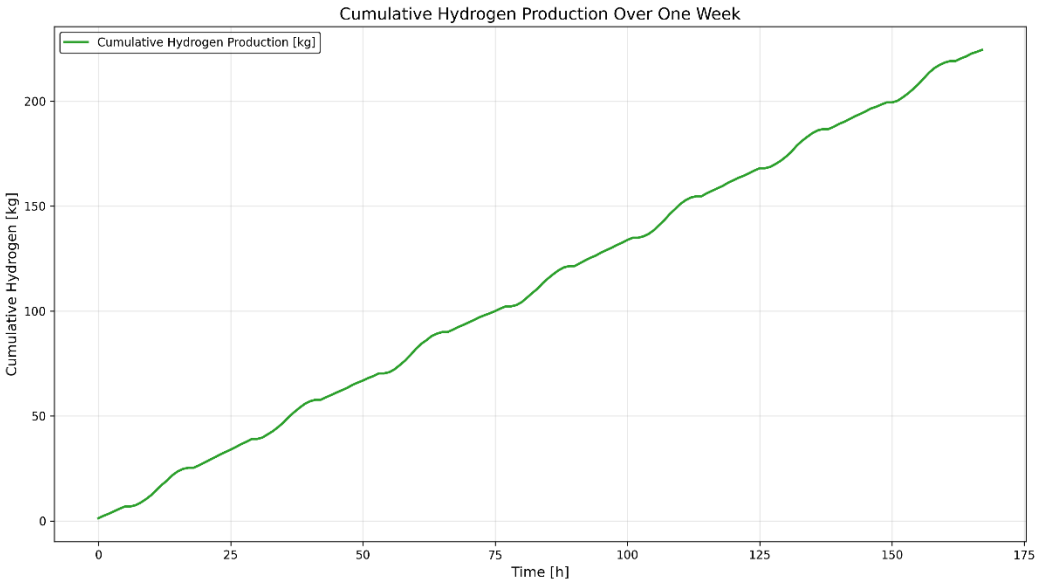

Figure 5.25: Cumulative Hydrogen Production Over One Week

This figure shows the hydrogen output over one week; it shows that the system almost meets the target of 35kg of hydrogen a day but not fully. This shortfall is primarily due to the energy inefficiencies including the electrolyser's conversion inefficiencies and the losses that occur between charging and discharging that result in less usable energy than required. Furthermore, the battery capacity could be sized up to meet the demand however it would be unrealistic.

Case2: Cloudy day

For this case, the data for the solar irradiance follow a generic cloudy day with minimal irradiance values that still peak a little around the afternoon then drop completely during the night. It also fluctuates a lot during the day to show an unstable pattern. The figure below will display the solar power profile along with the electrolyser and battery power profile:

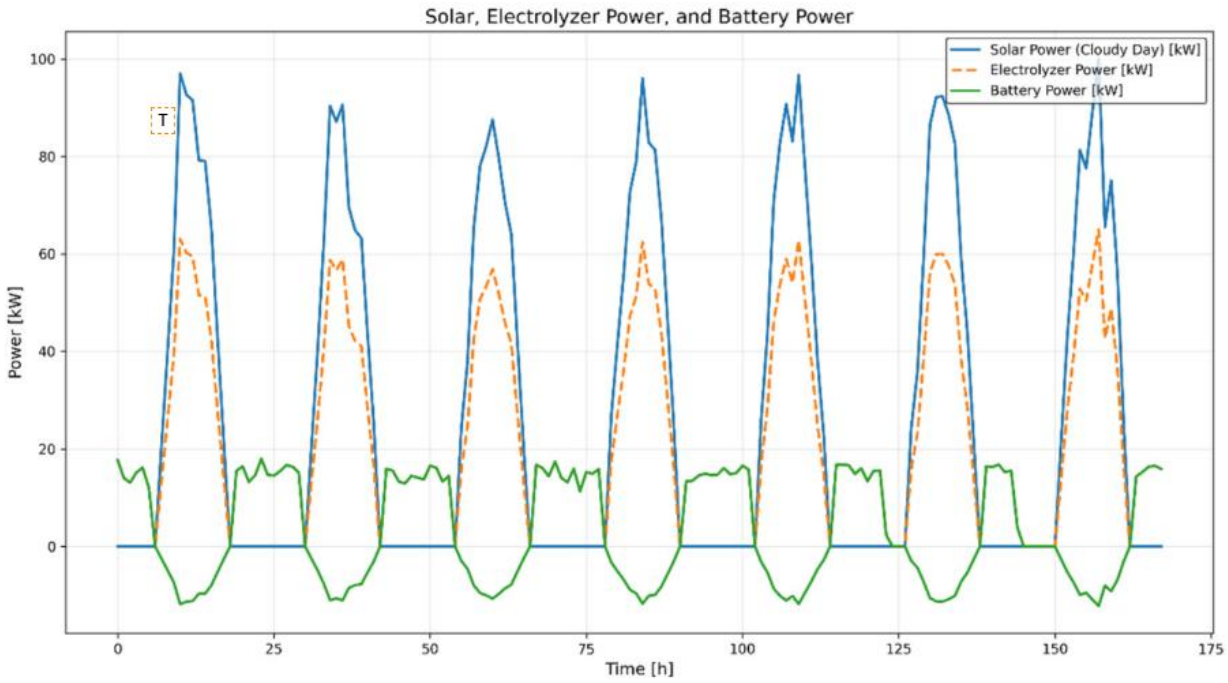

Figure 5.26: Solar, Electrolyzer Power, and Battery Power for Cloudy Day Profile

The graph shows the power profile over a 7day period under cloudy conditions where irradiance is reduced compared to sunny conditions. The solar power curve demonstrates a more flattened profile with peaks reaching a maximum of 60kw, significantly lower than the output observed during sunny days. This directly impacts the electrolyser's power where it operates at reduced capacity. The battery shows increases fluctuations reflecting the need for a battery discharge more frequently. Since the solar generation is low, the system relies heavily on the battery storage to maintain the electrolyser operation during daytime and nighttime. As a result, the battery discharges at irregular intervals throughout the day overall affecting the system's ability to supply the electrolyser with the adequate power.

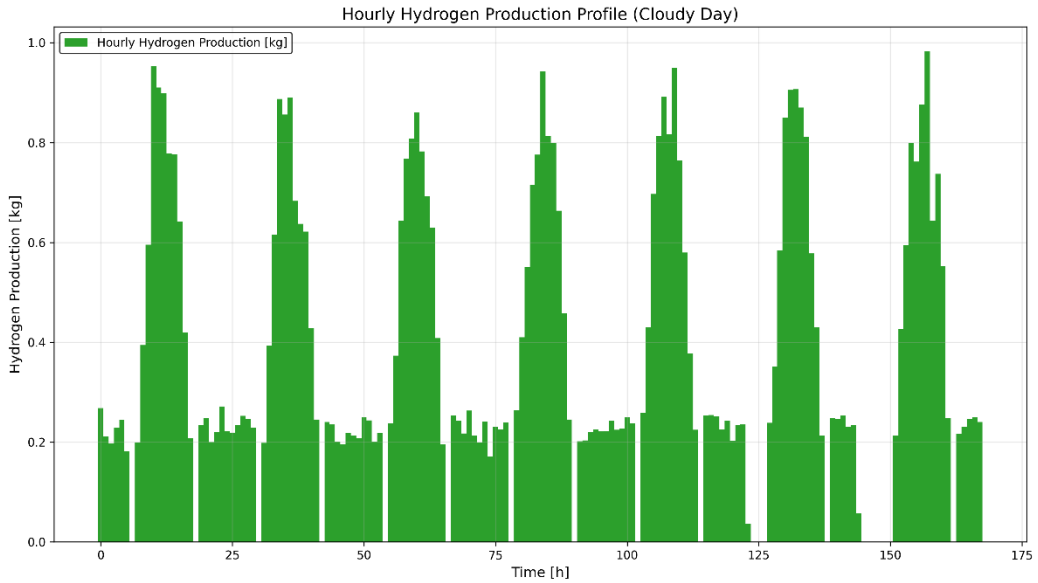

Figure 5.27: Hourly Hyrogen Production Profile on a Cloudy Day

The overall hydrogen production is noticeably lower compared to sunny days with smaller peaks and increased variability. The system relies more on the battery system leading to a more erratic production as energy from the solar panels is insufficient. This graph demonstrates the impact of cloudy conditions on the electrolyser's ability to maintain consistent hydrogen output, resulting in lower and more unstable production throughout the day and night highlighting the need for an alternative solution if the goal is to have a stable hydrogen production.

5.2 Hybrid Solar and Wind System

The hybrid configuration combining PV and Wind energy was simulated to evaluate its capacity to maintaine the continuous operation of the electrolyser system. Unlike the purely solar configuration, this model introduces a complementary energy source to address production intermittency and improve the nighttime energy supply. The objective here it to assess how this addition will affect the overall power balance, the charging and discharging behaviour of the battery system and the stability of the electrolyser's hydrogen production over a week.

This part is structured the same as the solar system section, it will show the system's operation under two cases: a sunny day and a cloudy day. The data used as well are the same used for the solar system and for the wind it also follows a generic profile for wind speed during different

climates. The idea to add the wind comes from the need to compensate for energy during nighttime especially at times when solar irradiance is very low and also reduce the battery dependence.

Throughout the 7day simulation, the system dynamically allocates the available renewable power between the electrolyser and the battery.

Case1: Sunny Day

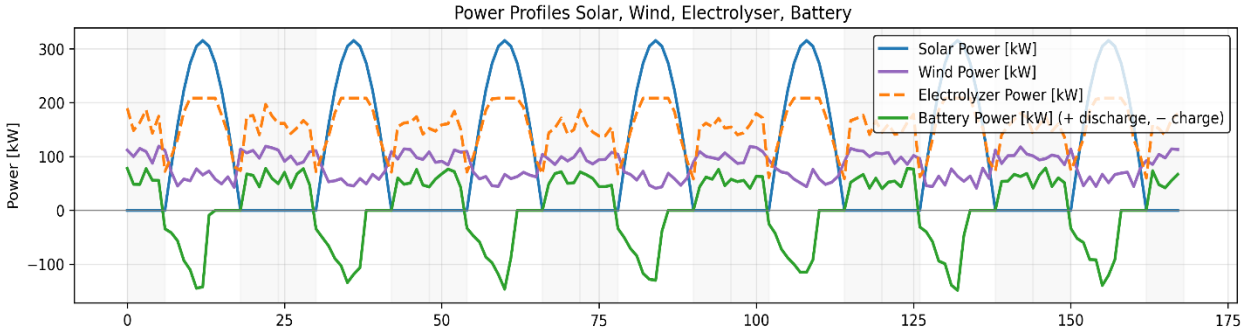

Figure 5.28: Solar, Wind , Electrolyser and Battery power for a Sunny Day Profile

The power profile for the sunny day shows a complementarity between solar and wind generation in maintaining a balance supply to the electrolyser. The solar power curve follows a clear pattern of peaking around midday and dropping to zero at night while the wind remained relatively stable and lower with moderate fluctuations extending throughout the day and the night. The battery is charging actively during periods of high solar irradiance and discharges at night to supplement wind energy and sustain the electrolyser's operation.

The electrolyser power closely follows the solar generation during the day, operating near its nominal range and remains consistently above the wind profile at night due to the additional support from the battery. This ensures a more stable hydrogen production even during solar inactivity. The overall profile shows a good improvement and mitigation of energy gaps showing how solar and wind energy complement each other well during periods of sunny days.

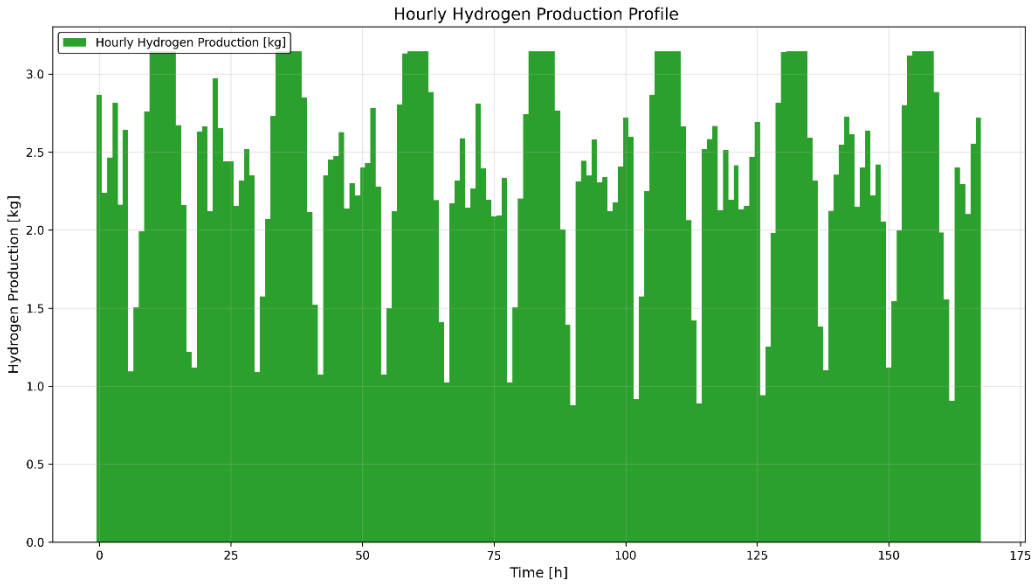

Figure 5.29: Hourly Hydrogen Production Profile on a Sunny Day

This figure shows that the hybrid solar wind system sustains a relatively continuous hydrogen output throughout the simulated week, with clear variations linked to fluctuations. Periods of elevated hydrogen production correspond to hours of strong solar input and combined wind support, while lower segments are due to reduced energy availability or battery recharging intervals. Although this system maintains a nonzero hydrogen production generation even during nighttime, the production remains uneven with recurrent short-term fluctuations. Now we will see how the system behaves under cloudy conditions to assess whether its efficiency at producing hydrogen is affected.

Case2: Cloudy Days

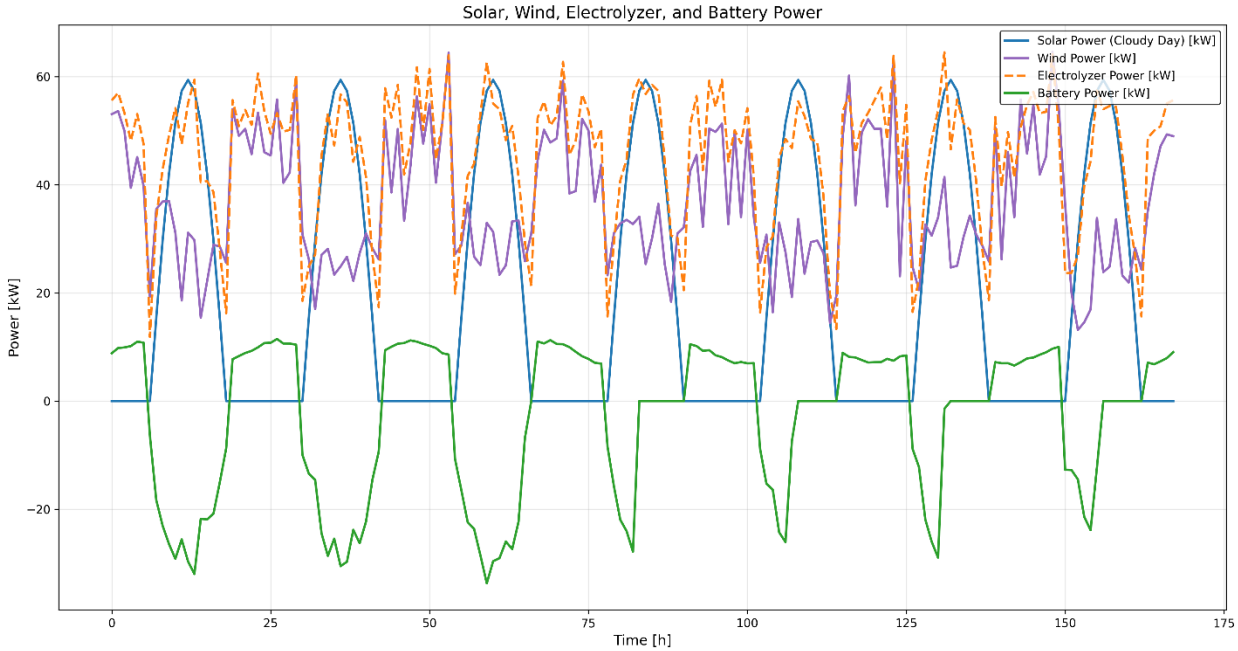

Figure 5.30: Solar, Wind, Electrolyser and Battery Power on a Cloudy Day

This shows us how the hybrid system behaves on a cloudy day when solar, wind and the battery all work together to power the electrolyser. During the day, the solar panels provide low amount of of power, but it is the one responsible for powering the electrolyser and charging the battery with low amountss of power considering the wind power is low during the day. At night, the electrolyser keeps running at a lower but steady rate by taking energy from the wind and the battery. Because of this combined input, the electrolyser's power stays above the wind curve, showing how the battery is helping maintain the operation. However, as seen in the figure the battery charges and discharges at slow rates, this keeps the hydrogen production going despite low power input but clearly not enough to generate the needed amounts of hydrogen.

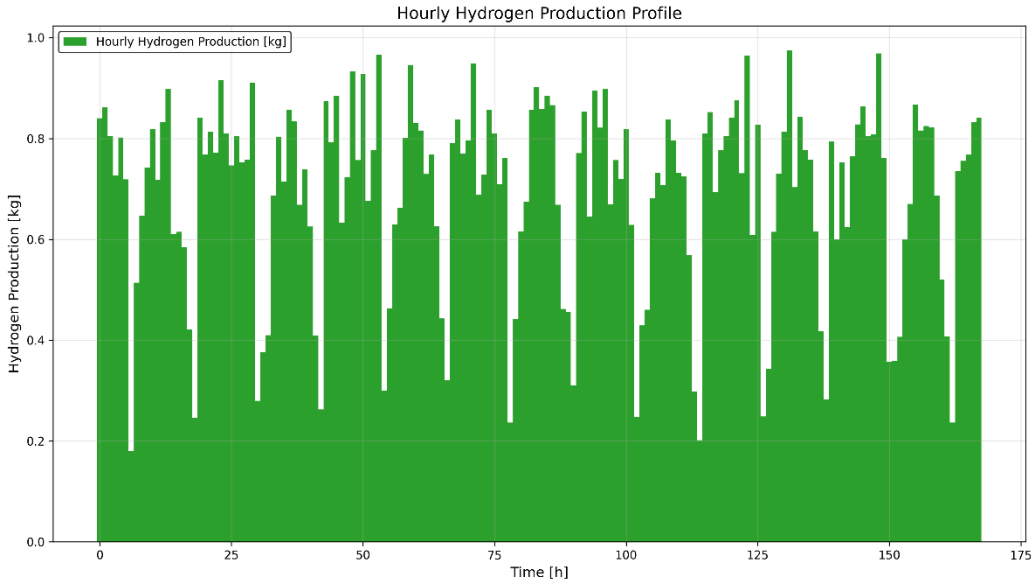

Figure 5.31: Hourly Hydrogen Production Profile on a Cloudy Day

This profile shows a clear improvement compared to the standalone solar configuration, particularly during nighttime hours. The addition of wind energy and battery storage allows the electrolyser to maintain partial operation after sunset, preventing complete shutdown and enabling more consistent hydrogen generation throughout the 24-hour cycle. This hybrid configuration smooths the production curve a little and reduces long periods of inactivity, highlighting the benefit of adding another renewable source. However, despite this improvement, the overall hydrogen production output remains below the required target of 35kg. The fluctuations and reduced nighttime production indicate that while the system gains resilience, it still operates under minimal energy management.

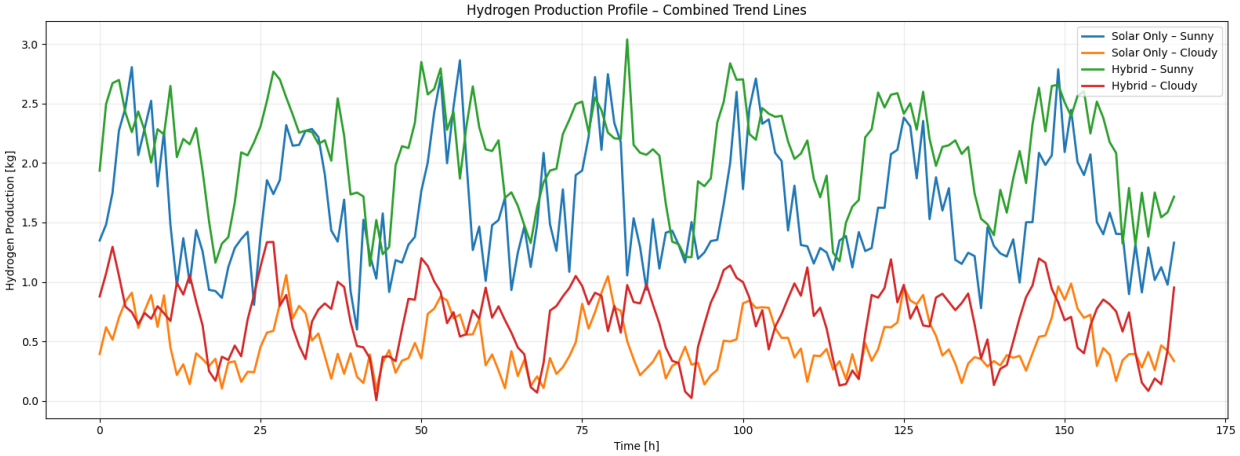

Figure 5.32: Hydrogen Production Profile Combined Trends

The combined hydrogen production trend reveals a system that is highly dynamic and strongly dependent on the underlying energy source characteristics, particularly solar irradiance and wind availability. Across all four scenarios, the hourly hydrogen output shows big fluctuations, reflecting the intermittent and variable nature of renewable energy inputs. These variations point to the need for advanced control strategies and optimization mechanisms to coordinate energy flow between the subsystems. Proper optimization would help maximize the hydrogen yield, stabilize operation under fluctuations especially considering the weather data used for these systems are generic while real-world data is far more fluctuating and intermittent.

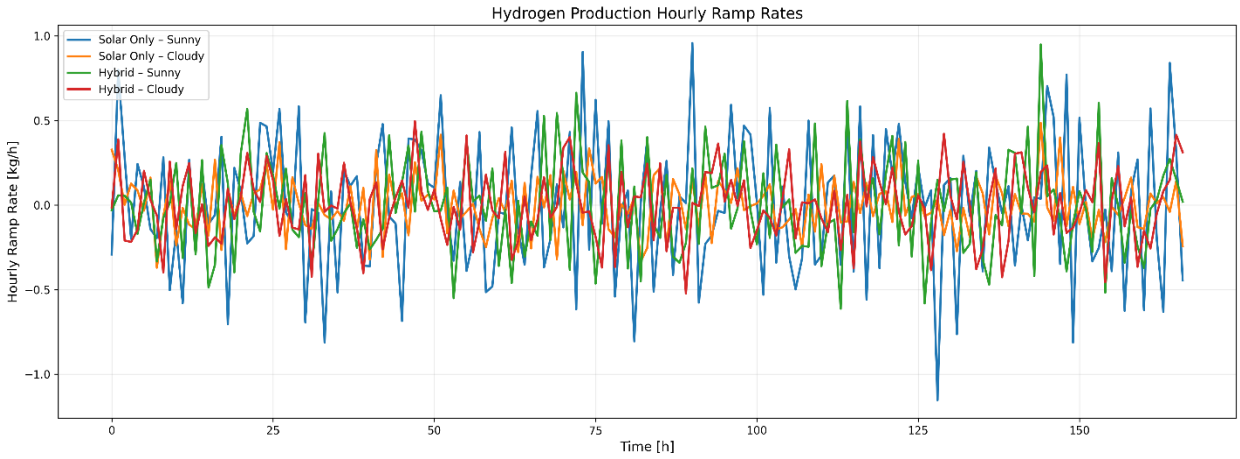

Figure 5.33: Hydrogen Production Hourly Ramp Rate

The ramp rate analysis shows how strongly hydrogen production depends on the variability of the renewable energy sources. The solar only system exhibits the most sever fluctuations with sharp and negative spikes caused by the rapid changes in irradiance, indicating highly unstable input power and significant stress on the electrolyzer. The hybrid system produces more stable ramp rates for both sunny and cloudy conditions as wind energy smooths out the rapid swings. Overall, this comparison proves how hybridization reduces variability and reduces ramp-rate stress on the PEM electrolyzer. However it is not enough as the system exhibits still exhibits major fluctuations.

5.3 Hybrid Solar Wind Optimized System

For this section, the same approach will follow for the results starting with the behaviour of the system under high irradiance during sunny days.

Case 1:Sunny Days

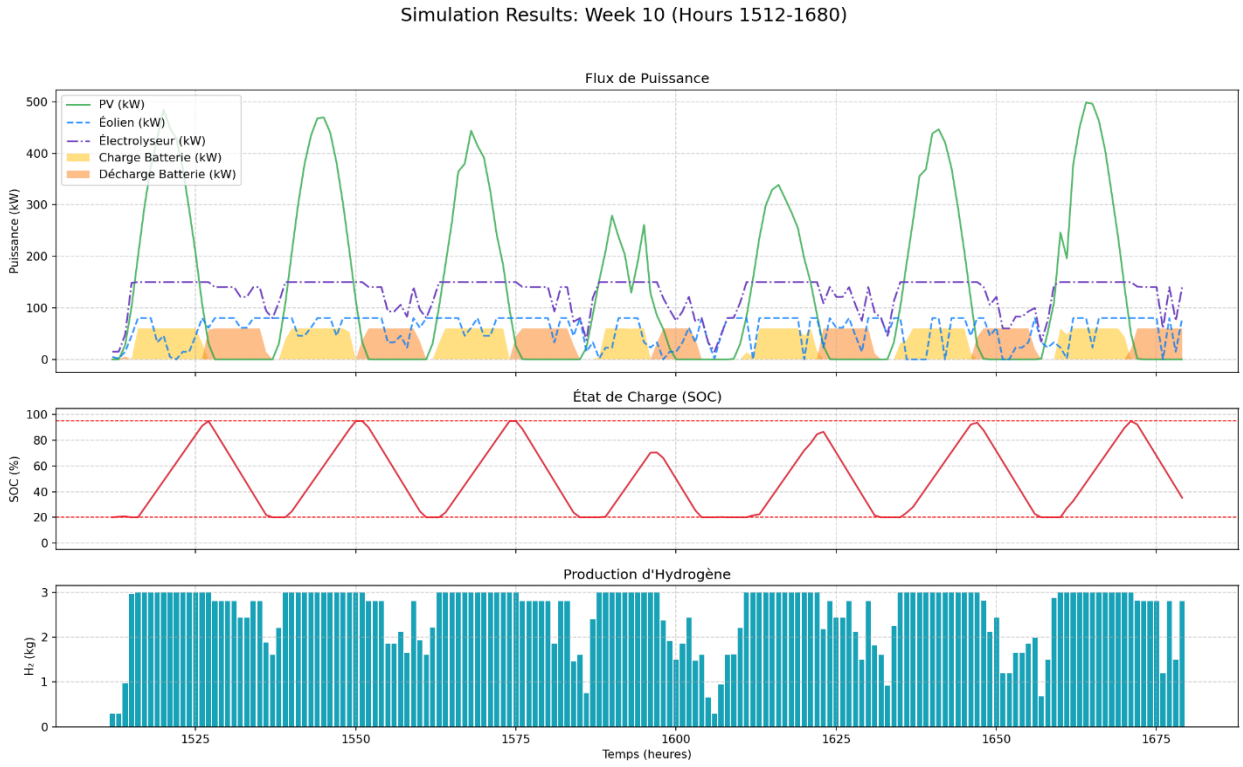

Figure 5.34: Power Flows, Battery SOC, and Hydrogen Production During Sunny days

The hydrogen production throughout a sunny week is not heavily dependent on the fluctuations in solar and wind power because the optimized hybrid sizing and PSO-based control strategy maintain adequate power to the electrolyzer throughout the day. The combined PV and Wind profile, supported by the battery at 17%, reducing the impact of short-term variability on the electrolyzer's operating power. As a result the hydrogen ouput remains within a consistent range of 2-3kg/h despite marked changes in renewable generation.

Case2: Cloudy days

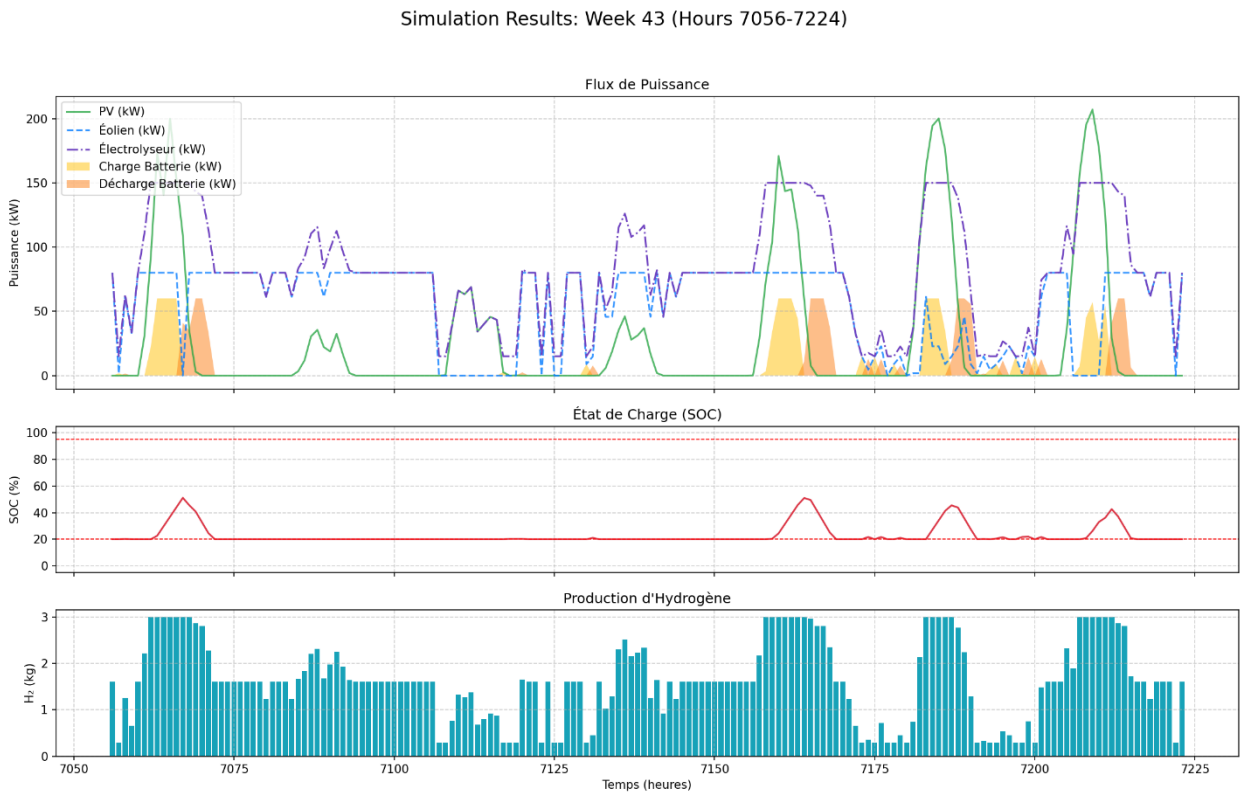

Figure 5.35: Power Flows, Battery SOC, and Hydrogen Production During Cloudy days

During cloudy days, the renewable availability is reduced, with PV production providing only short peaks and wind remaining highly variable. As a result the battery frequently operates near iits minimum SOC and offers only limited support to the electrolyzer. Even under these constrained conditions, hydrogen production does not collapse, instead, it fluctuates between roughly 0.5-2kg/h. Although overall output decreases compared to high-resource periods, the system avoids

extended shutdowns, showing that the optimization approach mitigates the impact of the weak renewable conditions on hydrogen production.

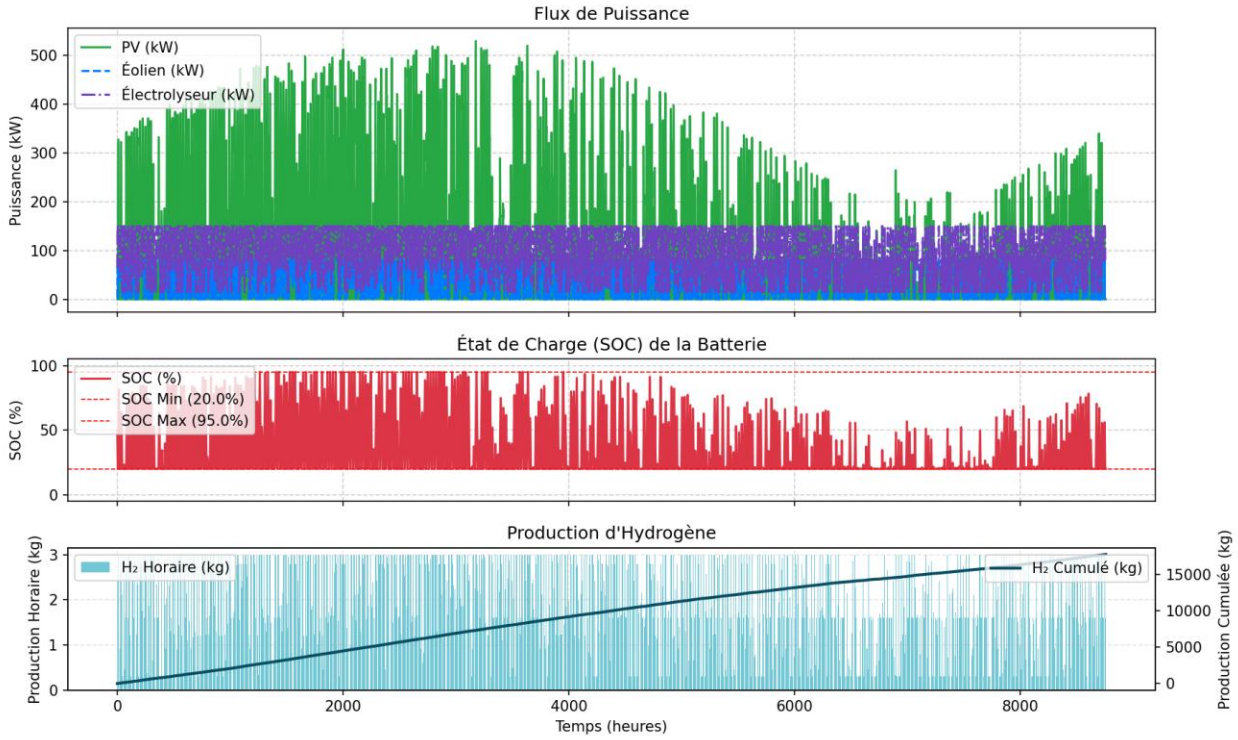

Figure 5.36: Annual Power Flows, Battery SOC, and Hydrogen Production of the Optimized PV–Wind–Battery–PEM System

The annual simulation results confirm the effectiveness of the optimized hybrid configuration; the electrolyzer operates with a specific energy consumption of 50Kwh/kg. The system maintains a high electrolyzer capacity factor of 0.67, significantly above typical off-grid hybrid installations, without relying on oversizing or excessive storage. Solar and wind supply 85% averagely over the year with the battery compensating for the rest preventing power shortages. The battery cycles within a 20-95% SoC window, charging fully in high-resource months and supporting partial-load operation during renewable deficits. This design enables a total annual hydrogen production of nearly 17.8 tonnes. The cumulative hydrogen production grows consistently throughout the year, demonstrating that the system achieves both high efficiency and high utilization under realistic intermittency.

Table 5.4: Operating Bounds of the Hybrid PV–Wind–Battery–Electrolyzer System

Component	Min	Max
PV Power (kW)	0	529.95
Wind Power (kW)	0	80
Electrolyzer Power (kW)	15	150
Battery Power (kW)	-60	60
Hydrogen Production (kg/h)	0.3	3
Battery SoC (%)	20%	95%
Curtailment (kW)	0	389

Table 5.5: State-of-the-Art Utilization Factors for PEM Electrolyzers in Hybrid Off-Grid Architectures

System Type	Value	Remarks	Ref.
Hybrid–wind–solar–battery (multiple global case studies)	53.7% (Miami case), up to ∼70% in wind-dominant climates	Wind-rich sites display high hydrogen production.	[44]
PV–and–Hybrid PV/Wind (System A & B)	9.20% (Sys A), 20.2% (Sys B)	Heavy PV-dependent systems display low capacity factors due to strong sensitivity to irradiance variability.	[45]
Hybrid–PV–Wind–Battery	41.5% (A), 65.5% (B), ≈66% (C), 82.0% (D)	Excess renewable generation and large battery sizing result in high hyrgoen production.	[46]
Hybrid off-grid systems (review)	61.34%	Benchmarks system-level performance limits in hybrid renewable configurations.	[47]
This Study	**67.6%**	**Achieves electrolyzer utilization levels typically requiring oversized renewable or storage systems.**	–

The hybrid solar-wind microgrid combined with MPC, DT and PSO achieves performance levels that exceed those reported for comparable off-grid PEM electrolyzer systems. The electrolyzer operates with an annual capacity factor of 0.676 which is aligned with the high end of hybrid systems that rely on substantial oversizing or large storage (up to 82% [149]).

This configuration maintains a good utilization without oversizing the renewable generation: PV

is sized at 1x the electrolyzer rating and wind at 0.53x, and the battery provides only 40% of the electrolyzer rated power with an average duration of 6.7h to maintain the system at a feasible economic standard. The system consistently stabilizes hydrogen production despite pronounced hourly fluctuations in irradiance and wind speed.

During high-resource conditions, hydrogen output remains within a narrow 2-3kg/h band. The battery contributes an average of 13-17% of the electrolyzer input power depending on the week, primarily during morning-evening transitions and cloudy periods. This modest cycling contribution is enabled by the MPC penalty structure and DT trajectory selection, which together constrain the SoC to the 20-98% admissible band while preventing deep cycling and excessive ramping.

Under worst-case renewable availability (week 43), hydrogen production remains between 0.5-2.5 kg/h, avoiding full outages despite sustained low irradiance and weak wind speed values. The control architecture in the system preserves continuity of operation rather than prioritizing instantaneous yield. The PSO post-optimization improves the operational smoothness of the electrolyzer by tuning ramp limits and the swarm converges toward a solution that reduces hourly hydrogen standard deviation for a flatter production trajectory.

Relative to state-of-the-art performance benchmarks (Table 4.6), the system achieves utilization levels typically reported only with a significant overcapacity, high curtailment ratios or very large battery banks. This software optimization can substitute for hardware oversizing while improving the system's feasibility and reducing capital intensity in off-grid hydrogen microgrids.

CHAPTER 6 CONCLUSION AND RECOMMENDATIONS

This study assesses a hybrid solar-wind microgrid supplying a PEM electrolyzer along with a battery storage under real year-long meteorological conditions.

The first part of the work presents a solar standalone microgrid without control and optimization to understand the relationship between hydrogen production and the intermittency of the renewable generation. The second part integrates a wind source to complement the solar generation and to evaluate its impact on hydrogen production. Both systems proved a high dependency on the variable renewable generation, with the solar system providing little to no energy during nighttime and experiencing systems shutdowns due to restricted battery sizing while the hybrid system is functional during nighttime due to the wind generation yet still highly dependent on the intermittency of the hybrid renewable sources.

The last part studies the same system but adds control and optimization along with accurate meteorological data. The system demonstrated continuous hydrogen production without grid support or large energy storage systems or oversized renewable generation. It achieved a high annual utilization level and consistent specific energy performance while respecting the operational bounds. The hydrogen production pattern differs from the renewable generation pattern unlike in the first two systems. In addition, a fully interactive simulation interface was developed to allow users to modify system sizing, control settings and renewable inputs, making the entire framework reproducible and easily adaptable to new design scenarios or new geographical locations.

6.1 Contributions

- This works demonstrates a high electrolyzer capacity factor without relying on oversized renewable generation, large wind shares or large battery storage. The control and energy flow coordination strategy maintains a stable hydrogen output under real meteorological variability, proving the system performance can be maximized through optimized operation rather than large capacity scaling.

- This study uses a virtual DT to allow system performance, failure modes and control strategies to be tested before real deployment. It reduces design uncertainty, accelerates prototyping and supports informed decision making before real world experimental evaluation.

- The study introduces an interactive simulation interface that allows users to modify component sizing, control settings and environmental inputs. This enables rapid testing of multiple design scenarios, helps identify operational bottlenecks and makes the framework adaptable to new locations or new system configurations.

- The analysis is performed over a complete year using real meteorological data along with the electrolyzer system incorporating practical operational limits to avoid oversimplifications associated with averaged or synthetic data, which makes the simulation realistic and suitable for reliability analysis.

6.2 Limitations and Future Work

- Electrolyzer degradation and lifetime modeling: The model does not include long-term PEM electrolyzer degradation mechanisms such as membrane thinning and catalyst aging. As a result, it is not possible to have a lifetime performance assessment. Future work should explore integrating detailed degradation models as this will allow for accurate predictions of the dynamic operation and its durability.

- Techno-Economic and cost assessment: This study focuses on technical feasibility but does not evaluate cost or the levelized cost of hydrogen (LCOH) therefore it limits the economic interpretation of this work. Therefore, future work should add a techno-economic layer that includes CapEX/OpEX and LCOH calculations.

- Hydrogen Utilization pathways: The analysis focuses only on hydrogen production and does not address how the produced hydrogen would be stored, transported or used (e.g., mobility, industry, injection into pipelines, reconversion to electricity). Therefore extending the framework to model downstream hydrogen handling would enable complete system-level assessments and help determine the suitability of the system for different deployment contexts.

REFERENCES

[1] Yang, F., Ibrahim, R. L., Ajide, K. B., & Al-Faryan, M. A. S. (2024). Examining the ecological effects of energy transition, environmental technology, and structural change in BRICS economies: Implications for sustainable development. *Energy Sources, Part B: Economics, Planning, and Policy*, *19*(1). https://doi.org/10.1080/15567249.2024.2419956

[2] Environmental and Energy Study Institute, "Fact Sheet: Climate, Environmental, and Health Impacts of Fossil Fuels," EESI, Jun. 2021. [Online]. Available: https://www.eesi.org/papers/view/fact-sheet-climate-environmental-and-health-impacts-of-fossil-fuels-2021

[3] Den Elzen, M., Forsell, N., Roelfsema, M., Van Soest, H., Hof, A. F., & Admiraal, A. (2016). Contribution of the G20 economies to the global impact of the Paris agreement climate proposals. *Climatic Change*, *137*(3–4), 655–665. https://doi.org/10.1007/s10584-016-1700-7

[4] S. K. Rose, R. Richels, G. Blanford, and T. Rutherford, "The Paris Agreement and next steps in limiting global warming," *Climatic Change*, vol. 142, no. 1–2, pp. 255–270, Mar. 2017, doi: 10.1007/s10584-017-1935-y.

[5] A. Le, N. Domingo, N. Rodrigo, and S. Senaratne, "Policy Mapping for Net-Zero-Carbon Buildings: Insights from Leading Countries," *Buildings*, vol. 13, no. 11, p. 2766, Nov. 2023, doi: 10.3390/buildings13112766.

[6] H. Xu, "Facilitating full and effective implementation of the Paris Agreement for carbon neutrality vision," *Carb Neutrality*, vol. 1, no. 1, Jan. 2022, doi: 10.1007/s43979-022-00014-8.

[7] W. Hammond, J. Axsen, and E. Kjeang, "How to slash greenhouse gas emissions in the freight sector: Policy insights from a technology-adoption model of Canada," *Energy Policy*, vol. 137, p. 111093, Nov. 2019, doi: 10.1016/j.enpol.2019.111093.

[8] Government of British Columbia, *CleanBC: Roadmap to 2030*, Victoria, BC, Canada: Government of British Columbia, 2021. [Online]. Available: https://cleanbc.gov.bc.ca/about-cleanbc/

[9] Government of Alberta, *Technology Innovation and Emissions Reduction (TIER) Regulation*, Edmonton, AB, Canada: Government of Alberta, 2023. [Online]. Available: https://www.alberta.ca/technology-innovation-and-emissions-reduction-regulation

[10] International Carbon Action Partnership (ICAP), “Canada – Québec Cap-and-Trade System,” ICAP ETS Map, 2025. [Online]. Available: https://icapcarbonaction.com/en/ets/canada-quebec-cap-and-trade-system. [Accessed: Oct. 20, 2025]

[11] IRENA, *World Energy Transitions Outlook 2022: 1.5°C Pathway*, International Renewable Energy Agency, Abu Dhabi, 2022. [Online]. Available: https://www.irena.org/publications/2022/Mar/World-Energy-Transitions-Outlook-2022

[12] Lasseter, R. H. (2011). *Smart distribution: Coupled microgrids*. Proceedings of the IEEE, 99(6), 1074–1082. https://doi.org/10.1109/JPROC.2011.2114630

[13] C. Sulzberger, Thomas Edison’s 1882 Pearl Street Generating Station, August 2011.

[14]Canada's electricity generation, 2022," Statistics Canada, https://www150.statcan.gc.ca/n1/daily-quotidien/231030/dq231030c-eng.htm

[15] M. Arunachalam and D. S. Han, “Efficient solar-powered PEM electrolysis for sustainable hydrogen production: an integrated approach,” *emergent mater.*, vol. 7, no. 4, pp. 1401–1415, Apr. 2024, doi: 10.1007/s42247-024-00697-y.

[16] M. Reuß, J. Reul, T. Grube, M. Langemann, S. Calnan, M. Robinius, R. Schlatmann, U. Rau, and D. Stolten, "Solar hydrogen production: a bottom-up analysis of different photovoltaic–electrolysis pathways," *Sustainable Energy Fuels*, vol. 3, no. 3, pp. 801-813, 2019. Available: https://doi.org/10.1039/C9SE00007K.

[17] IEA, *Global Hydrogen Review 2023*, International Energy Agency, Paris, 2023. [Online]. Available: https://www.iea.org/reports/global-hydrogen-review-2023

[18] Angelico, R., Bianchi, B., Catalano, P., & Giametta, F. (2025). Green Hydrogen for Energy Transition: A Critical Perspective. *Energies*, *18*(2), 404. https://doi.org/10.3390/en18020404

[19] C. Liu *et al.*, “Influence of Power Fluctuation on Ni-Based Electrode Degradation and Hydrogen Evolution Reaction Performance in Alkaline Water Splitting: Probing the Effect of Renewable Energy on Water Electrolysis,” *Catalysts*, vol. 14, no. 5, p. 307, May 2024, doi: 10.3390/catal14050307.

[20] [N. Agrawal, A. Agarwal, and T. Kanumuri, “A dual-purpose novel converter for optimized hybrid energy system,” *Eng. Res. Express*, vol. 7, no. 1, p. 015307, Jan. 2025, doi: 10.1088/2631-8695/ada33c.

[21] T. Lundblad, M. Taljegard, and F. Johnsson, “Centralized and decentralized electrolysis-based hydrogen supply systems for road transportation – A modeling study of current and future costs,” *International Journal of Hydrogen Energy*, vol. 48, no. 12, pp. 4830–4844, Nov. 2022, doi: 10.1016/j.ijhydene.2022.10.242.

[22] M. Perkel, “Why Jupyter is data scientists’ computational notebook of choice,” *Nature*, vol. 563, no. 7729, pp. 145–146, 2018.

[23] A. Maliat, S. Kotian, and D. Ghahremanlou, “Assessment of a Hybrid Renewable Energy System Incorporating Wind, Solar, and Storage Technologies in Makkovik, Newfoundland and Labrador,” *JSE*, vol. 3, no. 2, pp. 87–104, June 2024, doi: 10.56578/jse030203.

[24] K. E. Gan, T. Weis, D. Yamazaki, T. Y. Gan, O. Taikan, and H. Schüttrumpf, “Enhancing Renewable Energy Systems, Contributing to Sustainable Development Goals of United Nation and Building Resilience Against Climate Change Impacts,” *Energy Tech*, vol. 11, no. 11, Sept. 2023, doi: 10.1002/ente.202300275.

[25] J. Brauns and T. Turek, “Alkaline Water Electrolysis Powered by Renewable Energy: A Review,” *Processes*, vol. 8, no. 2, p. 248, Feb. 2020, doi: 10.3390/pr8020248.

[26] M. K. Senapati, P. K. Nayak, S. R. Samantaray, and C. Pradhan, “Improved power management control strategy for renewable energy-based DC micro-grid with energy storage integration,” *IET Generation Trans & Dist*, vol. 13, no. 6, pp. 838–849, Sept. 2018, doi: 10.1049/iet-gtd.2018.5019.

[27] G. N. S. Oliveira, M. A. Mohamed, M. H. N. Marinho, A. Ilinca, and T. Costa, “Comprehensive case study on the technical feasibility of Green hydrogen production from photovoltaic and battery energy storage systems,” *Energy Science & Engineering*, vol. 12, no. 10, pp. 4549–4565, Sept. 2024, doi: 10.1002/ese3.1905.

[28] H. Sayed-Ahmed, Á. I. Toldy, and A. Santasalo-Aarnio, “Dynamic operation of proton exchange membrane electrolyzers—Critical review,” *Renewable and Sustainable Energy Reviews*, vol. 189, p. 113883, 2024. doi: 10.1016/j.rser.2023.113883.

[29] F. Zhang, P. Zhao, M. Niu, and J. Maddy, “The survey of key technologies in hydrogen energy storage,” *International Journal of Hydrogen Energy*, vol. 41, no. 33, pp. 14535–14552, Sept. 2016. doi: 10.1016/j.ijhydene.2016.05.293.

[30] S. G. Nnabuife, A. K. Hamzat, J. Whidborne, B. Kuang, and K. W. Jenkins, “Integration of renewable energy sources in tandem with electrolysis: A technology review for green hydrogen production,” *International Journal of Hydrogen Energy*, vol. 107, pp. 218–240, 2025, doi: 10.1016/j.ijhydene.2024.06.342

[31] International Renewable Energy Agency (IRENA), *World Energy Transitions Outlook 2023: 1.5°C Pathway*, Abu Dhabi, United Arab Emirates, 2023. [Online]. Available: https://www.irena.org/publications/2023/Jun/World-Energy-Transitions-Outlook-2023

[32] T. Li, M. Eremia, and M. Shahidehpour, “Interdependency of Natural Gas Network and Power System Security,” *IEEE Trans. Power Syst.*, vol. 23, no. 4, pp. 1817–1824, Nov. 2008, doi: 10.1109/tpwrs.2008.2004739.

[33] S. G. Nnabuife, A. K. Hamzat, J. Whidborne, B. Kuang, and K. W. Jenkins, “Integration of renewable energy sources in tandem with electrolysis: A technology review for green hydrogen production,” *International Journal of Hydrogen Energy*, vol. 107, pp. 218–240, 2025, doi: 10.1016/j.ijhydene.2024.06.342

[34] H. Sayed-Ahmed, Á. I. Toldy, and A. Santasalo-Aarnio, “Dynamic operation of proton exchange membrane electrolyzers—Critical review,” *Renewable and Sustainable Energy Reviews*, vol. 189, p. 113883, 2024. doi: 10.1016/j.rser.2023.113883.

[35] D. Virah-Sawmy, F. J. Beck, and B. Sturmberg, “Ignore variability, overestimate hydrogen production – Quantifying the effects of electrolyzer efficiency curves on hydrogen production from renewable energy sources,” *International Journal of Hydrogen Energy*, vol. 72, pp. 49–59, 2024, doi: 10.1016/j.ijhydene.2024.05.360

[36] H. Sayed-Ahmed, Á. I. Toldy, and A. Santasalo-Aarnio, "Dynamic operation of proton exchange membrane electrolyzers—Critical review," *Renewable and Sustainable Energy Reviews*, vol. 189, p. 113883, 2024. doi: 10.1016/j.rser.2023.113883.

[37] Z. Wang *et al.*, "Optimizing Energy Management and Case Study of Multi-Energy Coupled Supply for Green Ships," *JMSE*, vol. 11, no. 7, p. 1286, June 2023, doi: 10.3390/jmse11071286.

[38] C. M. Colson, B. Asghari, M. H. Nehrir, and R. K. Sharma, "Improving Sustainability of Hybrid Energy Systems Part II: Managing Multiple Objectives With a Multiagent System," *IEEE Trans. Sustain. Energy*, vol. 5, no. 1, pp. 46–54, Jan. 2014, doi: 10.1109/tste.2013.2269319.

[39] M. S. Saleem and N. Abas, "A solar assisted grid-tied polygeneration system for hydrogen and electricity production: Future of energy transition from electrons to molecules," *International Journal of Hydrogen Energy*, vol. 69, pp. 559–569, 2024, doi: 10.1016/j.ijhydene.2024.05.082

[40] O. F. Guler, O. Sen, C. Yilmaz, and M. Kanoglu, "Performance evaluation of a geothermal and solar-based multigeneration system and comparison with alternative case studies: Energy, exergy, and exergoeconomic aspects," *Renewable Energy*, vol. 200, pp. 1517–1532, 2022, doi: 10.1016/j.renene.2022.10.064.

[41] S. Di Fraia, R. Figaj, M. Shah, and L. Vanoli, "Biomass-Driven Polygeneration Coupled to Power-to-X: An Energy and Economic Comparison Between On-Site Electric Vehicle Charging and Hydrogen Production," *Energies*, vol. 17, no. 21, 5479, 2024, doi: 10.3390/en17215479.

[42] M. S. Saleem and N. Abas, "A solar assisted grid-tied polygeneration system for hydrogen and electricity production: Future of energy transition from electrons to molecules," *International Journal of Hydrogen Energy*, vol. 69, pp. 559–569, 2024, doi: 10.1016/j.ijhydene.2024.05.082.

[43] W. K. Hussam, E. M. Barhoumi, M. Abdul-Niby, and G. J. Sheard, "Techno-economic analysis and optimization of hydrogen production from renewable hybrid energy systems: Shagaya Renewable Power Plant—Kuwait," *International Journal of Hydrogen Energy*, vol. 58, pp. 56–68, 2024, doi: 10.1016/j.ijhydene.2024.01.153.

[44] E. B. Ssekulima, A. Al Hinai, M. B. Anwar, and M. S. El Moursi, "Wind speed and solar irradiance forecasting techniques for enhanced renewable energy integration with the grid: a review," *IET Renewable Power Gen*, vol. 10, no. 7, pp. 885–989, Aug. 2016, doi: 10.1049/iet-rpg.2015.0477.

[45] M. B. E. Dabbagh, M. Saad, A. Oukaour, and H. Ibrahim, “Efficient control of DC microgrid with hybrid PV–fuel cell and energy storage systems,” *Energies*, vol. 14, no. 11, p. 3234, 2021, doi: 10.3390/en14113234

[46] D. Wei, L. Zhang, A. A. Alotaibi, J. Fang, A. H. Alshahri, and K. H. Almitani, “Transient simulation and comparative assessment of a hydrogen production and storage system with solar and wind energy using TRNSYS,” *International Journal of Hydrogen Energy*, 2022, doi: 10.1016/j.ijhydene.2022.02.157

[47] A. Dezhdar, E. Assareh, N. Agarwal, A. Bedakhanian, S. Keykhah, and F. Y. Fard, “Transient optimization of a new solar–wind multigeneration system for hydrogen production, desalination, clean electricity, heating, cooling, and energy storage using TRNSYS,” *Renewable Energy*, vol. 208, pp. 512–537, 2023, doi: 10.1016/j.renene.2023.03.019

[48] M. B. Abdelghany, F. Gao, H. H. Zeineldin, and A. Al-Durra, “A Coordinated Multitimescale Model Predictive Control for Output Power Smoothing in Hybrid Microgrid Incorporating Hydrogen Energy Storage,” *IEEE Trans. Ind. Inf.*, vol. 20, no. 9, pp. 10987–11001, Sept. 2024, doi: 10.1109/tii.2024.3396343.

[49] O. A. Aguirre, R. Luna-Romero, M. Morales-Menendez, and E. Rodriguez-Toral, “Control strategies for alkaline water electrolyzers: A survey,” *Int. J. Hydrogen Energy*, article in press, 2024. [Online]. Available: https://www.sciencedirect.com/science/article/pii/S0360319924036012

[50]X. Dong, J. Yang, C. Zhang, Y. Yan, and J. Mao, “Generalized Dynamic Predictive Control for Nonlinear Systems Subject to Mismatched Disturbances With Application to PMSM Drives,” *IEEE Trans. Ind. Electron.*, vol. 71, no. 1, pp. 954–964, Jan. 2024, doi: 10.1109/tie.2023.3245213.

[51] V. A. Martínez López, H. Ziar, J. W. Haverkort, M. Zeman, and O. Isabella, “Dynamic operation of water electrolyzers: A review for coupling with renewable energy systems,” *Renew. Sustain. Energy Rev.*, vol. 182, art. no. 113407, Aug. 2023

[52] A. H. D. Christensen, J. S. Jensen, and S. K. Kær, “Nonlinear model predictive control for dynamic operation of an alkaline electrolyzer,” *J. Process Control*, vol. 140, art. no. 104310, Jan. 2025.

[53] B. Endrődi, C. A. Trapp, I. Szén, I. Bakos, M. Lukovics, and C. Janáky, “Challenges and opportunities of the dynamic operation of PEM water electrolyzers,” *Energies*, vol. 18, no. 9, p. 2154, Apr. 2025.

[54] H. Zou, Y. Li, L. Wang, and C. Zhang, “Novel control strategies for multi-electrolyzer systems in large-scale alkaline water hydrogen production: Enhancing renewable energy utilization and electrolyzer lifespan,” *SSRN Electronic Journal*, preprint, 2025. [Online]. Available: https://papers.ssrn.com/abstract=5173240

[55] S. Chaudhary, B. D. Shivahare, V. Kumar, S. K. Gupta, P. Singh, and M. Diwakar, “Metaheuristic Optimization Algorithms and Recent Applications: A Comprehensive Survey,” in *Proc. 2023 Int. Conf. on Computational Intelligence, Communication Technology and Networking (CICTN)*, Ghaziabad, India, Apr. 20–21, 2023, doi: 10.1109/CICTN57981.2023.10140511.

[56] J. Kennedy and R. Eberhart, “Particle swarm optimization,” in *Proc. IEEE Int. Conf. Neural Networks (ICNN)*, Perth, Australia, 1995, pp. 1942–1948. doi: 10.1109/ICNN.1995.488968

[57] R. Storn and K. Price, “Differential evolution – A simple and efficient heuristic for global optimization over continuous spaces,” *J. Global Optimization*, vol. 11, no. 4, pp. 341–359, Dec. 1997. doi: 10.1023/A:1008202821328

[58] O. A. Aguirre, R. Luna-Romero, M. Morales-Menendez, and E. Rodriguez-Toral, “Control strategies for alkaline water electrolyzers: A survey,” *Int. J. Hydrogen Energy*, article in press, 2024.[Online].Available: https://www.sciencedirect.com/science/article/abs/pii/S0360319924036012

[59] S. Bandarua and K. Deb, “Metaheuristic Techniques,” Michigan State University College of Engineering, 2016. [Online]. Available: https://www.egr.msu.edu/~kdeb/papers/c2016029.pdf.

[60] A. M. Nassef, M. A. Abdelkareem, H. M. Maghrabie and A. Baroutaji, “Review of Metaheuristic Optimization Algorithms for Power Systems Problems,” *Sustainability*, vol. 15, no. 12, Art. no. 9434, 2023. doi:10.3390/su15129434. [Online]. Available: https://www.mdpi.com/2071-1050/15/12/9434. MDPI

[61] K. Rajwar, S. Das and K. Deep, “An exhaustive review of the metaheuristic algorithms for search and optimization: taxonomy, applications, and open challenges,” 2023. [Online]. Available:

https://zeus.inf.ucv.cl/~bcrawford/UAH_CHARLA-MAYO-22-2023/1-An%20exhaustive%20review%20of%20the%20metaheuristic%20algorithms.pdf.

[62] A. Alorf et al., “A survey of recently developed metaheuristics and their optimization capability,”2023.[Online]Available: https://www.sciencedirect.com/science/article/pii/S0952197622006121.

[63] M.-H. Lin, J.-F. Tsai, and C.-S. Yu, “A Review of Deterministic Optimization Methods in Engineering and Management,” *Mathematical Problems in Engineering*, vol. 2012, Art. ID 756023, pp. 1–15, Jun. 2012. doi:10.1155/2012/756023. [Online]. Available: https://www.hindawi.com/journals/mpe/2012/756023/

[64] K. E. Fahim, “A State-of-the-Art Review on Optimization Methods and Applications in Renewable Energy Systems,” *Sustainability*, vol. 15, no. 15, Art. no. 11837, 2023. doi:10.3390/su151511837. [Online]. Available: https://www.mdpi.com/2071-1050/15/15/11837

[65] O. Bamisile, M. Dagbasi, and T. Nawaz, “Towards Renewables Development: Review of Optimization Methods for Hybrid Renewable Energy Systems,” *Heliyon*, vol. 10, no. 4, p. e13513, Apr.2024.[Online].Available: https://www.sciencedirect.com/science/article/pii/S240584402413513X

[66] D. E. Kvasov, “Metaheuristic vs. Deterministic Global Optimization Algorithms: A Comparative Study on Multiextremal Test Problems,” *Applied Mathematics and Computation*, vol. 320,pp.485-497,2018.[Online].Available: https://www.sciencedirect.com/science/article/abs/pii/S0096300317303028

[67] [1] A. Nouh, A. Almalih, F. Mohamed, M. Faraj, and A. Almalih, “Hybrid of Meta-Heuristic Techniques Based on Cuckoo Search and Particle Swarm Optimizations for Solar PV Systems Subjected to Partially Shaded Conditions,” *jsesd*, vol. 13, no. 1, pp. 114–132, Mar. 2024, doi: 10.51646/jsesd.v13i1.178.

[68] J. Kennedy and R. Eberhart, *Particle Swarm Optimization*, Proceedings of IEEE International Conference on Neural Networks, vol. 4, pp. 1942-1948, Dec. 1995.

[69] L. Frison, J. De Schutter, and M. Diehl, “MPC for Renewable Energy Systems,” *Syscop*, 2023.[Online].Available: https://www.syscop.de/files/2023ss/MPC4RES/MPC_for_RES_script.pdf.

[70] M. A. Syed, and M. Khalid, “An Intelligent Model Predictive Control Strategy for Stable Solar-Wind Renewable Power Dispatch Coupled with Hydrogen Electrolyzer and Battery Energy Storage,” *Int. J. Energy Res.*, vol. 47, no. 8, pp. 3745–3762, 2023. [Online]. Available: https://doi.org/10.1155/2023/4531054.

[71] A. Elgammal and T. Ramlal, “Optimal Model Predictive Frequency Control Management of Grid Integration PV/Wind/FC/Storage Battery Based Smart Grid Using Multi Objective Particle Swarm Optimization MOPSO,” *WSEAS TRANSACTIONS ON ELECTRONICS*, vol. 12, pp. 46–54, July 2021, doi: 10.37394/232017.2021.12.7.

[72] M. Alharbi and Z. Iqbal, “Optimal Energy Management and Prediction for Hybrid Renewable Systems,” *Frontiers in Energy Research*, vol. 11, Article 1416201, 2024. [Online]. Available: https://www.frontiersin.org/articles/10.3389/fenrg.2024.1416201/full.

[73] G. Mbasso, Y. Himeur, F. Almakhles, T. Sutikno, and H. Malik, “Digital twins in renewable energy systems: A comprehensive review,” *Energy Strategy Reviews*, vol. 53, p. 101814, 2025.

[74] [1] K. Bassey, B. Antwi, A. Ntiakoh, J. Opoku-Boateng, and A. Juliet, “Digital twin technology for renewable energy microgrids,” *Eng. sci. technol. j.*, vol. 5, no. 7, pp. 2248–2272, July 2024, doi: 10.51594/estj.v5i7.1319.

[75] A. Q. Al-Shetwi, M. Al-Hazmi, and H. Malik, “Digital twin technology for renewable energy, smart grids, energy storage, and systems,” *IET Smart Grid*, vol. 8, no. 1, pp. 233–245, 2025.

[76] A. A. A. Ardebili, Y. Ding, M. R. Elbassioni, and R. K. Malik, “Digital twins of smart energy systems: A systematic literature review on enablers, design, management and computational challenges,” *Energy Informatics*, vol. 7, no. 2, pp. 115–132, 2024.

[77] J. Yuan, J. Ma, K. L. Man, and Z. Tian, “Digital Twin Integration With Data Fusion for Enhanced Photovoltaic System Management: A Systematic Literature Review,” *IEEE Open J. Power Electron.*, vol. 5, pp. 1045–1058, Jan. 2024, doi: 10.1109/ojpel.2024.3422021.

[78] G. Mbasso, Y. Himeur, F. Almakhles, T. Sutikno, and H. Malik, “Digital twins in renewable energy systems: A comprehensive review,” *Energy Strategy Reviews*, vol. 53, p. 101814, 2025.

[79] A. A. A. Ardebili, Y. Ding, M. R. Elbassioni, and R. K. Malik, “Digital twins of smart energy systems: A systematic literature review on enablers, design, management and computational challenges,” *Energy Informatics*, vol. 7, no. 2, pp. 115–132, 2024.

[80] A. Mchirgui, A. Quadar, N. Kraiem, and A. Lakhssassi, “The applications and challenges of digital twin technology in smart grids: A comprehensive review,” *Applied Sciences*, vol. 14, no. 23, p. 10933, 2024.

[81] W. Sun, Y. Zhou, Y. Zhang, and W. Ma, “An Introduction to Digital Twin Standards,” *GetMobile: Mobile Comp. and Comm.*, vol. 26, no. 3, pp. 16–22, Oct. 2022, doi: 10.1145/3568113.3568119.

[82] A. M. Madni, S. D. Lucero, and C. C. Madni, “Leveraging Digital Twin Technology in Model-Based Systems Engineering,” *Systems*, vol. 7, no. 1, p. 7, Jan. 2019, doi: 10.3390/systems7010007.

[83] MathWorks, *“Solar Cell,”* Simscape Electrical Documentation, 2024. [Online]. Available: https://www.mathworks.com/help/sps/ref/solarcell.html

[84]S. Singh, S. Manna, A. K. Akella, and M. I. Hasan Mansoori, “Implementation of Perturb & Observe MPPT Technique using Boost converter in PV System,” Institute Of Electrical Electronics Engineers, July 2020, pp. 1–4. doi: 10.1109/cispsse49931.2020.9212203.

[85] MathWorks, *“Average-Value DC–DC Converter,”* Simscape Electrical Documentation, 2024. [Online]. Available: https://www.mathworks.com/help/sps/ref/averagevaluedcdcconverter.html

[86] MathWorks, *“Solar Cell,”* Simscape Electrical Documentation, 2024. [Online]. Available: https://www.mathworks.com/help/sps/ref/solarcell.html

[87] European Commission, Joint Research Centre (JRC), *Photovoltaic Geographical Information System (PVGIS)*, 2024. [Online]. Available: https://re.jrc.ec.europa.eu/pvg_tools/en/

[88] M. J. Rana and M. A. Abido, “Energy management in DC microgrid with energy storage and model predictive controlled AC–DC converter,” *IET Generation Trans & Dist*, vol. 11, no. 15, pp. 3694–3702, July 2017, doi: 10.1049/iet-gtd.2016.1934.

[89] S. J. Moura, M. Krstic, and N. A. Chaturvedi, “Adaptive PDE Observer for Battery SOC/SOH Estimation,” American Society Of Mechanical Engineers, Oct. 2012, pp. 101–110. doi: 10.1115/dscc2012-movic2012-8800.

[90] H. A. Mohamed, H. A. Khattab, G. A. Morsy, and A. Mobarka, “Design, control and performance analysis of DC-DC boost converter for stand-alone PV system,” Institute Of Electrical Electronics Engineers, Dec. 2016, pp. 101–106. doi: 10.1109/mepcon.2016.7836878.

[91] S. Sood et al., “Generic Dynamical Model of PEM Electrolyser under Intermittent Sources,” Energies, vol. 13, no. 24, p. 6556, Dec. 2020, doi: 10.3390/en13246556.

[92] J. Liu et al., “Experimental Investigation of PEM Water Electrolyser Stack Performance Under Dynamic Operation Conditions,” J. Electrochem. Soc., vol. 171, no. 5, p. 054521, May 2024, doi: 10.1149/1945-7111/ad4d1f.

[93] G. N. S. Oliveira, M. A. Mohamed, M. H. N. Marinho, A. Ilinca, and T. Costa, “Comprehensive case study on the technical feasibility of Green hydrogen production from photovoltaic and battery energy storage systems,” Energy Science & Engineering, vol. 12, no. 10, pp. 4549–4565, Sept. 2024, doi: 10.1002/ese3.1905.

[94] R. Wagner, S. M. Pedersen, M. S. Courtney, I. Antoniou, and H. E. Jørgensen, “The influence of the wind speed profile on wind turbine performance measurements,” Wind Energy, vol. 12, no. 4, pp. 348–362, Sept. 2008, doi: 10.1002/we.297.

[95] “Data Download for Montréal,” WeatherStats, Accessed: Nov. 24, 2025. *Online*. Available: https://montreal.weatherstats.ca/download.html

[95] S. Adak, “Power Factor Analysis of Grid-Connected Solar Inverter under Different Irradiance Levels throughout the Day,” Energies, vol. 17, no. 15, p. 3632, July 2024, doi: 10.3390/en17153632.

[96] N. Jargalsaikhan, H. Masrur, A. Iqbal, S. S. Rangarajan, S. Byambaa, and T. Senjyu, “A control algorithm to increase the efficient operation of wind energy conversion systems under extreme wind conditions,” *Energy Reports*, vol. 8, pp. 11429–11439, Sept. 2022, doi: 10.1016/j.egyr.2022.08.243.

[97] M. A. Syed and M. Khalid, “An Intelligent Model Predictive Control Strategy for Stable Solar-Wind Renewable Power Dispatch Coupled with Hydrogen Electrolyzer and Battery Energy

Storage," *International Journal of Energy Research*, vol. 2023, pp. 1–17, Mar. 2023, doi: 10.1155/2023/4531054.

[98] J. Liu *et al.*, "Experimental Investigation of PEM Water Electrolyser Stack Performance Under Dynamic Operation Conditions," *J. Electrochem. Soc.*, vol. 171, no. 5, p. 054521, May 2024, doi: 10.1149/1945-7111/ad4d1f.

[99] M. A. Arce, J. M. Guerrero, A. J. Calderón, and F. Jurado, "Model predictive control of hybrid renewable energy systems with battery storage and electrolyzer for hydrogen production," *Renewable Energy*, vol. 141, pp. 300–312, Oct. 2019.

[100] A. B. Shafiee, H. Karimi, and M. Saif, "Digital twin-based predictive control for renewable-hydrogen hybrid systems," *IEEE Transactions on Energy Conversion*, vol. 37, no. 3, pp. 2158–2170, Sept. 2022.

[101] J. Kennedy and R. Eberhart, "Particle swarm optimization," in Proceedings of the IEEE International Conference on Neural Networks, Perth, WA, Australia, vol. 4, pp. 1942–1948, Dec. 1995.

[102] A. Khalilnejad, A. Sundararajan, and A. I. Sarwat, "Optimal design of hybrid wind/photovoltaic electrolyzer for maximum hydrogen production using imperialist competitive algorithm," Journal of Modern Power Systems and Clean Energy, vol. 6, no. 1, pp. 40–49, 2018.

[102] S. G. Nnabuife, A. K. Hamzat, J. Whidborne, B. Kuang, and K. W. Jenkins, "Integration of renewable energy sources in tandem with electrolysis: A technology review for green hydrogen production," International Journal of Hydrogen Energy, vol. 107, pp. 218–240, Mar. 2025, doi: 10.1016/j.ijhydene.2024.06.342.

[103] K. K. Kurramovich, A. A. Abro, A. I. Vaseer, S. R. Ali, M. Murshed, and S. U. Khan, "Roadmap for carbon neutrality: the mediating role of clean energy development-related investments.," Environ Sci Pollut Res, vol. 29, no. 23, pp. 34055–34074, Jan. 2022, doi: 10.1007/s11356-021-17985-3.

[104] Z. Ziobrowski and A. Rotkegel, "Assessment of Hydrogen Energy Industry Chain Based on Hydrogen Production Methods, Storage, and Utilization," Energies, vol. 17, no. 8, p. 1808, Apr. 2024, doi: 10.3390/en17081808.

[105] F. Zhao, Z. Liu, X. Liu, and F. Bai, “A Review on Renewable Energy Transition under China’s Carbon Neutrality Target,” Sustainability, vol. 14, no. 22, p. 15006, Nov. 2022, doi: 10.3390/su142215006.

[106] P. Ge, Q. Hu, Q. Wu, Y. Ding, X. Dou, and Z. Wu, “Increasing operational flexibility of integrated energy systems by introducing power to hydrogen,” IET Renewable Power Gen, vol. 14, no. 3, pp. 372–380, Jan. 2020, doi: 10.1049/iet-rpg.2019.0663.

[107] J. Witte, H. Madi, U. Elber, P. Jansohn, and T. J. Schildhauer, “Grid-neutral hydrogen mobility: Dynamic modelling and techno-economic assessment of a renewable-powered hydrogen plant,” International Journal of Hydrogen Energy, vol. 78, pp. 52–67, June 2024, doi: 10.1016/j.ijhydene.2024.05.331.

[108] S. Samsatli and N. J. Samsatli, “The role of renewable hydrogen and inter-seasonal storage in decarbonising heat – Comprehensive optimisation of future renewable energy value chains,” Applied Energy, vol. 233–234, pp. 854–893, Nov. 2018, doi: 10.1016/j.apenergy.2018.09.159.

[109] R. Borup, J. Brouwer, and T. Krause, “Hydrogen is Essential for Industry and Transportation Decarbonization,” Electrochem. Soc. Interface, vol. 30, no. 4, pp. 79–84, Dec. 2021, doi: 10.1149/2.f18214if.

[110] A. Franco and M. Rocca, “Renewable Electricity and Green Hydrogen Integration for Decarbonization of ‘Hard-to-Abate’ Industrial Sectors,” Electricity, vol. 5, no. 3, pp. 471–490, July 2024, doi: 10.3390/electricity5030024.

[111] Q. Hassan, H. M. Salman, A. Z. Sameen, and S. Algburi, “Assessment of industrial-scale green hydrogen production using renewable energy,” Proceedings of the Institution of Mechanical Engineers, Part A: Journal of Power and Energy, vol. 238, no. 3, pp. 569–587, Nov. 2023, doi: 10.1177/09576509231219339.

[112] W. Su, J. Wang, and J. Roh, “Stochastic Energy Scheduling in Microgrids With Intermittent Renewable Energy Resources,” IEEE Trans. Smart Grid, vol. 5, no. 4, pp. 1876–1883, July 2014, doi: 10.1109/tsg.2013.2280645.

[113] S. G. Nnabuife, A. K. Hamzat, K. A. Quainoo, C. K. Darko, and C. K. Agyemang, “Innovative Strategies for Combining Solar and Wind Energy with Green Hydrogen Systems,” Applied Sciences, vol. 14, no. 21, p. 9771, Oct. 2024, doi: 10.3390/app14219771.

[114] E. Kuhnert, K. Mayer, M. Heidinger, C. Rienessel, V. Hacker, and M. Bodner, “Impact of intermittent operation on photovoltaic-PEM electrolyzer systems: A degradation study based on accelerated stress testing,” International Journal of Hydrogen Energy, vol. 55, pp. 683–695, Dec. 2023, doi: 10.1016/j.ijhydene.2023.11.249.

[115] F. Dawood, M. Anda, and G. Shafiullah, “Stand-Alone Microgrid with 100% Renewable Energy: A Case Study with Hybrid Solar PV-Battery-Hydrogen,” Sustainability, vol. 12, no. 5, p. 2047, Mar. 2020, doi: 10.3390/su12052047.

[116] P. S. Kumar, K. V. S. M. Babu, V. Ramu, R. P. S. Chandrasena, and G. N. Srinivas, “Energy Management System for Small Scale Hybrid Wind Solar Battery Based Microgrid,” IEEE Access, vol. 8, pp. 8336–8345, Jan. 2020, doi: 10.1109/access.2020.2964052.

[117] R. Keller, E. Rauls, M. Hehemann, M. Müller, and M. Carmo, “An adaptive model-based feedforward temperature control of a 100 kW PEM electrolyzer,” Control Engineering Practice, vol. 120, p. 104992, Dec. 2021, doi: 10.1016/j.conengprac.2021.104992.

[118] M. Nasser, T. F. Megahed, S. Ookawara, H. Hassan, and M. Abd El-Hady, “A review of water electrolysis-based systems for hydrogen production using hybrid/solar/wind energy systems,” Environmental Science and Pollution Research, vol. 29, pp. 86994–87018, 2022.

[119] V. Papadopoulos, J. Desmet, J. Knockaert, and C. Develder, “Improving the utilization factor of a PEM electrolyser powered by a 15 MW PV park by combining wind power and battery storage – feasibility study,” International Journal of Hydrogen Energy, vol. 43, pp. 16468–16478, 2018.

[120] J. L. Llamazares, M. I. García, J. I. San Martín, and A. Ramos-Hernanz, “Stability analysis of an off-grid hybrid power plant for hydrogen production,” Renewable Energy and Power Quality Journal, vol. 23, 2025.

[121] B. W. Tuinema, M. J. M. van der Meulen, P. H. F. M. Leufkens, and H. Polinder, “Modelling of large-size electrolysers for real-time simulation and study of the possibility of frequency support by electrolysers,” unpublished manuscript, 2020.

[122] H. Khajeh, S. Seyyedeh-Barhagh, and H. Laaksonen, “Optimized operation of hybrid wind-hydrogen system to provide flexibility for transmission system needs,” IEEE Transactions on Sustainable Energy, vol. 16, no. 3, pp. 1576–1587, Jul. 2025.

[123] MathWorks, “Solar Cell,” Simscape Electrical Documentation, 2024. [Online]. Available: https://www.mathworks.com/help/sps/ref/solarcell.html

[124] S. Singh, S. Manna, A. K. Akella, and M. I. Hasan Mansoori, “Implementation of Perturb & Observe MPPT Technique using Boost converter in PV System,” Institute Of Electrical Electronics Engineers, July 2020, pp. 1–4. doi: 10.1109/cispsse49931.2020.9212203.

[125] MathWorks, “Average-Value DC–DC Converter,” Simscape Electrical Documentation, 2024. [Online]. Available: https://www.mathworks.com/help/sps/ref/averagevaluedcdcconverter.html

[126] P. Sanjeevikumar, F. Blaabjerg, P. W. Wheeler, J. Loncarski, and G. Grandi, “A simple MPPT algorithm for novel PV power generation system by high output voltage DC-DC boost converter,” Institute Of Electrical Electronics Engineers, Jan. 2015, pp. 214–220. doi: 10.1109/isie.2015.7281471.

[127] M. Hosseinpour, A. Seifi, S. H. Hosseini, and M. Ahmadi, “A new transformerless buck-boost converter with improved voltage gain and continuous input current,” IET Power Electronics, vol. 17, no. 4, pp. 534–550, Feb. 2024, doi: 10.1049/pel2.12671.

[128] MathWorks, “Solar Cell,” Simscape Electrical Documentation, 2024. [Online]. Available: https://www.mathworks.com/help/sps/ref/solarcell.html

[129] European Commission, Joint Research Centre (JRC), Photovoltaic Geographical Information System (PVGIS), 2024. [Online]. Available: https://re.jrc.ec.europa.eu/pvg_tools/en/

[130] M. J. Rana and M. A. Abido, “Energy management in DC microgrid with energy storage and model predictive controlled AC–DC converter,” IET Generation Trans & Dist, vol. 11, no. 15, pp. 3694–3702, July 2017, doi: 10.1049/iet-gtd.2016.1934.

[131] S. J. Moura, M. Krstic, and N. A. Chaturvedi, “Adaptive PDE Observer for Battery SOC/SOH Estimation,” American Society Of Mechanical Engineers, Oct. 2012, pp. 101–110.

[132] M. A. Syed and M. Khalid, “An Intelligent Model Predictive Control Strategy for Stable Solar-Wind Renewable Power Dispatch Coupled with Hydrogen Electrolyzer and Battery Energy Storage,” International Journal of Energy Research, vol. 2023, pp. 1–17, Mar. 2023, doi: 10.1155/2023/4531054.

[133] H. A. Mohamed, H. A. Khattab, G. A. Morsy, and A. Mobarka, “Design, control and performance analysis of DC-DC boost converter for stand-alone PV system,” Institute Of Electrical Electronics Engineers, Dec. 2016, pp. 101–106. doi: 10.1109/mepcon.2016.7836878.

[134] R. Wagner, S. M. Pedersen, M. S. Courtney, I. Antoniou, and H. E. Jørgensen, “The influence of the wind speed profile on wind turbine performance measurements,” Wind Energy, vol. 12, no. 4, pp. 348–362, Sept. 2008, doi: 10.1002/we.297.

[135] M. Bilgili, S. Tumse, B. Sahin, and M. Tontu, “Effect of Growth in Turbine Size on Rotor Aerodynamic Performance of Modern Commercial Large-Scale Wind Turbines,” Arab J Sci Eng, vol. 46, no. 8, pp. 7185–7195, Jan. 2021, doi: 10.1007/s13369-021-05364-6.

[136] N. Jargalsaikhan, H. Masrur, A. Iqbal, S. S. Rangarajan, S. Byambaa, and T. Senjyu, “A control algorithm to increase the efficient operation of wind energy conversion systems under extreme wind conditions,” Energy Reports, vol. 8, pp. 11429–11439, Sept. 2022, doi: 10.1016/j.egyr.2022.08.243.

[137] “Data Download for Montréal,” WeatherStats, Accessed: Nov. 24, 2025. *Online*. Available: https://montreal.weatherstats.ca/download.html

[138] S. Sood et al., “Generic Dynamical Model of PEM Electrolyser under Intermittent Sources,” Energies, vol. 13, no. 24, p. 6556, Dec. 2020, doi: 10.3390/en13246556.

[139] S. Gharibzadeh, R. Motallebzadeh, S. Jafarmadar, and A. Ebrahimpour, “Comprehensive optimization of an integrated energy system for power, hydrogen, and freshwater generation using high-temperature PEM fuel cell,” Case Studies in Thermal Engineering, vol. 56, p. 104181, Mar. 2024, doi: 10.1016/j.csite.2024.104181.

[140] S. Sood et al., “Generic Dynamical Model of PEM Electrolyser under Intermittent Sources,” Energies, vol. 13, no. 24, p. 6556, Dec. 2020, doi: 10.3390/en13246556.

[141] M. A. Arce, J. M. Guerrero, A. J. Calderón, and F. Jurado, “Model predictive control of hybrid renewable energy systems with battery storage and electrolyzer for hydrogen production,” Renewable Energy, vol. 141, pp. 300–312, Oct. 2019.

[142] A. B. Shafiee, H. Karimi, and M. Saif, “Digital twin-based predictive control for renewable-hydrogen hybrid systems,” IEEE Transactions on Energy Conversion, vol. 37, no. 3, pp. 2158–2170, Sept. 2022.

[143] J. Kennedy and R. Eberhart, “Particle swarm optimization,” in Proceedings of the IEEE International Conference on Neural Networks, Perth, WA, Australia, vol. 4, pp. 1942–1948, Dec. 1995.

[144] A. Khalilnejad, A. Sundararajan, and A. I. Sarwat, “Optimal design of hybrid wind/photovoltaic electrolyzer for maximum hydrogen production using imperialist competitive algorithm,” Journal of Modern Power Systems and Clean Energy, vol. 6, no. 1, pp. 40–49, 2018.

[145] M. Alharthi, “An analysis of hybrid renewable energy-based hydrogen production and power supply for off-grid systems,” Processes, vol. 12, 2024.

[146] T. Papadopoulos, P. Stathopoulos, and P. Tsiakaras, “Improving the utilization factor of a PEM electrolyzer powered by a 15 MW solar park,” International Journal of Hydrogen Energy, vol. 43, no. 1, pp. 214–226, 2018.

[147] M. Nasser, T. F. Megahed, S. Ookawara, and H. Hassan, “A review of water electrolysis–based systems for hydrogen production using hybrid/solar/wind energy systems,” Environmental Science and Pollution Research, vol. 29, pp. 86994–87018, 2022.

[148] M. Alharthi, “An analysis of hybrid renewable energy-based hydrogen production and power supply for off-grid systems,” Processes, vol. 12, 2024.

[149] T. Papadopoulos, P. Stathopoulos, and P. Tsiakaras, “Improving the utilization factor of a PEM electrolyzer powered by a 15 MW solar park,” International Journal of Hydrogen Energy, vol. 43, no. 1, pp. 214–226, 2018.

[150] M. Nasser, T. F. Megahed, S. Ookawara, and H. Hassan, “A review of water electrolysis–based systems for hydrogen production using hybrid/solar/wind energy systems,” Environmental Science and Pollution Research, vol. 29, pp. 86994–87018, 2022.

APPENDIX

APPENDIX A SENSITIVITY ANALYSIS

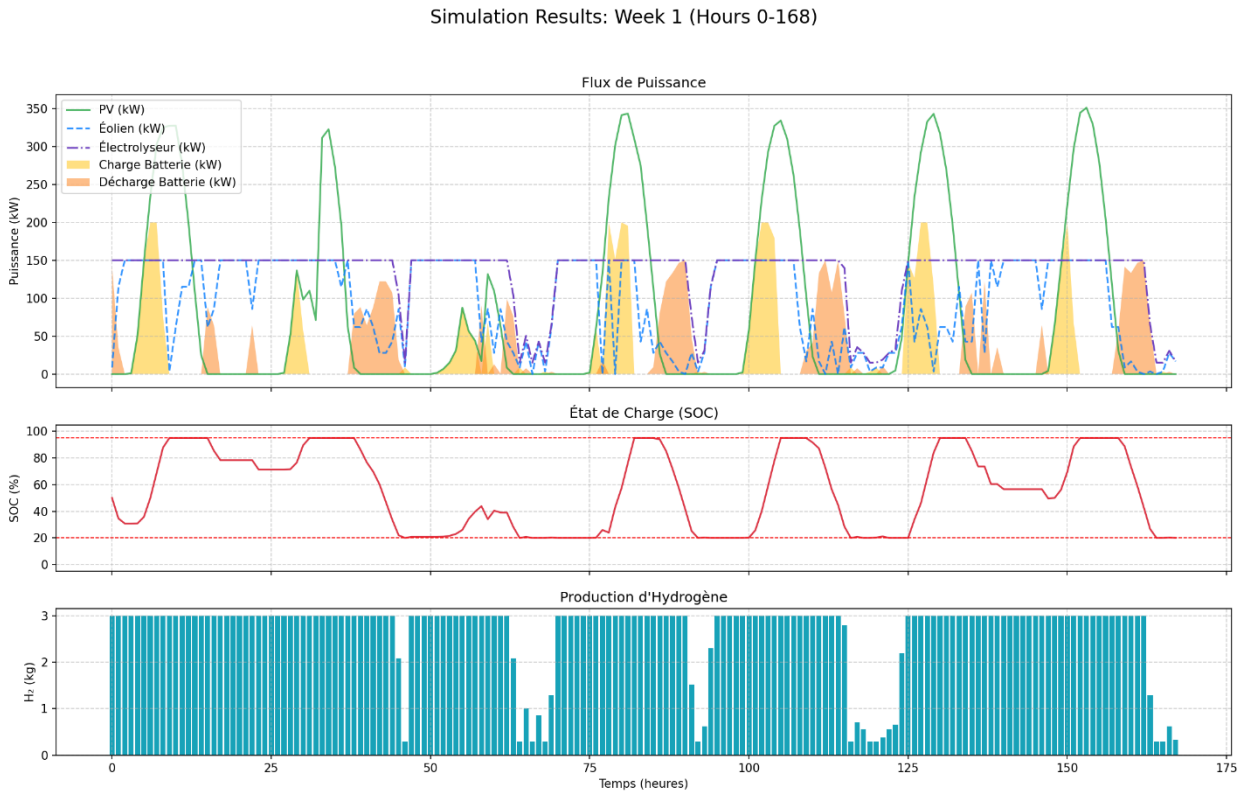

Figure A7.37: Weekly Simulation of Power Flows, SOC Dynamics, and Hydrogen Output Under the Oversized Renewable and Large-Battery Configuration on a Cloudy Day

In this scenario, the renewable generation and storage capacities were intentionally oversized relative to the electrolyzer rating in order to evaluate the upper bound of system performance. The PV system was oversized by 67% while the wind was oversized by 25% compared to the study. The battery capacity was also doubled. Under these conditions the electrolyzer operated with a capacity factor of 0.88, which is exceptionally high for a fully renewable, off-grid microgrid. Achieving that capacity factor confirms what was found in the literature that with oversizing of RE source and battery capacities, capacity factors could reach more than 80%. The hydrogen objective

reaching almost 140% indicates that the system produces way more hydrogen than the nominal target.

Curtailed energy represented 25% of the produced energy even though this scenario was simulated for a cloudy day, this reveals that the system is unproportionally oversized that even diminished irradiance does not prevent renewable overflow.

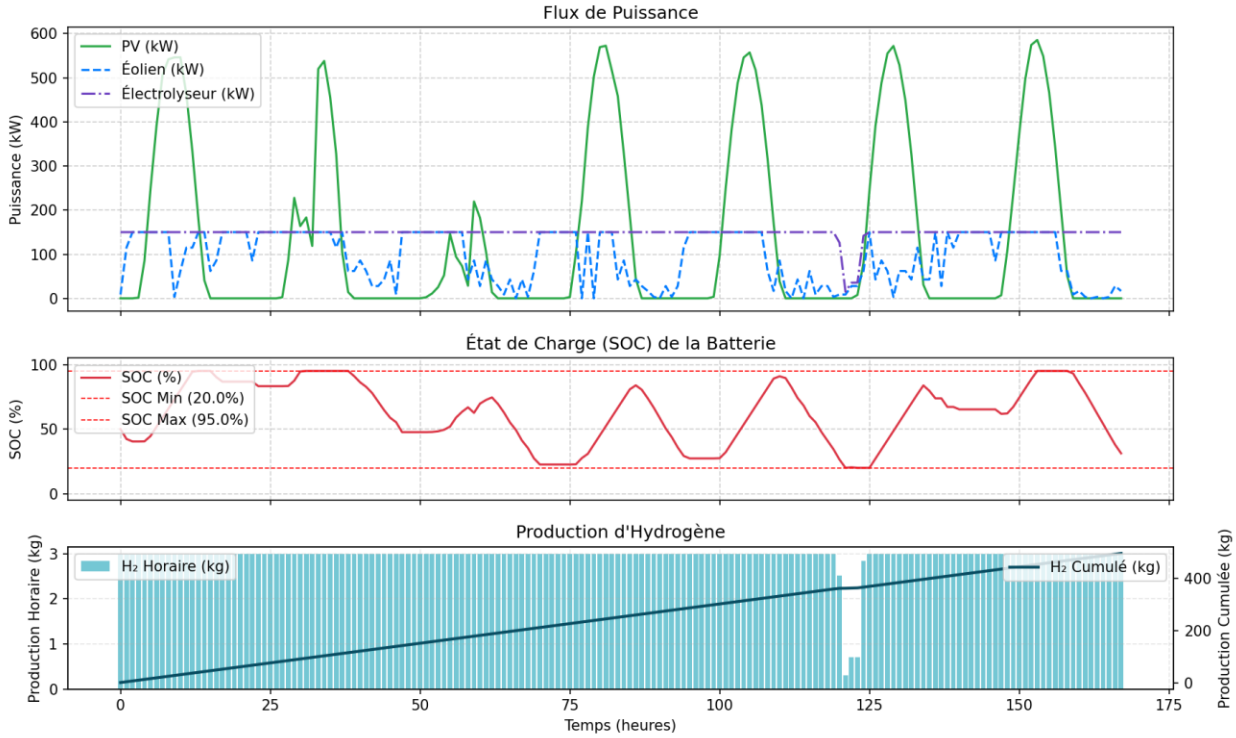

Figure A7.38: Weekly Simulation of Power Flows, SOC Dynamics, and Hydrogen Output Under the Oversized Renewable and Large-Battery Configuration on a Cloudy Day

During a sunny week, the electrolyzer starts behaving as a fixed based load, absorbing as much renewable energy as its limits allows while the battery handles any short-term mismatch. Once the battery reaches its upper SoC limit, any surplus renewable generation is curtailed.

APPENDIX B USER INTERFACE SAMPLE

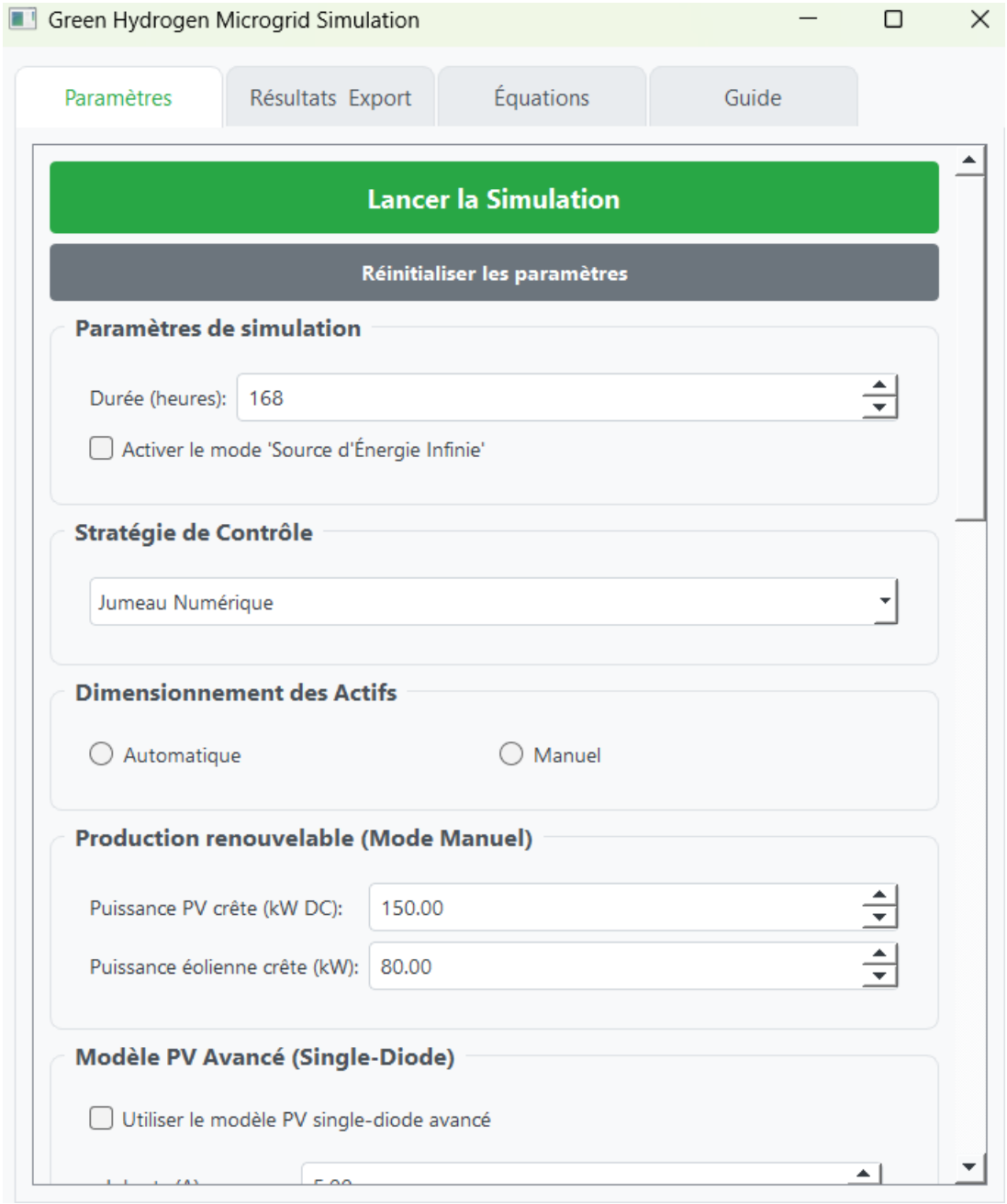

Figure A7.39: User Interface for Configuring Electrolyzer Parameters and Weather Inputs

This panel allows the user to define the simulation duration, choose the control strategy, and select between automatic or manual sizing. It also provides manual inputs for the PV and wind rated capacities used in the simulation.

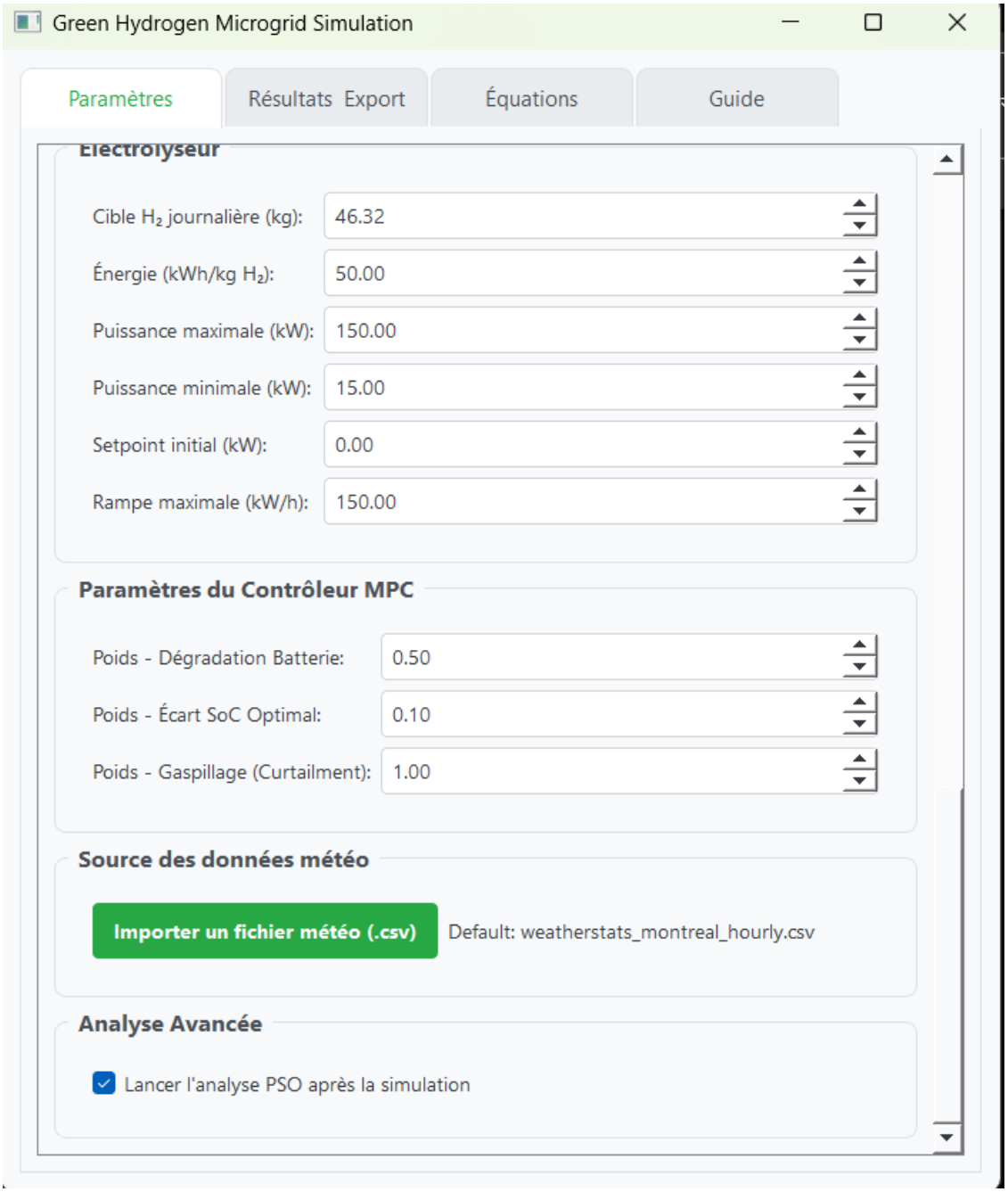

Figure A7.40: User Interface for Configuring Electrolyzer Parameters and Weather Inputs

This panel displays the adjustable electrolyzer parameters such as daily hydrogen target, energy consumption per kilogram and power limits. It allows the user to import meteorological input for the simulation and choose whether or not to run the PSO post optimization.

APPENDIX C CODE SAMPLES

- **MPC code sample :**

```
import numpy as np
from scipy.optimize import minimize

class MPCController:
    def __init__(self, parameters):

        self.p = parameters
        self.electrolyzer_hourly_target_kw = self.p.get('ELECTROLYZER_DAILY_TARGET_KWH', 2500) / 
        self.p_elec_previous_kw = self.p.get('ELEC_SETPOINT_KW', 0)

    def solve(self, current_soc, renewable_forecast_kw):

        horizon = min(self.p.get('PREDICTION_HORIZON', 24), len(renewable_forecast_kw))
        if horizon == 0:
            return 0, 0

        num_vars = 4 * horizon

        def objective(x):
            p_elec = x[0:horizon]
            p_batt = x[horizon:2*horizon]
            p_batt_abs = x[2*horizon:3*horizon]
            p_curtail = x[3*horizon:num_vars]

            cost_elec_production = -np.sum(p_elec) * self.p.get('W_ELECTROLYZER_TARGET', 1.0)
            cost_degradation = np.sum(self.p.get('W_BATTERY_DEGRADATION', 0.5) * p_batt_abs)
            soc_path = self._calculate_soc_path(current_soc, p_batt, horizon)
            cost_soc_deviation = np.sum(self.p.get('W_SOC_DEVIATION', 0.1) * ((soc_path[1:] - sel
            cost_curtailment = np.sum(self.p.get('W_CURTAILMENT', 1.0) * p_curtail)

            return cost_elec_production + cost_degradation + cost_soc_deviation + cost_curtailmen

        constraints = []

        for i in range(horizon):
            def power_balance(x, i=i):
                return renewable_forecast_kw[i] - x[i] - x[i + horizon] - x[i + 3*horizon]
            constraints.append({'type': 'eq', 'fun': power_balance})

        def soc_constraints(x):
            p_batt = x[horizon:2*horizon]
            soc_path = self._calculate_soc_path(current_soc, p_batt, horizon)
            min_soc_violations = soc_path[1:] - self.p.get('BATT_SOC_MIN', 0.2)
            max_soc_violations = self.p.get('BATT_SOC_MAX', 0.95) - soc_path[1:]
            return np.concatenate([min_soc_violations, max_soc_violations])
        constraints.append({'type': 'ineq', 'fun': soc_constraints})

        ramp_max = self.p.get('ELEC_RAMP_MAX_KW_PER_H', 150)
        def ramp_constraints(x):
            p_elec = x[0:horizon]
            ramps = np.diff(p_elec, prepend=self.p_elec_previous_kw)
            return np.concatenate([ramp_max - ramps, ramp_max + ramps])
        constraints.append({'type': 'ineq', 'fun': ramp_constraints})

        def abs_batt_constraints(x):
            p_batt = x[horizon:2*horizon]
            p_batt_abs = x[2*horizon:3*horizon]
            return np.concatenate([p_batt_abs - p_batt, p_batt_abs + p_batt])
        constraints.append({'type': 'ineq', 'fun': abs_batt_constraints})

        elec_bounds = [(self.p.get('ELEC_MIN_POWER_KW', 15), self.p.get('ELEC_MAX_POWER_KW', 150)
        batt_bounds = [(-self.p.get('BATT_DISCHARGE_MAX_KW', 500), self.p.get('BATT_CHARGE_MAX_KW
        max_abs_batt = max(self.p.get('BATT_CHARGE_MAX_KW', 500), self.p.get('BATT_DISCHARGE_MAX_
```

```
    curtail_bounds = [(0, None)] * horizon
    bounds = elec_bounds + batt_bounds + batt_abs_bounds + curtail_bounds

    x0 = np.concatenate([
        np.full(horizon, self.electrolyzer_hourly_target_kw),
        np.zeros(horizon),
        np.zeros(horizon),
        np.zeros(horizon)
    ])

    result = minimize(objective, x0, bounds=bounds, constraints=constraints, method='SLSQP',

    if result.success:
        p_elec_opt = result.x[0]
        p_batt_opt = result.x[horizon]
    else:
        p_elec_opt = min(self.p.get('ELEC_MAX_POWER_KW', 150), renewable_forecast_kw[0] if le
        p_elec_opt = max(self.p.get('ELEC_MIN_POWER_KW', 15), p_elec_opt)
        p_batt_opt = (renewable_forecast_kw[0] if len(renewable_forecast_kw) > 0 else 0) - p_

    self.p_elec_previous_kw = p_elec_opt

    return p_elec_opt, p_batt_opt

def _calculate_soc_path(self, initial_soc, p_batt_trajectory, horizon):

    soc_path = np.zeros(horizon + 1)
    soc_path[0] = initial_soc

    charge_eff = self.p.get('BATT_CHARGE_EFF', 0.95)
    discharge_eff = self.p.get('BATT_DISCHARGE_EFF', 0.92)
    capacity = self.p.get('BATT_CAPACITY_KWH', 2500)
    time_step = self.p.get('TIME_STEP_H', 1)

    for i in range(horizon):
        power = p_batt_trajectory[i]
        if power >= 0:
            soc_change = (power * time_step * charge_eff) / capacity
        else:
            soc_change = (power * time_step) / (discharge_eff * capacity)
        soc_path[i+1] = soc_path[i] + soc_change

    return soc_path
```

- **DT code sample :**

```python
import numpy as np

class DigitalTwinController:

    def __init__(self, params):
        self.p = params
        self.last_run_strategies = None

    def solve(self, current_soc, renewable_forecast):
        forecast_clean = np.nan_to_num(np.array(renewable_forecast), nan=0.0)

        strategies = {
            "max_hydrogen": self.simulate_strategy(current_soc, forecast_clean, "max_hydrogen"),
            "charge_battery": self.simulate_strategy(current_soc, forecast_clean, "charge_battery
            "balanced": self.simulate_strategy(current_soc, forecast_clean, "balanced"),
        }

        self.last_run_strategies = strategies
        best_strategy_name = "max_hydrogen"
        best_strategy = strategies[best_strategy_name]

        if best_strategy is None:
            return 0, 0

        return best_strategy['p_elec'][0], best_strategy['p_batt'][0]

    def simulate_strategy(self, current_soc, renewable_forecast, strategy_name):
        horizon = len(renewable_forecast)
        p_elec = np.zeros(horizon)
        p_batt = np.zeros(horizon)
        soc = np.zeros(horizon + 1)
        soc[0] = current_soc

        for t in range(horizon):
            renewable_power = renewable_forecast[t]
            soc_t = soc[t]

            energy_to_soc_min = (soc_t - self.p['BATT_SOC_MIN']) * self.p['BATT_CAPACITY_KWH']
            dischargeable_power_soc = (energy_to_soc_min / self.p['TIME_STEP_H']) * self.p['BATT_
            dischargeable_power_kw = min(self.p['BATT_DISCHARGE_MAX_KW'], dischargeable_power_soc

            energy_to_soc_max = (self.p['BATT_SOC_MAX'] - soc_t) * self.p['BATT_CAPACITY_KWH']
            chargeable_power_soc = (energy_to_soc_max / self.p['TIME_STEP_H']) / self.p['BATT_CHA
            chargeable_power_kw = min(self.p['BATT_CHARGE_MAX_KW'], chargeable_power_soc)

            p_elec_target = 0
            if strategy_name == "max_hydrogen":
                p_elec_target = renewable_power + dischargeable_power_kw
            elif strategy_name == "charge_battery":
                p_elec_target = 0
            elif strategy_name == "balanced":
                p_elec_target = self.p.get('ELEC_SETPOINT_KW', self.p['ELEC_MAX_POWER_KW'] / 2)

            p_elec[t] = np.clip(p_elec_target, 0, self.p['ELEC_MAX_POWER_KW'])
            if p_elec[t] < self.p['ELEC_MIN_POWER_KW']:
                p_elec[t] = 0

            required_batt_power = renewable_power - p_elec[t]
            p_batt[t] = np.clip(required_batt_power, -dischargeable_power_kw, chargeable_power_kw

            p_elec[t] = renewable_power - p_batt[t]
            p_elec[t] = max(0, p_elec[t])
```

```
            soc_change = 0
            if p_batt[t] > 0:
                soc_change = (p_batt[t] * self.p['TIME_STEP_H'] * self.p['BATT_CHARGE_EFF']) / se
            elif p_batt[t] < 0:
                soc_change = (p_batt[t] * self.p['TIME_STEP_H']) / (self.p['BATT_DISCHARGE_EFF'] 

            soc[t+1] = np.clip(soc_t + soc_change, self.p['BATT_SOC_MIN'], self.p['BATT_SOC_MAX']

        return {"p_elec": p_elec, "p_batt": p_batt, "soc": soc}

    def evaluate_strategies(self, strategies):
        best_strategy = None
        best_score = -np.inf

        w_h2 = self.p.get('W_ELECTROLYZER_TARGET', 1.0)
        w_soc = self.p.get('W_SOC_DEVIATION', 0.1)
        soc_optimal = self.p.get('BATT_SOC_OPTIMAL', 0.6)

        for name, results in strategies.items():
            if results is None or np.any(np.isnan(results['p_elec'])) or np.any(np.isnan(results[
                continue

            total_h2_energy = np.sum(results['p_elec'])
            final_soc_deviation = np.abs(results['soc'][-1] - soc_optimal)

            score = (w_h2 * total_h2_energy) - (w_soc * final_soc_deviation)

            if score > best_score:
                best_score = score
                best_strategy = name

        return best_strategy
```

- **Code Logic for the Interface (PyQt5)**

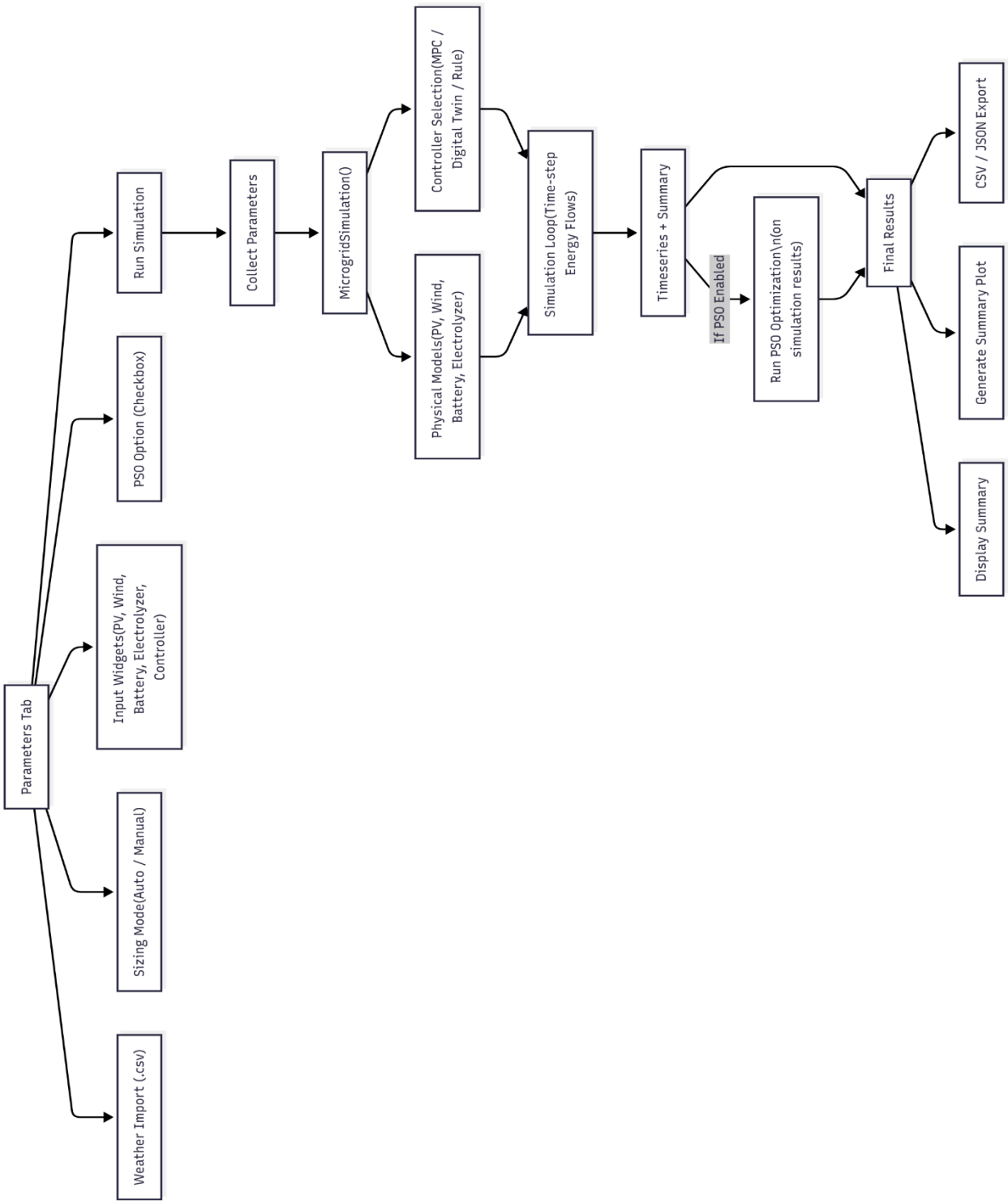

Figure A7.41: Flow Diagram for the Code Logic for the Interface

- **Code Sample : Parameter Extraction & Simulation Executio**

```
def run_simulation(self):
    if self.soc_min_spin.value() >= self.soc_max_spin.value():
        QMessageBox.critical(self, "Erreur", "SOC min < SOC max");
        return

    params = SYSTEM_PARAMETERS.copy()
    params['SIMULATION_HOURS'] = self.duration_spin.value()
    params['CONTROLLER_TYPE'] = self.controller_combo.currentText()
    params['USE_INFINITE_SOURCE_MODE'] = self.infinite_source_checkbox.isChecked()
    params['USE_AUTOMATIC_SIZING'] = self.radio_auto.isChecked()

    if params['USE_AUTOMATIC_SIZING']:
        if self.max_prod_checkbox.isChecked():
            params['SIZING_OVERSIZING_FACTOR'] = 2.0
            params['SIZING_BATT_AUTONOMY_H'] = 24
        else:
            params['SIZING_OVERSIZING_FACTOR'] = self.oversizing_factor_spin.value()
            params['SIZING_BATT_AUTONOMY_H'] = self.autonomy_hours_spin.value()
    else:
        params['PV_PEAK_POWER_KW'] = self.solar_spin.value()
        params['WIND_P_RATED_KW'] = self.wind_spin.value()

    if hasattr(self, 'adv_pv_checkbox') and self.adv_pv_checkbox.isChecked():
        params['PV_ADV_PARAMS'] = {
            'iph_stc': self.iph_stc_spin.value(),
            'is_stc': self.is_stc_spin.value(),
            'rs': self.rs_spin.value(),
            'rsh': self.rsh_spin.value(),
            'n': self.n_spin.value(),
            'voc_stc': self.voc_stc_spin.value()
        }

    params['BATT_CAPACITY_KWH'] = self.battery_kwh_spin.value()
    params['BATT_CHARGE_MAX_KW'] = self.batt_charge_spin.value()
    params['BATT_DISCHARGE_MAX_KW'] = self.batt_discharge_spin.value()
    params['BATT_RAMP_MAX_KW_PER_H'] = self.batt_ramp_spin.value()
    params['BATT_SOC_MIN'] = self.soc_min_spin.value()
    params['BATT_SOC_MAX'] = self.soc_max_spin.value()

    params['ELECTROLYZER_DAILY_TARGET_KWH'] = self.h2_target_spin.value() * self.energy_per_kg_sp
    params['energy_per_kg'] = self.energy_per_kg_spin.value()
    params['ELEC_MAX_POWER_KW'] = self.elec_max_power_spin.value()
    params['ELEC_MIN_POWER_KW'] = self.elec_min_power_spin.value()
    params['ELEC_SETPOINT_KW'] = self.elec_setpoint_spin.value()
    params['ELEC_RAMP_MAX_KW_PER_H'] = self.elec_ramp_spin.value()

    params['W_BATTERY_DEGRADATION'] = self.w_batt_deg_spin.value()
    params['W_SOC_DEVIATION'] = self.w_soc_dev_spin.value()
    params['W_CURTAILMENT'] = self.w_curtailment_spin.value()

    if self.weather_file_path:
        params['WEATHER_DATA_PATH'] = self.weather_file_path

    try:
        sim = MicrogridSimulation(params)
        sim.run(use_physical_models=hasattr(self, 'adv_pv_checkbox') and self.adv_pv_checkbox.isC
        self.current_sim = sim
        self.sim_results = sim.results['timeseries']
    except Exception as e:
        QMessageBox.critical(self, "Erreur", str(e))
        return

    self.update_plot_placeholder()
    self.tabs.setCurrentIndex(1)
```